SISSA
Scuola
Internazionale
Superiore di
Studi Avanzati

Neuroscience Area – PhD course in

NEUROBIOLOGY

Exploring hybrid networks made by neurons and progenitor cells

Candidate:

Teresa Sorbo

Supervisor:

Laura Ballerini

Academic Year 2018-19

List of contents

1 ABSTRACT 1

2 INTRODUCTION 2

2.1 REGENERATIVE MEDICINE 2

Stem Cells discovery 3

2.2 NEURONAL REPLACEMENT STRATEGIES 6

Endogenous recruitment from neurogenic sources 6

Injury-induced neurogenesis 8

Transplantation of neurogenic cells 9

2.3 NEURAL PROGENITOR CELLS (NPCS): *IN VITRO* AND *IN VIVO* STUDIES 12

2.4 *IN VITRO* CO-CULTURES 15

2.5 POST-NATAL CIRCUITS 17

Hippocampal neurons culture 17

Dopaminergic neurons culture 20

3 AIMS 22

4 PAPERS 24

4.1 NEURONAL PROGENITOR CELL-IDENTITY SPECIFIED BY SYNAPTIC INTEGRATION TO POSTNATAL HIPPOCAMPAL CIRCUITS IN CULTURE 24

Abstract 24

Introduction 24

Results 25

Discussion 31

Materials and Methods 33

Figure and figure legends 39

4.2 FETAL NEURAL PROGENITORS CONTRIBUTE TO POSTNATAL CIRCUITS FORMATION *EX VIVO*: AN ELECTROPHYSIOLOGICAL INVESTIGATION 49

Abstract 49

Introduction 50

Material and methods 50

Results 53

Discussion *55*
Conclusions *55*
Reference *56*
5 APPENDIX 60
5.1 EXPLOIT EARLY ACTIVITY TO EVALUATE INTEGRATION RATE 60
Materials and Methods *60*
Results and discussions *60*
5.2 THE IMPACT OF CONDITIONED MEDIA ON FNPCS DEVELOPMENT 62
Methods *62*
Results and discussions *63*
5.3 PAIR PULSE RATIO 65
Methods *65*
Results and discussions *65*
5.4 DOPAMINERGIC NEURONS AND FNPCS 67
Methods *67*
Results and discussions *67*
5.5 *FOXG1* UPREGULATION ENHANCES NEOCORTICAL PROJECTION NEURON ACTIVITY. 73
6 FINAL REMARKS 97
7 REFERENCES 100

List of figures

Figure 1. Origin of stem cells in the mammalian embryo. 5
Figure 2. Overview of three neuronal replacement strategies. 7
Figure 3. Distinction between lineage and potential of NSCs 11
Figure 4. Lineage trees of neurogenesis. 13
Figure 5. Schematic representation of different co-culture experiments. 16
Figure 6. Main hippocampal cell populations. 19
Figure 7. Three dopamine pathways and their related cognitive processes. 20
Figure 8. Exploit early activity to evaluate integration rate 61
Figure 9. The impact of conditioned media 64
Figure 10. The impact of astrocytes 64
Figure 11. Pair Pulse Ratio 66
Figure 12. Dopaminergic neurons 68
Figure 13. SNC-VTA neurons' membrane passive properties 69
Figure 14. Spontaneous Post Synaptic activity in SNC-VTA cultures 70
Figure 15. Pair recordings in SNC-VTA cultures 71

1 ABSTRACT

Neuronal stem cells (NSCs) and primitive progenitors (NPCs) play an essential role in homeostasis of the central nervous system (CNS). Due to their ability to differentiate into specific lineages, the possibility to manipulate these cell types could have a tremendous impact on future therapeutic approaches for brain or spinal cord injuries or degenerative diseases charachterized by neuronal loss. Thus, the study of the pathways involved in self-renewal and lineage-specific differentiation of stem cells is a pillar step to generate specific cell types required for clinical applications.

We focused on fetal NPCs, a more committed subpopulation of NSCs, which are mostly cultured *in vitro* as neurospheres given their ability to proliferate and differentiate in all neuronal cell types. We tested wheter fNPCs could integrate among post-mitotic neurons and communicate with them by culturing them in co-culture *in vitro* system. This possibility was investigated by co-culturing fNPCS within hippocampal neurons, within dopaminergic neurons, obtained from substantia nigra compacta (SNc) and ventral tegmental area (VTA) and within cortical astrocytes.

Our results suggest the capability of fNPCs to differently change their phenotype and cell development depending on the neural circuit they interact with.

We further examined the main players responsible for such changes, including the soluble component released by different cell types and the firing properties of neurons.

2 INTRODUCTION

2.1 Regenerative medicine

The term “regenerative medicine” was coined by William A. Haseltine in 2000. Nowadays, it describes any biomedical approach inducing endogenous, or exogenous (transplanted) cell-based repair of damaged tissues or, more in general, tissue engineering approaches to replace diseased or injured tissues and organs. Ultimately, regenerative medicine seeks to replace tissue or organs that have been damaged by diverse disease or traumatic etiologies. By bringing together experts in biology, chemistry, computer science, engineering, genetics, medicine, robotics and other fields, regenerative medicine is already facing some of the most challenging medical problems humankind must deal with.

The National Institutes of Health in 2010 defined regenerative medicine as “the process of creating living, functional tissues to repair or replace tissue or organ function lost due to age, disease, damage or congenital defects”. The main strategy adopted in regenerative medicine to replace diseased cells, tissues, or organsis is augmenting natural or inducing latent regenerative processes. Underlying these goals is the manipulation – expansion and differentiation – of stem cells, which are the primary source for organ homeostasis, maintenance and tissue regeneration.

In the majority of mammalian species including human, tissue injuries are normally repaired by formation of fibrous scar tissue (Klussmann and Martin-Villalba, 2005, Sun and Weber , 2000). However, in various experiemntal conditions, the potential to promote tissue re-growth *in vitro* and in animal models clearly emerged. For example, stem cells, derived from umbilical cord blood, placental, adipose, and embryonic tissues, have been used in animal models to promote growth of cartilage, bone, and other connective tissues by producing factors known to promote tissue growth (Goldberg et al., 2017). Human mesenchymal stem cells (MSCs) are demonstrated to produce proteoglycans and glycosaminoglycans, which are integral components of a healthy intervertebral disc (Sobajima et al., 2008). In addition to stem cells, *in vitro* and *in vivo* studies using platelet-rich plasma (PRP), which contains high concentrations of

growth factors, demonstrated that PRP may induce smooth muscle cell proliferation (Ross et al., 1974) and bone regeneration (Hokugo et al., 2005, Kanthan et al., 2011).

Although the current literature is very promising, to better understand how regenerative technologies can be used in the treatment of patients with diverse conditions, focused research is still needed. More specifically, the use of *in vitro* and *in vivo* studies may be a solid way to better elucidate the cellular mechanisms by which regenerative agents lead to improvements in disadvantaged conditions (McCormick and Hooten, 2018).

Stem Cells discovery

Tissue-resident stem cells and primitive progenitors play an essential role in homeostasis of most organs; indeed, they are a very attractive source of cells as they can be obtained from patients at relative ease and transplanted autologously. The ability to direct embryonic stem cells (ESCs) or stem cells from different adult tissues to differentiate into specific lineages will have a tremendous impact on future therapeutic approaches. Thus, the study of the molecular pathways involved in self-renewal and lineage-specific differentiation of embryonic and somatic stem cells is a pillar step to generate specific cell types required for clinical applications. The ESCs were described first in 1981 when Martin used normal mouse blastocysts cultured in embryonal carcinoma cells (ECC)-conditioned medium (Martin, 1981), whereas Evans and Kaufman (1981) used a co-culture system in which cells derived from the inner cell mass (ICM) of delayed mouse blastocysts were grown on a layer of mitotically inactivated mouse embryonic fibroblast (MEF) as feeder cells (Kaufman, 1981). After these two first reports – considered milestones of the field - ESCs were shown to contribute to all tissues of chimeric mice following injection into blastocysts.

In normal conditions, mammalian development requires the specification of over 200 cell types from a single totipotent cell. Therefore, the investigation of the regulatory networks that are responsible for pluripotency in ESCs is fundamental to understand mammalian development and realizing therapeutic potential. These embryo-derived stem cells have been categorized using different names (embryonic stem cells (ESCs), embryonal carcinoma cells (ECCs), and embryonic germ cells (EGCs); described in Figure 1). Despite these distinctions, the different cells may display several overlapping **fetaures** and embryo-derived stem cells are definitely unified by some distinct advantages when compared to adult stem cells. They are easier to identify, isolate and maintain as established stem-cell lines so that they can be kept in culture basically indefinitely,

serving as an ‘on-demand’ reservoir of precursor cells. In the past decades, many intrinsic factors, essential for maintaining an ESC phenotype, have been identified (Boiani and Schöler, 2005) such as the octamer-binding transcription factor-4 (OCT-4) (Nichols et al., 1998), Nanog (Novo et al., 2016) and extrinsic factors as the leukemia inhibitory factor (LIF) (Jeff et al., 1988) which is a precursor of the only pathway defined in detail by the interaction of the transmembrane glycoprotein-130 (gp130). Because pluripotency is a fundamental biological function in multicellular organisms, it must be conserved among different types of stem cell. There is considerable interest in finding ways to perpetuate the pluripotency of embryo-derived cell lines, and such knowledge is crucial for many potential biomedical applications related to tissue regeneration and thus to regenerative medicine (Conrad and Huss, 2005).

Pluripotent cells of the embryo are tracked in green (Figure 1). From left to right, the morula-stage mouse embryo holds a core of pre-ICM (inner cell mass). At this stage, embryonic stem cell (ESC) and trophoblast stem cell (TSC) cell lines can be derived in vitro, and implantation occurs in vivo. As the blastocyst fully expands (and undergoes implantation in vivo), the ICM delaminates giving rise to a primitive ectoderm and a primitive endoderm layer. At this stage, pluripotent cell lines that are known as embryonal carcinoma cells (ECCs) can be derived from the primitive ectoderm — whether they are distinct from ESCs has not been resolved (Pan et al., 2016). At E6 and subsequent stages, the experimental ability to derive ESCs, TSCs and ECCs from the mouse embryo is progressively lost, and the in vivo embryo will start gastrulating. The Figure 1 was modified from (Boiani and Schöler, 2005).

In a similar way to mice, cell lines resembling ESCs have also been established from certain primates (Thomson and Marshall, 1997), including humans (Thomson et al., 1998). However, cell lines from embryos of different mammalian species have been notoriously more difficult to establish or propagate without losing pluripotency and therefore should be defined as “ESC-like cells” (Stadtfeld and Hochedlinger, 2010). ESCs unique characteristics to indefinite self-renewal and pluripotency allow them to remain genetically normal even after 140 cycles of division (Suda et al., 1987). Indeed, ESCs are great promise in regenerative medicine as they provide a source of cells with the potential to differentiate into various cell types to repair different injured tissues. Recent developments in methodologies allow to better isolate and culture embryonic and somatic stem cells leading to concrete new applications for clinical and preclinical trials. The field of regenerative medicine in clinical practice is still in its debut and a great amount of

experimentation and optimization is needed to refine all the conditions for derivation of different cell lineages. The question of which stem cell source will be optimal for each disease/tissue condition and the issue of host-rejection, among the others, remain to be answered. On the way to the clinic, several obstacles must be overcome, but when they will be resolved, the true potential of stem cell therapies will be realized.

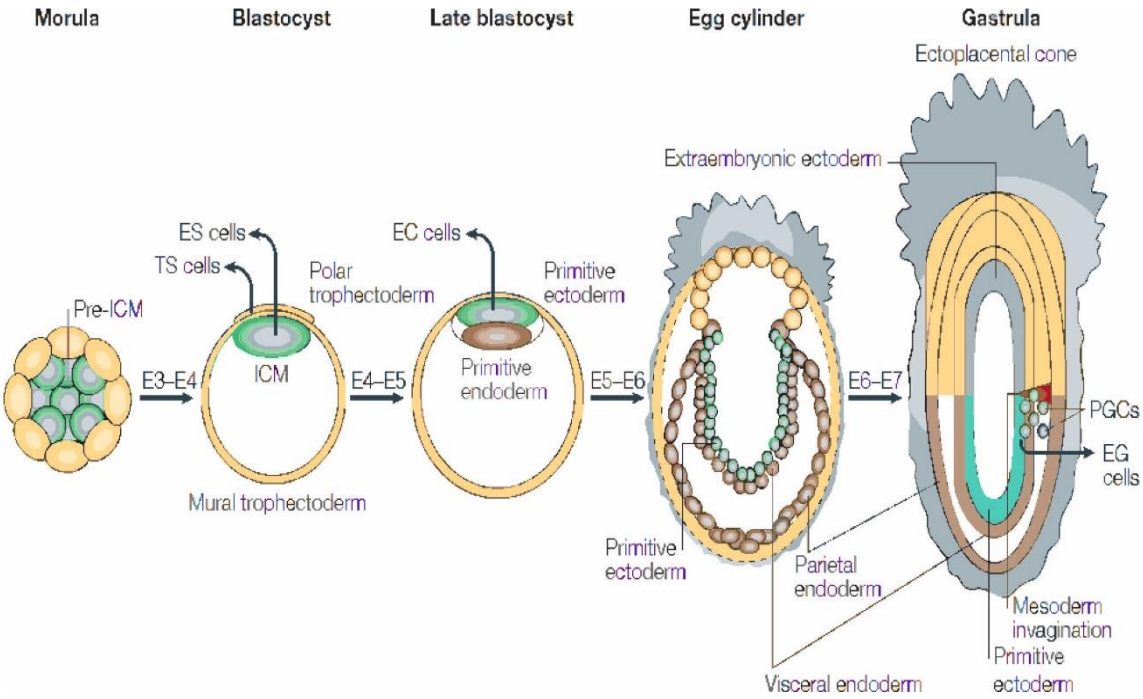

Figure 1. Origin of stem cells in the mammalian embryo

Pluripotent cells of the embryo are tracked in green. From left to right, the morula-stage mouse embryo holds a core of pre-ICM (inner cell mass). At this stage, embryonic stem cell (ESC) and trophoblast stem cell (TSC) cell lines can be derived in vitro, and implantation occurs in vivo. As the blastocyst fully expands (and undergoes implantation in vivo), the ICM delaminates giving rise to a primitive ectoderm and a primitive endoderm layer. At this stage, pluripotent cell lines that are known as embryonal carcinoma cells (ECCs) can be derived from the primitive ectoderm — whether they are distinct from ESCs has not been resolved. At E6 and subsequent stages, the experimental ability to derive ESCs, TSCs and ECCs from the mouse embryo is progressively lost, and the in vivo embryo will start gastrulating. This figure was modified from (Boiani and Schöler, 2005).

2.2 Neuronal replacement strategies

Central nervous system (CNS) degeneration or damage lead to irreversible neuronal loss resulting in functional deficits which may cause highly debilitating pathologies. As patients acquire permanent disabilities, the impact on families, societies and patients themselves becomes a significant health and economic **encumbrance**. The available treatments tend to rescue the remaining neurons, to compensate the lack of synaptic function or to promote functional plasticity or simply to alleviate symptoms,. Indeed, CNS injury can, to some extent, "awake" mechanisms of plasticity usually present during CNS development (Caleo, 2015). However, as expected when extensive injury takes place or progressive degenerative diseases, in which the brain accumulates dysfunction and inflammation, this plasticity may be limited (Lepeta et al., 2016). It is quite intuitive that the substitution of a dying neuron by a new one, within an extremely complex and intricate number of connections calibrated during network development, looks like an daunting challenge. Anyway, the crucial discovery that also the adult mammalian brain hosts neural stem cells (NSCs) that continuously generate newborn neurons capable to integrate into pre-existing neuronal circuitries, strengthen the neuronal integration hypothesis (Harel and Strittmatter, 2006). So far, three distinct strategies for neuronal replacement have been examined in depth: (1) endogenous recruitment from neurogenic niches or local cells (**Figure 2**a); (2) forced conversion of local glia to a neuronal fate (**Figure 2**b); (3) transplantation of exogenous cells from neuronal lineage (**Figure 2**c).

Endogenous recruitment from neurogenic sources

As already mentioned, even if constitutive neurogenesis is mostly restricted to early postnatal stages, it continues in the adult brain albeit much reduced during aging (Riddle and Lichtenwalner, 2007). The generation of new neurons in the adult brain was, for long time, considered with great skepticism, partly based on the conceptual question of how an organ specialized in information processing and storage may deal with a constant addition of new neurons (Gross, 2000). Now, the existence of neurogenesis in a few specific regions of the adult mammalian brain has been widely accepted even though is still poorly understood how adult-generated neurons affect the composition and function of the neuronal networks. In the mouse brain, NSCs have so far been detected in two former regions: the subventricular zone (SVZ) lining the lateral ventricles (Lim and Alvarez-Buylla, 2016) and in the subgranular zone (SGZ) of the hippocampal dentate gyrus (DG) (Gonçalves et al., 2016) (**Figure 2**a, left). A substantial turnover of dentate

granule cells (Spalding et al., 2013) suggests that adult hippocampal neurogenesis contributes to brain function also in humans since neurons constantly integrate and replace others in regions (Weinandy et al., 2011).

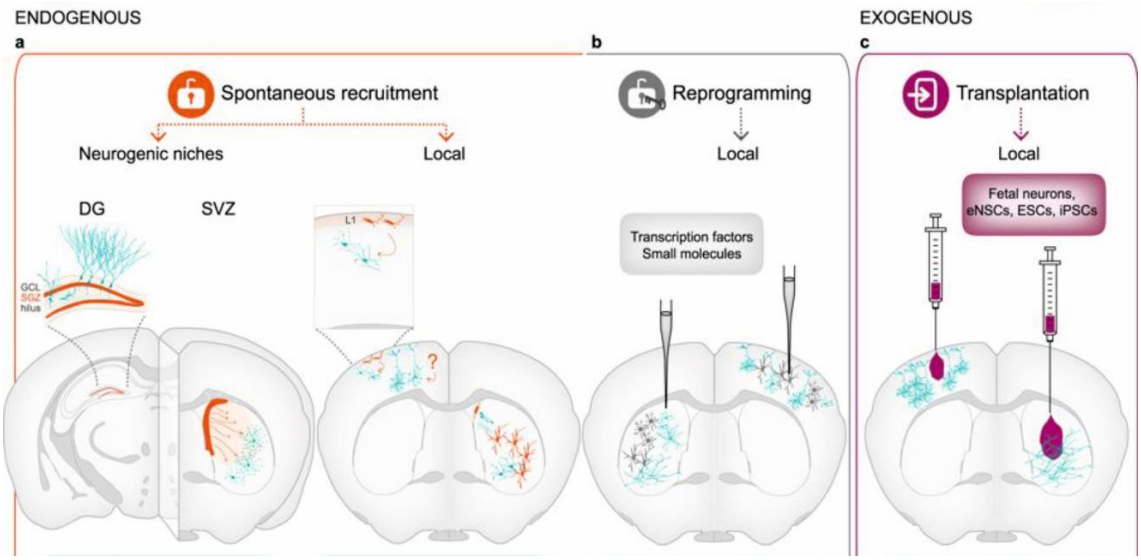

Figure 2. Overview of three neuronal replacement strategies.

Endogenous approaches (a) include a recruitment from the brain neurogenic niches like the hippocampal dentate gyrus (DG) and the subventricular zone (SVZ) or from latent local progenitors (cortical L1 or other) (spontaneous, as illustrated by the opened locker; orange), and (b) neuronal reprogramming which converts local glial cells into neurons (forced, as illustrated by the locker opened by a key that symbolizes the reprogramming transcription factors/small molecules; gray). (c) Exogenous approaches (purple) use different sources of donor cells for transplantation into the injured or diseased area, including fetal neurons, eNSCs-derived, ESC-derived and iPSC-derived neurons. Modified from (Grade and Götz, 2017).

This allows the study of the mechanisms regulating the synaptic integration of adult-born neurons in pre-existing networks and may help us understanding and engineering neuronal integration in non-neurogenic areas of the adult brain for circuits reconstruction or replacement. However, it is important to consider that mechanisms of synaptic competition and selective neuronal survival occur for instance in a fully functional circuit with already optimal neuronal numbers, like the dentate gyrus (DG) (Bergami and Berninger, 2012) and may hence differ in a setting where neuronal loss leaves gaps in the circuitry and unmatched synapses. Neuronal integration after injury or in

neurodegeneration must take place in a very different environment, often inflammatory, posing additional challenges for the newly integrating neurons.

Injury-induced neurogenesis

Even though brain insults perturb the homeostasis of adult neurogenic niches and the migratory routes of their progeny, a spontaneous recruitment of neuroblasts towards pathological sites is observed in a multitude of animal's brain models. Indeed, mobilization of neuroblasts from neurogenic niches occurs in response to stroke (Arvidsson et al., 2002), trauma (Kreuzberg et al., 2010) and Huntington's disease (HD) (Kandasamy et al., 2015) in animal models (Fig. 1a, left). This is fascinating because it implies that injury itself elicits a profound change in the neuronal subtype produced (Magnusson et al., 2014). Still questions arise about the neuronal subtype recruitment: how appropriate and to what extent can these new neurons connect in the target zone? Despite the observation that they are less prone to differentiate towards the neuronal fate (Li et al., 2010), they have been shown to form synaptic contacts (Yamashita et al., 2006), receive inhibitory and excitatory inputs (Hou et al., 2008), but eventually they fail to achieve long-term replacement of the degenerated neurons (Thored et al., 2006).

Besides cell mobilization from constitutive neurogenic niches, some studies suggested the generation of neurons from local latent precursors that are activated by the injury (**Figure 2**a, right). For instance, in the mice adult neocortex the differentiation into the same projection neuron subtype previously lost by apoptosis (Magavi et al., 2000) or into inhibitory neurons after cortical ischemia (Ohira et al., 2010) can suggest a probable local attempt for self-repair. Many other studies show increased plasticity of glial cells upon injury (Figure 2b) (Ninkovic and Götz, 2013) where reactive astrocytes isolated from the injured brain parenchyma exhibit NSC-like properties as shown in Figure 3 (Götz et al., 2015, Sirko et al., 2013, Buffo et al., 2008). Usually, reactive glial cells are not sufficiently re-specified to generate neurons in most injury conditions *in vivo*, but they seem capable to do so after ectopic grafting into the adult brain (Seidenfaden et al., 2006) and upon hypoxia in the postnatal mouse brain (Bi et al., 2011). Regardless of their source, new neurons can be considered relevant for cell replacement only if they fully mature into the neuronal subtype lost, integrate appropriately and survive for long term. As mentioned, in the cerebral cortex or in a HD rodent model, injury-induced neurons were able to extend correct long-range projections, but it remains unclear how injury induces neurons integration into brain circuits and if this neuronal replacement may

improve circuitry function. Furthermore, for the development of strategies that contemplate cell replacement by boosting this recruitment response, long-term survival is the major obstacle; the large majority of the newly recruited neurons dies in the first 6 weeks post-stroke (Lu et al., 2017). Although the neurogenic response persists for long time (Kokaia et al., 2006), it is not clear if it can be stimulated to efficiently achieve functionally relevant levels of neuronal replacement associated with a behavioral impact. While endogenous recruitment of neurons still lacks foundations for foreseeing a clinical application, a greater progress has been achieved by use of exogenous neurons or neurogenic cells in transplantation, discussed in the next section.

Transplantation of neurogenic cells

During development of the vertebrate CNS, neural stem cells (NSCs) and progenitor cells (NSPCs) are certainly the base for all CNS cell types generation, including neurons, astrocytes and oligodendrocytes (**Figure 3**) (Gao et al., 2014). Regarding their fate and specifications, an important hallmark of the CNS is its patterning – i.e. NSCs located at different positions express diverse fate determinants and progeny. However, it has been showed that upon exposure to growth factors *in vitro*, at least some neuronal cells can generate again all three types of cells - astrocytes, oligodendrocytes and neurons - supposedly due to the upregulation of gliogenic transcription factors mediated by epidermal growth factor (EGF) and sonic hedgehog (SHH) signaling pathways (Gabay et al., 2003). This implies that most NSCs can exhibit multipotency *in vitro* even after differentiation *in vivo* (Figure 3). Therefore, NSCs are a potential source of cells for replacement therapy, with the advantage that they can be readily isolated from the human brain (Widera et al., 2007). Focal pathologies with the loss of mainly one specific neuron subtype, such as the degeneration of substantia nigra pars compacta dopaminergic neurons in Parkinson's Disease (PD) are best suited for transplantation strategies. That is because of the precise brain regions to target and the known cell phenotype to replace, in contrast to the broad and non-cell-type-specific nature of neuronal degeneration in Alzheimer's Disease (AD) for which neuronal replacement strategies are very challenging. Stroke and brain trauma are also spatially restricted but offer greater challenges for neuronal replacement since various types of neurons die within the affected area and the formation of a glial scar is generally thought to be inhibitory to neurite outgrowth (Silver and Miller, 2004). There are also examples of such approach in case of

spinal cord injury (SCI) where the application of NPCs has been reported to enhance neural repair, protection and regeneration .

Yet, it is noteworthy that young transplanted neurons can readily extend axons and seemingly develop well when placed in scar-forming injuries, such as stroke (Tornero et al., 2013) and cortical aspiration (Michelsen et al., 2015). Mainly, the homing of NSCs to injury sites relies on a chemoattractant gradient of inflammatory soluble molecules released by the lesioned tissue (Martino and Pluchino, 2006). Neurons from fetal sources are superbly specified as they exactly derive from the brain region that generates the neuronal subtype affected by the disease. For instance, cells from the medial ganglionic eminence (MGE) transplanted into different brain regions develop into mature GABAergic neurons that enhance local synaptic inhibition (Larimer et al., 2017; Howard and Baraban, 2016). The same therapeutic strategy could also be beneficial for AD as well as other traumatic brain injury associated with interneuron dysfunction or loss, and consequent imbalance between excitation and inhibition.

In summary, fetal neurons have provided the most exciting results as donor cell population and have been applied in the clinical setting in PD patients (Barker et al., 2013). The achievements made until now hold great promise even though the limited availability of fetal neurons hinders fetal neuron-based cell therapies for neurological disorders and hence, efforts have been focused towards the use of expandable cell sources. Self-replicating multipotent NSCs form and can be propagated as neurospheres in suspension cultures (**Figure 3**), which is the most common culture system to guarantee the maintenance and expansion of multipotency (Ewald et al., 1992). The neurosphere provides a three-dimensional environment that can, to some extent, mimic the neurogenic niche from which the NSC is derived. When used and cultured appropriately, NSCs in neurospheres can expand and provide important information about the mechanisms that potentially control *in vivo* mechanisms (Reynolds and Weiss, 1996).

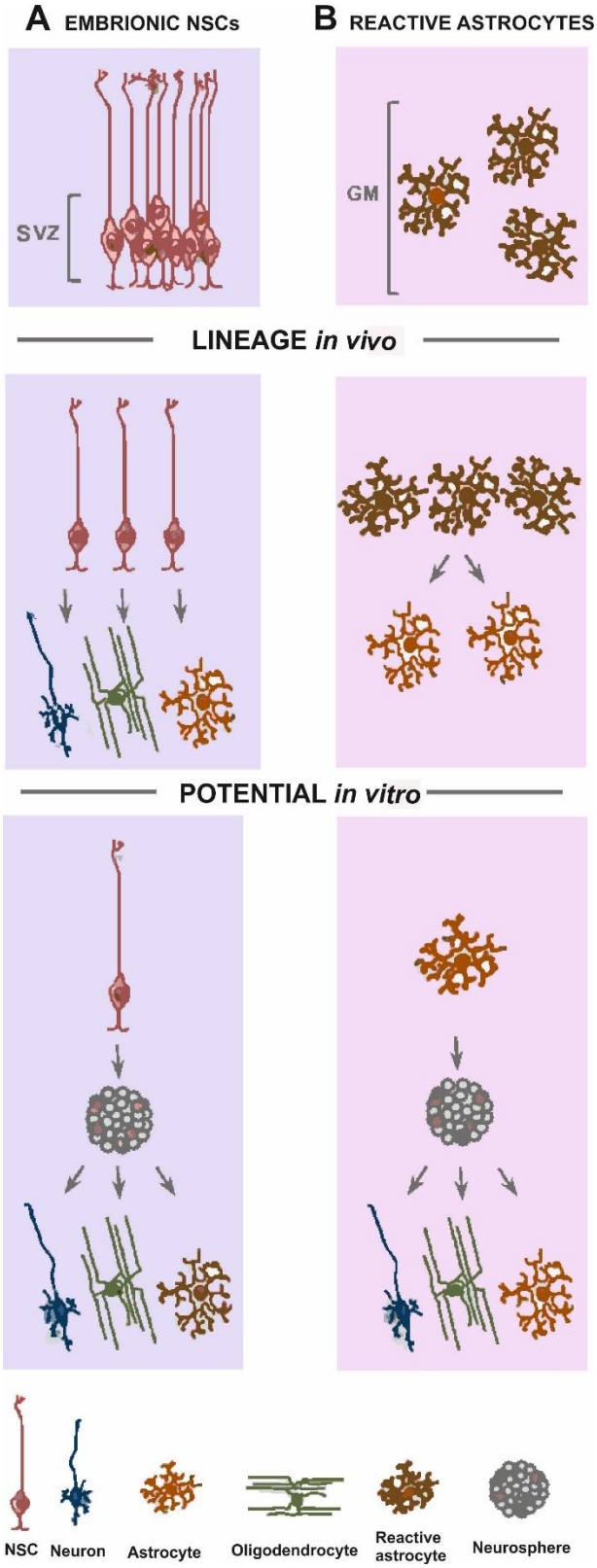

Figure 3. Distinction between lineage and potential of NSCs

Lineage is what a single cell does *in vivo*; potential is what a single cell can do when exposed to a different environment either by transplantation or in culture. SVZ, subventricular zone; GM, gray matter of cerebral cortex Image modified from (Götz et al., 2015)

2.3 Neural progenitor cells (NPCs): *in vitro* and *in vivo* studies

Usually, two criteria are applied to define a stem cell: self-renewal, ideally for an unlimited number of cell divisions, and multipotency, that is, the ability to give rise to numerous types of differentiated cell. For instance, NSCs are self-renewing, but not necessarily for an unlimited number of cell divisions. Initially, the self-renewal occurs by symmetrical cell divisions, which generate two daughter cells with the same fate; then they undergo asymmetric cell divisions in which one of the daughter cells remains a proliferating progenitor and the other one undergoes differentiation. Over time, NSCs can produce various neuron types (Wang et al., 2014) essential for circuit formation by changing their competence (Gao et al., 2014). Once NSCs have completed their set of neurogenic divisions, they typically undergo apoptosis or terminal division, or enter senescence and decrease proliferation. For this reason, the number of NSCs is low in post-embryonic animals, with only a few stem cells remaining in the adult brain (Ming and Song, 2011). Notably during development, before neurogenesis, the neural plate and neural tube are composed of a single layer of cells neuroepithelial (NE) cells, which can be considered stem cells. They first undergo symmetric, proliferative divisions, each of which generates two daughter stem cells (McConnell, 1995). These divisions are followed by many asymmetric, self-renewing divisions, each of which generates a daughter stem cell plus a more differentiated cell such as a neural progenitor cell (NPCs) or a neuron (**Errore. L'origine riferimento non è stata trovata.**).

Among NSCs, radial glial (RG) cells represent more fate-restricted progenitors than NE cells (Malatesta et al., 2000) so, as a consequence, most of the neurons in the brain derived, either directly or indirectly, from RG cells (Anthony et al., 2004). In fact, NSCs typically undergo symmetric, differentiating divisions, each of which generates two neurons — terminally differentiated, postmitotic cells. These types of division were first deduced from retroviral cell-lineage-tracing experiments (Luskin et al., 1988) and were subsequently shown directly in live time-lapse observations with brain slices (Chenn and McConnell, 1995) and isolated cells *in vitro* (Qian et al., 2000). Besides RG cells, another type of NSCs is the so-called basal progenitor (BP) (Noctor et al., 2004). BP originate from the mitosis of NE and RG cells at the apical surface of the basal side of the ventricular zone (Haubensak et al., 2004). They have been found to contribute to neurogenesis by undergoing symmetric cell divisions that generate two neuronal daughter cells. Therefore, BP might function to increase the number of neurons that are generated

from a given number of NSCs by allowing the occurrence of a further round of cell division. This concept is also supported by the correlation between the increasing in size of the subventricular zone and the number of neurons in the cerebral cortex during phylogeny (Smart et al., 2002).

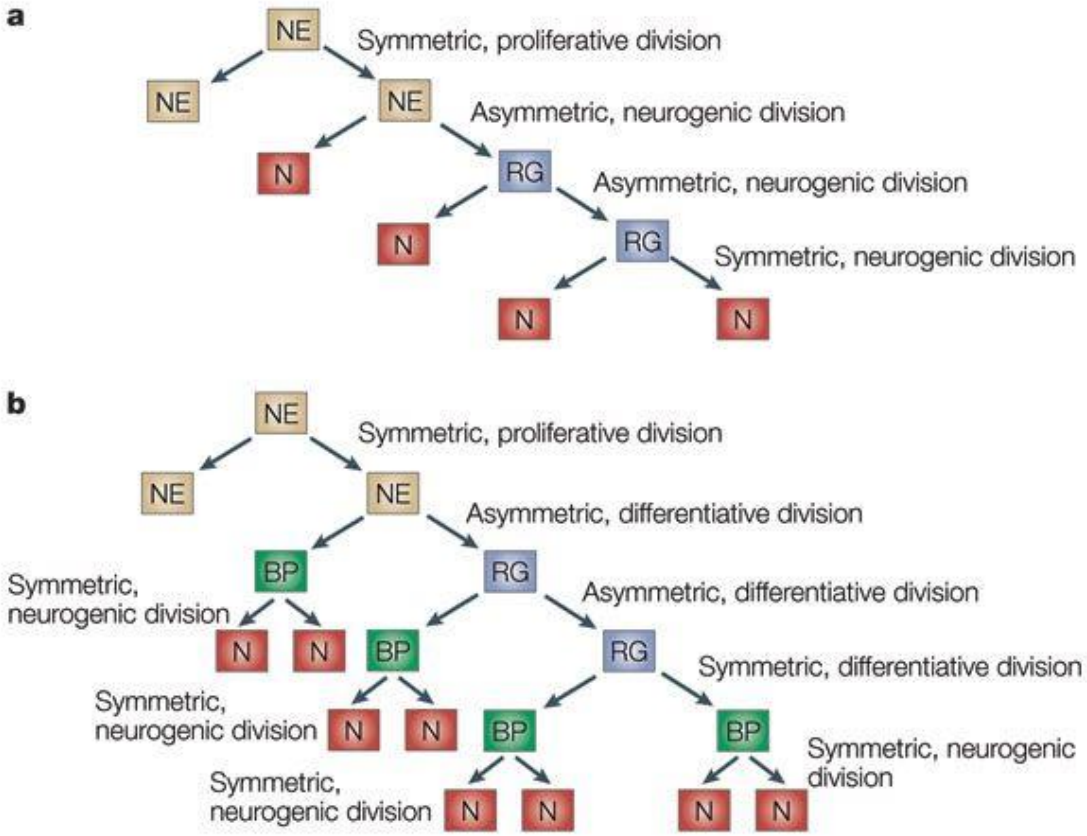

Figure 4. Lineage trees of neurogenesis

The lineage trees shown provide a simplified view of the relationship between neuroepithelial cells (NE), radial glial cells (RG) and neurons (N), within (**a**) and in (**b**) basal progenitors (BP) as cellular intermediates in the generation of neurons. They also show the types of cell division involved. Image modified from (Götz and Huttner, 2005).

Many studies provide evidence for the competence of grafted NS-NPCs to survive, migrate, and differentiate both *in vitro* and *in vivo* systems (Widera, 2004; Wu et al., 2012). Trials have been performed with NSCs obtained from different brain regions to better fit the injured area, knowing that local environments have a fundamental impact to regulate the fate choice of adult stem cells (Björklund and Lindvall, 2000). For example, in case of peripheral nerve injury (PNI), embryonic spinal cord neurons are best fitted as graft. In fact, these cells demonstrated, after transplantation into the injured distal nerve stump, the ability to sprout axons and reinnervate the target muscles tested (Zhang et al.,

2017). However it has been observed also that NSCs derived from adult hippocampus or spinal cord gave rise to neurons after grafting to the dentate gyrus, but not in the spinal cord (Shihabuddin et al., 2000). Anyway, it has been observed that after induction of hippocampal injury, grafted hippocampal NPCs migrated to the damaged area of the hippocampus *in vitro* and *in vivo*. Once they reached their destination, transplanted cells subsequently developed into functional neurons that keep integrating into the organotypic hippocampal network for at least 4 weeks after transplantation (Hofer et al., 2012). Hippocampal NPCs demonstrated, at 21 days *in vitro*, to express neurotransmitters, neurotransmitter receptors, and synaptic proteins consistent with those expressed in the mature hippocampus, but this was observed only in cultures grown in the presence of fibroblast growth factor 2 and brain-derived neurotrophic factor (Mistry et al., 2002).

Electrophysiology is a powerful tool to assess grafted cells phenotype and synptic integration (Hofer et al., 2012; Zhang et al., 2017). Indeed, by using electrophysiology it is possible to study synapses formation directly *in vivo* as reported from Tornero et al. (2017). These auhtors demonstrated, for the first time, that intracortical grafts of adult human iPSC-derived cortically fated neurons, receive direct synaptic inputs from stroke-injured brain tissue, and that these afferents are functional (Tornero et al., 2017). Studies *in vitro* combining MEAs and patch clamp technique (Stephens et al., 2012) investigated NPCs capability to generate neural networks - already documented in different conditions (Ban et al., 2006; Heikkilä et al., 2009) - and also to stimulate plasticity among silenced networks, such as those found in the stroke. MEAs offer long-term, label-free, and large-scale neuronal recording capabilities in entire networks therefore, the recent opportunities emerging from advances in cellular reprogramming techniques are strongly motivating the adoption of MEAs for readouts on cultures of human iPS-derived neurons (Malerba et al., 2018). There are many different examples of *in vivo* system where NPCs from primary CNS tissue and from cell cultures have been shown to integrate and differentiate after transplantation into developing brain (Fricker et al., 1999).

As stated before, ES-like cell lines features as donor cells (Ruschenschmidt et al., 2005) but local cellular environments are very important in controlling neurogenesis and, to note, adult NPCs grown in an environment nonpermissive for neurogenesis were unable to respond to excitation (Deisseroth et al., 2004).

Astrocytes surrounding neurons modulate the delivery of neurotransmitters, such as excitatory neurotransmitter glutamate (Hu et al., 2015). Indeed, glutamate transporter-1(GLT-1) in astrocytes clears 90 % of glutamate spilled over the synaptic cleft (Banasr

and Duman, 2007; Martinez-Lozada et al., 2016). It has been shown that downregulated expressed of GLT-1 in astrocytes in post-stroke depression (PSD) rat model is sufficient for inhibiting synaptic formation among NSC-derived neurons (Guo et al., 2013). This could also be related to the observed increased number of NSC-derived astrocyte *in vitro* when co-cultures with astrocytes (Yu et al., 2018). The increase in the proportion of NSC-derived astrocytes may be attributed to a compensatory mechanism to control ambient glutamate excess, but the mechanism(s) potentially inducing higher NSCs differentiation into neurons are unknown. Another study examined the regulation of adult-derived stem cells by different cell types, that may exist in the niche of proliferative cells in adult brains, and demonstrated that astrocytes from postnatal hippocampus can actively regulate neurogenesis from adult neural stem cells (Song et al., 2002).

2.4 *In vitro* co-cultures

Co-culture is a cell cultivation set-up, in which two or more different cells populations are grown with a variable degree of contact between them. Co-culture systems have long been used to study the interactions between cell populations and to gain more details incell–cell interaction features. Therefore, such systems have become of interest to synthetic biologists for studying and engineering complex multicellular systems (Goers et al., 2014). The are several motivations for using such a set-up that include: (1) studying natural interactions between different populations e.g. infection studies (Cottet et al., 2002) and other natural interactions (Tanouchi et al., 2012); (2) improving culturing success for certain populations to generate, for instance, experimental models and biomimetic environments of natural systems or artificial tissues (Moraes et al., 2012); (3) establishing interactions between populations (Figure 5). Mastering co-culture experiments allows the study of cell–cell interactions both natural and artificial at many levels and thus, the engineering of such new interactions. To reach high control over co-culture experiments we have to consider that such systems differ in many variables interlinked in their effects.

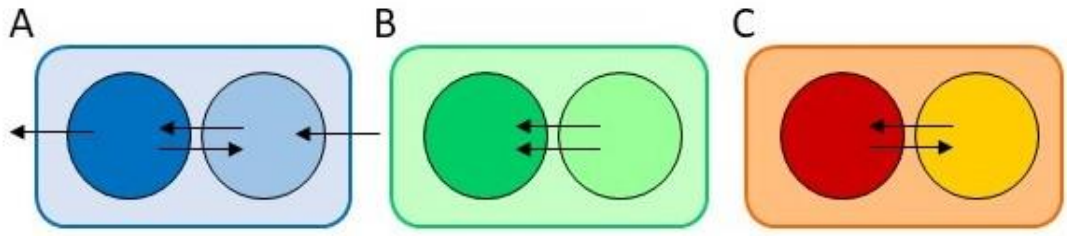

Figure 5. Schematic representation of different co-culture experiments

Studying natural interactions between populations (a). Improving cultivation success for a certain population (b). Establishing interactions between populations (c).

Co-cultures can differ in the number of distinct co-cultured populations, degree of similarity between populations or, covnersely, in the degree of separation between populations. Any information about the populations in a co-culture can potentially be used to control cell behavior even though studying interactions remains a major challenge and controlling them even more so.

A larger number of interacting populations increase the possibilities of complex reaction pathways -e.g. engineered microbial consortia useful for industrial applications (Brenner et al., 2008) - but also exponentialy complicates the experimental procedure. In fact, more than three interacting cell populations come along with an unmanageable level of complexity in terms of molecular interactions, leading to unpredictability and instability (Zeidan et al., 2010). To facilitate the study of system behavior, laboratory- based co-cultures usually involve only two populations. Generally, the aim is to characterize the activities and dynamics of each cell population in detail, as well as the interpopulation interactions. Both features are strongly affected also by the extracellular environment; hence growth medium composition obviously represents a fundamental factor to control the experimental set-up. Ultimately, the cellular phenotype emerging from the experiment is dependent upon the complex interactions between genotypes and environment. As stated at the beginning, depending on the experimental set-up and the different applications, there could be a variable degree of contact between the involved populations. Based on the idea that the systems should replicate the environment in which the co-culture will ultimately be used, the different cell populations can be in direct contact (if they are perfectly mixed, sometimes they are called mixed culture) or partially segregated. To establish valuable biomimetic *in vitro* models, especially in the case of mammalian tissue and other eukaryotic cell cultures, direct contact is required to preserve physiological behavior (Bidarra et al., 2011, Campbell et al., 2011). In such tuned

systems, also culture volume and cell density are very important factors to be considered. In a representative study investigating the embryonic developmental processes segregation and pattern formation, cell number in the co-culture was chosen to be comparable in size to an embryo, so that it was relevant to the natural biological system (Méhes et al., 2012). Studying natural cell–cell interactions will highlight new pathways for re-engineering cell populations and organisms but before these systems can be used in industrial, environmental or medical contexts, they must undergo rigorous testing for function and safety, especially in terms of process optimization.

Many works already cited in the previous chapter (2.3) took advantage of the co-culture system to simulate transplantation of exogenous NSCs (Deisseroth et al., 2004) or to evaluate different cells impact on NPCs differentaition (Song et al., 2002). The more common studies are based on the idea of exogenous cells, therefore it has been investigated the destiny of NSC-PCs added to bain slice cultures (Husseini et al., 2008) or lightly fixed dissociated cultures (Deisseroth et al., 2004). *In vitro* neuronal mixed cultures *per se* have not been investigated extensivel. Such an approach might be very usefull for the study of the diverse (synaptic) features otherwise hard to charachterize in more complex models.

2.5 Post-natal circuits

Hippocampal neurons culture

Conceivably one of the greatest appeals of *in vitro* neuronal cell culture is the wide experiemntal access to living neurons and synaptic networks provided by this model. In addition, low-density cultures are an ideal preparation for the investigation of many features because they are far less complex than neural tissue. It is preferable for neuroscientists to work with primary cultures instead of continuous (clonal) cell lines, because in such cell types the synapsys functionality is harder and slower to obtain (Xie et al., 2018). Primary CNS cell cultures are prepared from brain or spinal cord regions. However, hippocampal cultures benefit of a widespread popularity for many reasons, first for their relatively simplicity in terms of cell population. Most of the total neuronal population is represented by pyramidal neurons in addition to a variety of interneurons, fewer and morphologically distinguishable as describe in Figure 6 (Benson et al., 1994). The possibility to have such functional neurons well distributed in the culture allows the

study of cellular, subcellular and synaptic phenomena with a degree of resolution previously difficult to address, such as the dynamics of network formation and maturation, the synapse physiology, channels and receptors homeostasis, in addition to developmental and pharmacological studies. Primary dissociated hippocampal cultures were first introduced in the late seventies thanks to the enzymatic dissociation of hippocampi obtained from embryonic rats and subsequent plating on poly-lysine-treated coverslips in an enriched medium (Banker and Cowan, 1977).

Nowadays the stages of hippocampal neuron development *in vitro* have been well-characterized and are very consistent among different laboratories. Finally, as hippocampal cultures have been investigated for over 20 years, there is already an extensive database that provides the benchmark for new experiments (Kaech and Banker, 2007). A major focus of experimentation using hippocampal cultures concerns the study of events like dendritic development and branching, synaptogenesis and synaptic plasticity. For such studies, most investigators use cultures between 2 and 4 weeks *in vitro*. At this stage, hippocampal cultures have formed a very dense network because the peak of dendritic growth and synapse formation occurs during the second and third weeks in culture.

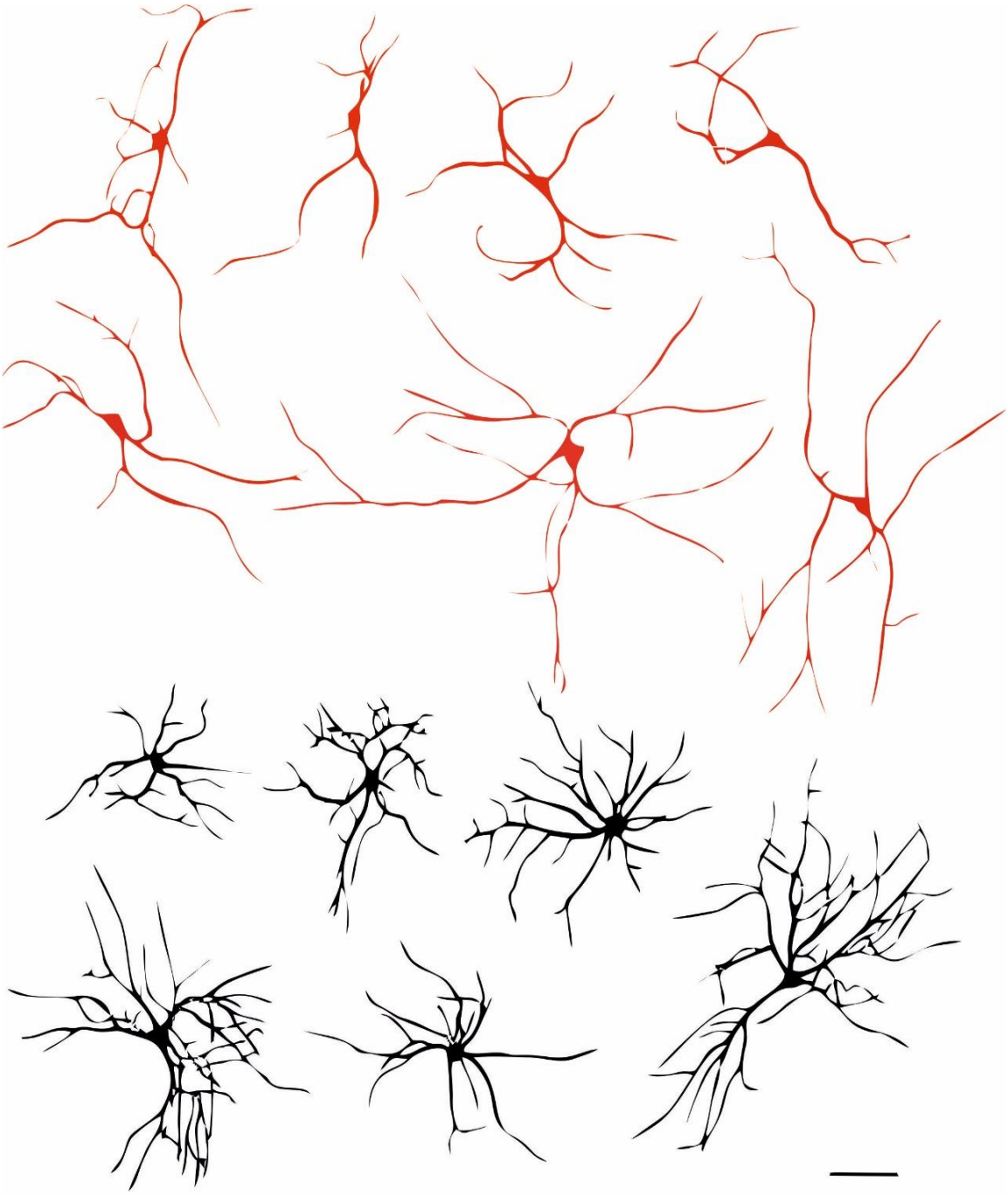

Figure 6. Main hippocampal cell populations

Drawings of MAP2-stained, GABA-immunopositive (red) and GABA-immunonegative (black) neurons. The GABAergic interneurons, shown in red, cover a wide spectrum of shapes but nevertheless resemble one another due to specific characteristics: the elongated dendritic arbors, the long dendritic segment lengths, and the relatively small number of primary dendritic branches. The non-GABAergic pyramidal cells shown in black have more radial dendritic arbors, shorter dendritic segment lengths and more consistently round cell somata. Scale bar = 100 µm. Image modified from (Benson et al., 1994).

Dopaminergic neurons culture

Midbrain dopaminergic neurons constitute the major source of dopamine in the mammalian CNS. The most prominent dopaminergic cell group resides in the ventral part of mesencephalon, which contains approximately 90 % of the total number of brain dopaminergic cells. The mesencephalic dopaminergic system has been subdivided into several nominal systems (**Figure 7**).

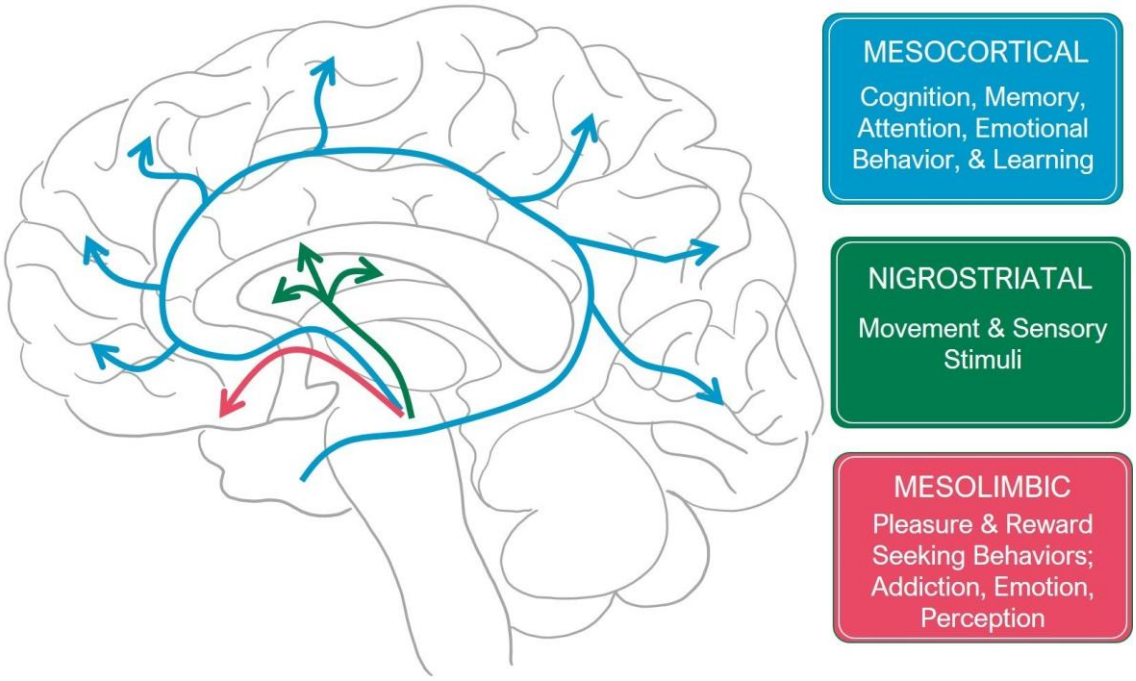

Figure 7. Three dopamine pathways and their related cognitive processes

Most of dopamine is generated deep in the midbrain, and it is released in many different areas across the brain. Image taken from http://sitn.hms.harvard.edu/flash/2018/dopamine-smartphones-battle-time.

Probably, the best known is the nigrostriatal system, which originates in the zona compacta of the substantia nigra (SNc) and extends its fibers into the dorsal striatum (**Errore. L'origine riferimento non è stata trovata.** green): the nigrostriatal pathway plays an essential role in voluntary motor movements control. The mesolimbic and mesocortical dopaminergic systems arise from dopaminergic cells present in the ventral tegmental area (VTA). The cells of the VTA project most prominently into the nucleus accumbens, olfactory tubercle but also innervate the septum, amygdala and hippocampus (**Figure 7** blue and pink); these dopaminergic systems are involved in emotion-based behavior including motivation and reward (Wise, 2004).

Considering the fact that dopaminergic system degradation is the basis of PD, the majority of the works present in literature about dopaminergic neurons is focused on the related disease. The first evidence of DA neurons in the SNc and VTA was given in the 70's (Aghajanian and Bunney, 1974), but only in the late 80's few studies started about the electrophysiological characterization of dissociated dopaminergic neurons obtained by rat midbrain (Grace and Onn, 1989). Anyway, the electrophysiological aspect of dissociated cells from SNc and VTA has been poorely considered, because the majority of works focalize on the molecular mechanisms underlying the loss in DA neurons, as main problem to overcome for PD recovery (Madrazo et al., 2019). In this frame, NS-NPCs gained a lot of attention thanks to the possiblity to guide their development toward the desired cell type i.e. dopaminergic in this case (Freed et al., 2001) as these cells also showed a good survival rate, up to 12 to 46 months after transplantation (Freed et al., 1992).

Anyway, as discussed above, the *in vitro* system, in its simplicity, represents an optimal way to investigate the basic aspects of cell to cell interactions. Therefore, with such system we could gain new insights about NPCs development among DA neurons and then, we could think about new and stronger strategies for PD neurons supply.

3 AIMS

Many questions still arise if we think to the exogenous transplantation as the most resolutive way to overcome brain damage. For instance, to which extent can the remaining brain parenchyma be as plastic to accommodate neurons in networks that suffered neuronal loss due to injury or neurological disease? Would the microenvironment be permissive for neuronal replacement and synaptic integration? Which cells can perform best? Can lost function be restored and how adequate is the new cells participation in the pre-existing circuitry?

The future in neuronal replacement therapy lies much in the field of neuronal circuits as a key to better understand neuronal networks and their functioning. As our understanding of neuronal circuits increases, neuronal replacement therapy should fulfill the lacking in network structure and function knowledge enough to incorporate neural circuitry research into regenerative medicine. This is a mandatory requisite to repair successfully brain injury. In this framework, electrophysiology appears to be the perfect techique to investigate neuronal circuits and accurately evaluate integration and synapse formation. By taking advantages of patch-clamp technique and hippocampal neurons dissociated cultures (a gold standard of *in vitro* neuronal cultures, very well characterized from an electrophysiological point of view), we investigated if and how fNPCs had the ability to synaptically interact with different neurons types when co-cultured and whether co-culturing affected the cell phenotype fate.

Several studies show that exogenous NSCs may develop into the correct neuronal cell type and eventually interact with the surrounding neurons after traspalntation, however a deep insights into the features of the synapses established between cells of different origin grown in close contact and wired together is lacking. We further investigated, considered the unexpected change in terms of morphology and development, type of synapses and neurotrasmitters adopted by fNPCs, the mechanistic factors that govern such changes, in particular those related to their functional integration in the postnatal cultured network. For instance, the intrinsic electrical component driven by mature neurons such as the auxiliary support activity completed by astrocytes have been considered fundamental aspect to investigate in the mixed cultures. Finally, we addressed newtork collective behaviour and fNPCs contibution in hippocampal mixed cultrues as well as the functional integration of fNPCs in SNc cultures. These results are included in this thesis as submitted

manuscript drafts. Additional work has been conducted in characterizing the integration rate due to conditioned media, the physiological membrane features of fNPCs in mixed cultures and the role of FOXg1 in neuronal development. Such collateral studies are reported separately in the Appendix.

4 PAPERS

4.1 Neuronal progenitor cell-identity specified by synaptic integration to postnatal hippocampal circuits in culture

Teresa Sorbo[1], Mattia Musto[1] and Laura Ballerini[1*]

1 International School for Advanced Studies, SISSA via Bonomea 265 34136 Trieste, Italy

* Corresponding author: Laura Ballerini, laura.ballerini@sissa.it

Abstract

During development, fetal neuronal progenitors (fNPCs) play an essential role in the construction of central nervous system (CNS) functional circuits. In this process, cell diversification and neuronal subtypes ability to form specific synaptic connections are crucial steps. Here we investigated by immunofluorescence and confocal microscopy a mixed culture system where rat fNPCs, labeled by enhanced green fluorescent protein (eGFP), differentiation is guided by postnatal hippocampal circuits reconstruction in vitro. Integrating fNPCs into active synaptic networks favored their development into glutamatergic phenotype and fNPCs synaptic contribution to the emergent activity was investigated by single and paired patch clamp recordings. We further examined the main players responsible for fNPCs identity specification, including network synaptic activity triggered by firing of action potentials and postnatal neuroglia microvesicles (MVs) release, a vectorized system able to transfer signaling molecules from neuroglia to neurons. We hypothesized that both signaling pathways influenced fNPCs destiny.

Introduction

Tissue-resident stem cells and primitive progenitors crucially contribute to the homeostasis of the CNS (Xu et al., 2017) and represent a very attractive source of cells in regenerative medicine since they can be potentially isolated from patients and transplanted autologously. Despite its promises, regenerative medicine translation in clinical practice is still in its debut and a great amount of experimentation and optimization is needed to refine all the conditions for ad hoc derivation of different cell lineages. Several investigations provided evidence for the competence of grafted neural stem cells (NSCs) to survive, migrate, and differentiate both in vitro and in vivo systems (Widera et al., 2007; Wu et al., 2012; Yin et al., 2019). There are several different

examples of in vivo systems where NSCs or neural progenitor cells (NPCs) from primary CNS tissue and from cell cultures have been shown to integrate and differentiate after transplantation into the developing brain (Fricker et al., 1999), or, more recently, into diseased brain (Upadhya et al., 2019; Yin et al., 2019). Therefore, NSCs and NPCs-like lines have the potential to feature as donor cells (Ruschenschmidt et al., 2005) and their controlled manipulation might have enormous impact in future developments of regenerative medicine. Among the factors that influence progenitors destiny, the local micro-environment was found crucial in controlling grafted-NPCs diversification into different cell identities (Deisseroth et al., 2004). We focused on fNPCs, a more committed subpopulation of NSCs, which are mostly cultured in vitro as neurospheres, given their ability to proliferate and differentiate in all brain cell phenotypes (Gao et al., 2014). We specifically investigate fNPCs, expressing green fluorescent protein (eGFP), differentiation and functional, synaptic, integration when grafted for > 2 weeks into cultured hippocampal networks. We exploited a cultured system to assess the fNPCs identity when cultured alone or when co-cultured into postnatal hippocampal networks. By single cell or paired electrophysiology recordings we further investigated the formation and nature of synapses to and from fNPCs, in particular we measured monosynaptic contacts with neighbor hippocampal neurons or fNPCs and we assessed the impact of fNPCs on the emerging network activity, measured as basal, spontaneous synaptic activity. We further dissected the influence of firing activity and of neuroglia MVs release on fNPCs differentiation.

Results

To investigate the formation and neurotransmitter identity of synaptic networks developed by fNPCs when cultured alone or when co-cultured with postnatal primary hippocampal neurons, and to gain insights into fNPCs neuronal identity and ability to synaptically integrate to postnatal circuits, we compared three cultured systems: hippocampal, fNPCs and mixed cultures, where fNPCs and primary hippocampal cells were seeded in 1:1 ratio (sketched in Figure 1B; see methods). To identify fNPCs, we used green fluorescent protein-labeled (eGFP; see methods) fNPCs, such cells have been shown to proliferate as neurospheres in the presence of growth factors (such as EGF and FGF; Supplementary Figure S1; see methods), and retained their proliferation ability for 7 days after plating, as confirmed by BrdU labeling experiments (not shown).

We quantified the network size and the ratio between neuronal and glial cells after 15–17 days in vitro (DIV), using immunofluorescence markers of cytoskeletal components specific for neurons (class III β-tubulin) or astrocytes (glial fibrillary acidic protein, GFAP) in all culture groups (coverslips n = 10; n = 9 and n = 10 from ≥ 3 hippocampal, fNPCs and mixed culture series, respectively). In Figure 1A, representative fluorescence micrographs show the presence of β–tubulin- and GFAP-positive cells in all culture groups, conversely eGFP- positive cell were detected, as expected, only in fNPCs and in mixed cultures, and were double stained for β–tubulin or GFAP in both conditions, with a minority (< 16 % in both fNPCs and mixed cultures) of cells positive only to eGFP. When comparing the total cell density (bar plot in Figure 1C), in mixed cultures we measured increased values (350 ± 10 cells/mm^2, 453 ± 33 cells/mm^2, 530 ± 36 cells/mm^2, hippocampal, fNPCs and mixed respectively; $P < 0.001$). However, in all culture groups the neuron/glial cell ratio (expressed in %) remained unaltered (32 % in mixed cultures; 33 % in hippocampal; 27 % in fNPCs). In Figure 1D, bar plots quantify double positive neurons for β–tubulin and eGFP, to estimate the amount of fNPCs neurons positive for eGFP in cultures. Apparently, fNPCs differentiated into neurons when cultured alone in standard culturing medium conditions (see methods) and were detected as eGFP double positive cells in 56 % of cases (69 ± 7 cells/mm2 in fNPCs alone), thus we cannot exclude, also in mixed cultures, the presence of fNPCs neurons which are not identifiable by eGFP positivity. Regardless eGFP-positive ones, β–tubulin-positive neuron density values were significantly higher in mixed cultures (167 ± 20 cells/mm^2) when compared to hippocampal and fNPCs ones (116 ± 7 cells/mm^2 and 123 ± 13 cells/mm^2, respectively; Bar plots in Figure 1D). These findings suggested that standard culturing conditions supports fNPCs proliferation as well as neuronal and glial differentiation. It is tempting to speculate that in mixed cultures the larger number of neurons detected be due to fNPCs residual proliferation.

In culture, neurons mature and develop functional synapses and display spontaneous collective electrical activity as a result of recurrent connections. To investigate cells membrane passive properties and synaptic activity, we used whole-cell patch-clamp technique. fNPCs and hippocampal neurons, after 15-17 days of in vitro growth were compared to aged matched mixed cultures (H_{mixed} and $fNPCs_{mixed}$). Hippocampal neurons when cultured alone (116.6 ± 38.7 pF and 203.9 ± 169.5 MΩ) or in H_{mixed} (105.2 ± 40.9 pF and 252.6 ± 236.7 MΩ) displayed similar values of passive membrane properties.

Interestingly, fNPCs (n = 112) displayed significant lower cell capacitance and higher input resistance (64.8 ± 19.5 pF and 446.9 ± 324.4 MΩ; see plot in Figure 2A) when compared to $fNPCs_{mixed}$ (96.4 ± 36.7 pF and 331.9 ± 258.3 MΩ respectively, n = 128), a result potentially indicative of an improved cell maturation (le Magueresse et al., 2011) when fNPCs are co-cultured with postnatal neurons. Resting membrane potential values (Figure 2B) are little or even not affected by the various culturing conditions, in particular $fNPCs_{mixed}$ value is – 60.5 ± 13.9 mV against the fNPCs alone one of – 60.2 ± 15.5 mV.

In all culture groups we monitored the occurrence of spontaneous, basal, postsynaptic currents (PSCs) as a clear evidence of functional synapse formation and as an index of network efficacy (representative traces in Figure 2C, in black hippocampal and H_{mixed} and in green fNPCs and $fNPCs_{mixed}$, respectively). Spontaneous synaptic activity in our recording conditions was manifested by inward currents made up by a mixed population of inhibitory (GABAA-receptor mediated) and excitatory (glutamate AMPA-receptor mediated) PSCs, typically characterized by different kinetic properties (Cellot et al., 2011).

PSCs recorded from hippocampal neurons (n = 152) were represented by inward currents of variable amplitude (representative traces are shown in black in Figure 2C, top) occurring at a frequency of 5.2 ± 4.4 Hz (Figure 2D). PSCs in fNPCs displayed a significant lower frequency (0.5 ± 0.5 Hz) when compared to hippocampal neurons (representative traces are shown in green in Figure 2C, note the different scale). Accordingly, fNPCs displayed also significant differences in the average amplitude values of the recorded PSCs (Figure 2E). To gain more insights on the synaptic identity in the neural network, we performed offline differential analysis of PSCs kinetic (see methods), in particular we measured the PSC decay (Lovat et al., 2005). Based on their kinetic, we identified slow decaying (τ = 25.2 ± 1.2 ms) PSCs presumably GABAA-receptor mediated events (Banks and Pearce, 2000) and fast decaying (τ = 5.1 ± 0.2 ms) events usually corresponding to AMPA-receptor mediated currents (Angulo et al., 1999). In hippocampal neurons fast events were the large majority of detected PSCs (~ 73 %); conversely, in fNPCs, slow events were more expresses (~ 58%).

H_{mixed} neurons (n = 111) retained the same characteristics of cells recorded in the hippocampal cultures described above (Figure 2C left panel, bottom recording in black). Interestingly, $fNPCs_{mixed}$ (eGFP-positive; n = 117; Figure 2C, right panel bottom recording in green) showed a strong increase in PSCs frequency (3.8 ± 3.2 Hz; Figure 2C and box plot in 2D) and amplitude (from 23.5 ± 19.6 pA in fNPCs to 41 ± 20.9 pA in

$fNPCs_{mixed}$; box plot in Figure 2E). In addition, $fNPCs_{mixed}$ showed now a majority (~ 68 %) of fast events.

These results indicated the occurrence of clear changes in fNPCs activity once integrated to the hippocampal network, leaving H_{mixed} unchanged, in particular the slow synaptic component seems downregulated. We pharmacologically addressed the contribution of $GABA_A$-receptor mediated transmission to network activity in all culture groups by administration of the specific $GABA_A$-receptor antagonist bicuculline (10 µM; n = 25 hippocampal neurons, n = 24 fNPCs, n = 19 H_{mixed}, n = 13 $fNPCs_{mixed}$) to weaken synaptic inhibition. As previously reported (Eisenman et al., 2015), the weakening of inhibition in hippocampal networks induced a switch from random activity to patterns of bursting and synchrony, leading to the appearance of slow-paced bursting in hippocampal, H_{mixed} and $fNPCs_{mixed}$ (representative traces and box plots summarizing bursts inter event interval and duration values in Figure 3A). On the contrary, in fNPCs, bicuculline virtually removed all PSCs and no patterned activity appeared (Figure 3A). The crucial role of GABAergic synapses in driving network activity in fNPCs suggested a prevalence of inhibitory neurons when fNPCs differentiate in standard medium alone.

This suggestion was strengthened by immunofluorescence experiments quantifying in all culture groups double positive cells for β-tubulin and GABA (representative images in Figure 3B). In accordance with the electrophysiological results, we detected a different distribution of GABAergic neurons (summarized in the bar plot of Figure 3B): 35 ± 3 double-positive cells/mm2 in hippocampal cultures (31% of total β-tubulin positive, n = 9 samples); 88 ± 8 double-positive cells/mm2 in fNPCs (68% of total β-tubulin positive, n = 12 samples) and in mixed culture (42% of total β-tubulin positive, n = 11 samples) the value is 58 ± 6 cells/mm2. To estimate $fNPCs_{mixed}$ differentiation into GABAergic neurons we further extrapolated the density of triple β-tubulin-GABA-eGFP-positive cells in co-culture (25 ± 2 cells/mm2 on a total of 50 ± 5 cells/mm2 β-tubulin III-eGFP positive ones). Thus, based on eGFP-positive cells, the amount of $fNPCs_{mixed}$ that differentiate into GABAergic neurons is reduced to 50 % and contributes to 70 % of GABAergic double positive cells in mixed cultures.

Thus far, although the previous results suggested a switch in identity in $fNPCs_{mixed}$ differentiated neurons, with a lower expression of GABAergic ones compared to fNPCs alone, it is hard to translate this information into $fNPCs_{mixed}$ integration and contribution to the hippocampal synaptic networks. Ultimately, are $fNPCs_{mixed}$ differentiating into glutamatergic neurons and contribute to glutamate-mediated synaptic transmission?

In the next set of experiments, we simultaneously patched clamped pairs of mono-synaptically coupled neurons in all three culture groups (sketched in Figure 4A). Paired recordings allow a detailed examination of the evoked transmissions of isolated synaptically coupled neurons of a known type (hippocampal, fNPCs, H_{mixed} and $fNPCs_{mixed}$). Action potentials (APs) were evoked in the presynaptic cell and the probability of finding mono-synaptically connected neurons in fNPCs cultures (n = 50 pairs) was very high (82 %) when compared to hippocampal neurons (51%, n = 59 pairs); a high probability of coupling was detected in mixed pairs (30 % H_{mixed} to $fNPCs_{mixed}$ and 32 % in vice versa pairs; n = 47 pairs) as depicted by the histograms in Figure 4B. Unitary post synaptic currents (uPSCs), were evoked in all pairs with a delay of 2.6 ± 0.25 ms, and were identified based on their decay time constant (representative traces are showed in Figure 4C). fNPCs pairs displayed 100 % of slow (τ = 25.3 ± 1.3 ms), probably GABAergic, uPSCs; this percentage was reduced to 68 % in hippocampal pairs, where 32 % of uPSCs displayed fast (τ = 4.8 ± 0.5 ms) decay, presumably representing glutamatergic connections. Mixed pairs have been evaluated in both directions: by having the $fNPCs_{mixed}$ firing on the H_{mixed} and vice versa, and behaved symmetrically, with 80 % of slow responses and 20 % of fast (τ = 4.7 ± 0.6 ms), probably glutamate mediated uPSCs (plot in Figure 4D).
These results suggested that when grafted to hippocampal postanal networks, fNPCs differentiated into neurons that belongs to both GABA and glutamate phenotypes, synaptically targeting both $fNPCs_{mixed}$ and H_{mixed} neurons.

We further explored which signaling might have instructed the different destiny of $fNPCs_{mixed}$, in particular whether the ongoing firing and synaptic activity of the network could influence fNPCs differentiation. We thus developed mixed cultures in the presence 1 µM tetrodotoxin (TTX), a Na+ voltage-gated channels blocker. 24 hours prior to recordings, fresh medium was replaced. fNPCsmixed treated with TTX showed significative differences in terms of cell capacitance, input resistance and PSCs frequency when compared to $fNPCs_{mixed}$ sister cultures developed without TTX (Figure 5A). $fNPCs_{mixed}$ capacitance was reduced in TTX (from 93.8 ± 24.7 pF to 70.6 ± 18.4 pF) with an increased input resistance (from 250.4 ± 128.1 MΩ to 453.7 ± 371.8 MΩ). In $fNPCs_{mixed}$ TTX treated, PSCs frequency was reduced from 5.7 ± 4 Hz to 2.7 ± 3.3 Hz (boxplot in Figure 5B and representative traces in Figure 5C). These results indicated that ongoing network activity might influence $fNPCs_{mixed}$ differentiation and identity,

however fNPCs alone are still displaying an apparently more immature electrophysiological phenotype. Since the cultured system contains also postnatal GFAP-positive astrocytes we wondered whether signals generated by these cells could influence fNPCs differentiation.

Brain intercellular communication comprise the shedding of microvesicles (MVs) from neuroglia (Raposo and Stoorvogel, 2013), a physiological form of cross talk between astrocytes and neurons. Extracellular vesicle signaling molecules, either stored within their cargo or embedded in their plasma membrane, modulate relevant processes in the development of CNS target cells (Théry et al., 2002). MVs are nanovesicles able to interact specifically with cells at local or distant sites and thus considered as a "vectorized" signaling system able to bind their target cells to transmit specific information.

We isolated MVs from mature cortical glia cultures (see methods). MVs presence was assessed by immunoblot analysis for the biomarker flotillin-1 (Rauti et al., 2016) of the supernatant collected from glial cultures, showing, as expected, the appearance of a thick band corresponding to flotillin-1 (Figure 6A), a signature of MVs release by neuroglia. Atomic force microscopy (AFM; Rauti et al., 2016) topographic reconstruction of re-suspended MVs pellet (Figure 6B) confirmed the presence of MVs detected by the immunoblot.

We thus compared fNPCs neurons treated with MVs (n = 92; see methods) with control fNPCs neurons (n = 55). Electrophysiological recordings showed a significative increase in PSCs frequency in MVs treated fNPCs (1.2 ± 1.2 Hz versus 0.5 ± 0.4 Hz) (Figure 6C, MVs treated fNPCs in magenta, control fNPCs in green). Interestingly, weakening of inhibition by bicuculline induced in MVs treated fNPCs the appearance of slow-paced bursting (2 cells out of 5 showed inter-burts-interval of 34.6 ± 5.6), reminiscent of that observed in $fNPCs_{mixed}$, while, as expected, almost blocked PSCs occurrence in fNPCs (Figure 6D).

As depicted in Figure 6F, double-positive neurons for β-tubulin and GABA were reduced in fNPCs from 76 ± 7 cells/mm^2 to 52 ± 4 cells/mm^2 when treated by MVs. This reduction in fNPCs differentiated GABAergic phenotype is reminiscent of that detected in $fNPCs_{mixed}$ and might contribute to the changes in network activity. This hypothesis is further supported by pair recordings, uPSCs recorded in pairs of fNPCs (n = 25) were 100 % represented by slow (τ 26.8 ± 2.2 ms) events, while in fNPCs treated by MVs pairs (n

= 42) 14 % of mono-synaptically connected neurons displayed fast decay (τ 5.1 ± 0.9 ms) uPSCs, suggestive of the appearance of glutamatergic synapses (Figure 6E).

Discussion

The main result of the current work is the reported ability of fNPCs to differentiate into neurons and to construct an active synaptic network when developed in standard medium. Notably, the development of mixed synaptic networks with post-mitotic hippocampal neurons tuned the fNPCs neuronal phenotype and their synapse specification, leading to the appearance of glutamatergic synapses and reducing the amounts of GABAergic cells derived from fNPCs.

We characterized fNPCs neurons based on their eGFP expression, however a percentage of fNPCs neurons were not eGFP positive, thus, in mixed cultures, we might have underestimated the amount of fNPCs and also the amount of fNPCs positive for GABA; however the presence of eGFP positive non GABAergic cells supports the different fNPCs destiny in mixed cultures, a result further strengthen by pair recordings (see below). Regarding the single cell patch clamp characterization, recordings form eGFP positive cells represented with no doubts fNPCs neurons in mixed cultures, but we cannot exclude that a small amount of hippocampal cells (i.e. eGFP negative) might have been indeed progenitors, we used the differences in passive membrane properties to functional isolate hippocampal neurons from fNPCs ones, thus reducing the potential sampling in this group of neurons belonging to the fNPCs population.

The electrophysiological properties of fNPCs maintained in cultures have been previously reported, although in diverse culturing conditions (Antonov et al., 2019; Heikkilä et al., 2009; Muth-Köhne et al., 2010). More recently, the synaptic integration of progenitor cells into postnatal networks has been increasingly investigated (Miskinyte et al., 2017), however e detailed analysis of unitary synaptic connections has, to our knowledge, not been described yet.

By pair recordings of mono-synaptically connected neurons we explored the role and contribution of fNPCs to the hippocampal synaptic network, and we assessed the presence of neurotransmission mediated by fast unitary synaptic events to and from fNPCs, which were never detected in fNPCs when cultured alone. Fast uPSCs were not pharmacologically or electrophysiologically characterized in the current work, however in the very same culture system (hippocampus) we have repeatedly reported the glutamate

AMPA-receptor mediated nature of such events (Cellot et al., 2011; Pampaloni et al., 2018; Rauti et al., 2019).

These changes in fNPCs destiny once grafted in postnatal neuronal networks is intriguing, since appropriate CNS circuit function requires balanced excitatory and inhibitory neurotransmission (Yizhar et al., 2011). The evidence that fNPCs-derived neurons were homeostatically integrated into the host synaptic network contributing by GABAergic and glutamatergic neurons to basal synaptic activity is relevant when targeting neuronal replacement in neuropathology approaches (Kopach et al., 2018).

Indeed, exploring the extent of afferent synaptic inputs to fNPCs-derived neurons originating from the host neurons and vice versa is a relevant issue and is increasingly explored by different experimental settings in vitro and in vivo, measuring the host-to-graft synaptogenesis (Avaliani et al., 2014; Miskinyte et al., 2017) as well as elucidating factors which control the neural conversion of grafted cells (Kopach et al., 2018). In this regard, our results indicate that spontaneous synaptic activity driven by APs generation contributes to fNPCs differentiation in mixed cultures, as in part expected (Lepski et al., 2013). More relevant is the role we suggested for glial derived MVs. This vectorized system of extracellular signaling may be significant during CNS development (Marzesco et al., 2005). MVs have been shown to tune synaptic activity via various transported molecules and signaling pathways as well as enabling the proliferation rate of stem cells (Feliciano et al., 2014). In particular, astrocyte-derived vesicles could variously affect immature neurons and mediate neuronal differentiation (Wang et al., 2011). We thus exploited the MVs cargoes obtained from pure glial cultures, as confirmed by western blot and AFM analysis (Rauti et al 2016), and we show how long-term fNPCs exposure to these vectors, tuned the differentiation of fNPCs neurons, providing synaptic networks reminiscent of those detected in mixed cultures.

In conclusion, our results convincingly indicate that fNPCs develop into a more mature electrical phenotype in presence of post-mitotic neurons. This appears to be the first work with a pure in vitro co-culture system to study electrophysiology, thus it could be a fundamental tool towards the understanding of fNPCs electrophysiological characteristics in the frame of neuronal replacement therapy in vivo.

Materials and Methods

Ethical statement

All animal procedures were conducted in accordance with the National Institutes of Health and with international and institutional standards for the care and use of animals in research, and after consulting with a veterinarian. All experiments were performed in accordance with European Union (EU) guidelines (2010/63/UE) and Italian law (decree 26/14) and were approved by the local authority veterinary service and by our institutional (SISSA-ISAS) ethical committee. All efforts to minimize animal suffering and to reduce the number of animals used were made. Animal use was approved by the Italian Ministry of Health, in agreement with the EU Recommendation 2007/526/CE(http://eur-lex.europa.eu/legal-content/EN/TXT/?uri=uriserv:OJ.L_.2007.197.01.0001.01.ENG&toc=OJ:L:2007:197:TOC).

Cell cultures

Hippocampal neurons

Primary cultures of hippocampal neurons were obtained from P3 rat pups (Wistar) by slightly modifying previously reported protocol (Cellot et al., 2011). Briefly, hippocampi were isolated and dissociated by following a three steps enzimatic procedure: (1) dissected hippocampi were first digested in the presence of trypsin (Sigma-Aldrich T1005) and deoxyribonuclease (DNAse - Sigma-Aldrich D5025-150KU) for 5 minutes at 37 °C and (2) then treated with trypsin inhibitor (Sigma-Aldrich T9003) for 10 minutes at 4 °C; (3) final mechanical dissociation was performed in presence of DNAse. Cells were filtered (0.70 µm), centrifuged (100 g for 5 m) and resuspended in culture medium. Culture medium was composed of Neurobasal™-A Medium (Gibco™ 10888022), 2 % B-27™ Supplement (Gibco™ 17504044), 1 % GlutaMAX™ Supplement (Gibco® 35050061) and 0.05 % gentamicin (50mg/mL) (Gibco® 15710-049). Samples were prepared by plating cells on poly-L-ornithine-coated (Sigma Aldrich P4957, 0.01 % solution) rectangular glass coverslips (Kindler, 12 x 24 mm, 0.17 mm thickness) at a density of 60000 cells/200 µL and incubated at 37 °C, 5% CO2 for 15-17 DIV.

Fetal neural progenitor cells (fNPCs)

fNPCs were isolated from E15 rat embryos (Wistar), by adding to the protocol reported by Aurand et al., 2014 the three enzymatic steps procedure described for the hippocampal

neurons. To allow specific identification, right after enzymatical and mechanical dissociation, fNPCs were engineered by incubation with lentiviral vectors encoding the enhanced green fluorescent protein (eGFP) under constitutive promoters (pGK). Before plating, fNPCs were kept in suspension as neurospheres for 2 days to allow proliferation (Supplementary Figure 1). Standard serum-free proliferation medium was composed of 3:1 Dulbecco's Modified Eagle's Medium (DMEM - Merck D5546): F-12 (Merck N4888), 1□ B-27™ Supplement, 2 mM L-glutamine (ThermoFisher 25060081), 100U/mL penicillin/streptomycin (ThermoFisher 15140122) plus the addition of 20 ng/mL basic fibroblast growth factor (bFGF) and epidermal growth factor (EGF). Before the plating, neurospheres were dissociated by using ACCUMAX (Sigma-Aldrich T7089) for 5 minutes at 37 °C, centrifuged (100 g for 5 m) and resuspended in culture medium. Samples were prepared by plating fNPCs at the same density and in the same culture medium described for the hippocampal neurons (see above).

Mixed cultures

Mixed cultures were obtained by incorporating dissociated fNPCs to primary hippocampal neurons in 1:1 ratio and plating the cells in the same conditions of controls. For experiments involving chronic treatment, mixed cultures were incubated at DIV 8 with a medium containing 1 µM tetrodotoxin (TTX – Latoxan L8503). At DIV 14 or 15 (after 6-7 d of incubation) medium was replaced with fresh one, without the blocker, 24 h prior to electrophysiological recordings. Control cultures were subjected to the same medium changes without TTX, following the procedure described by (Cellot et al., 2011).

Glial cultures

Primary brain glial cultures were obtained from P2−P3 rats (Wistar) cortices, as previously described (Calegari et al., 1999). Briefly, enzymatically dissociated cells were plated into plastic 150 cm2 flasks, incubated (37 °C; 5% CO2) and cultured for 21-25 DIV in culture medium consisting of DMEM (ThermoFisher 31966021), supplemented with 10% FBS (ThermoFisher 10500064), 100U/mL penicillin/streptomycin.

MVs isolation

DIV 21-25 glial cells were cultured in FBS-free glial medium for 24h before collecting MVs, in order to exclude any contribution of the MVs already present in the FBS. MVs were then isolated as already described (Rauti et al., 2016). Briefly, the 24h-conditioned

medium was collected and centrifuged at 300 x g for 15 minutes, in order to remove cell debris. The supernatant was then centrifuged at 20000 x g for 1 hour. The presence of MVs was confirmed with Western blot analysis for the MVs biomarker flotillin-1 (Al-Nedawi et al., 2009; Conde et al., 2005) and atomic force microscopy (AFM).

For the Western blot, as already described in Rauti et al., 2016, the pellet was resuspended in lysis buffer (50 mM Tris-HCl, pH 8.0, 150 mM NaCl, 1 % NP40, 0.1 % SDS), sonicated 3 × 10 s, and then boiled at 95 °C for 5 min. Samples were run on a 10 % polyacrylamide gel and were blotted onto nitrocellulose filters (Millipore, Italy). Filters were then blocked in PBS-Tween-20 (0.1 %) plus 5 % nonfat dry milk and incubated with the primary antibody antiflotillin-1 (BD Biosciences 610820dilution 1:1000) for 16 h at 4 °C. After three washes with PBS-Tween, filters were incubated with peroxidase-conjugated anti-mouse secondary antibody (dilution 1:1000). Immunolabeled ECL-exposed protein bands were visualized with UVI-1D software.

AFM measurements were performed as previously described (Rauti et al., 2016) . Briefly, the pellet of MVs was resuspended in PBS solution and a 15 μL drop of sample solution was placed and left to adsorb (30 min) onto a freshly peeled mica substrate. Vesicles were then fixed with 1% formaldehyde for 1 h (RT) in order to prevent their collapse during AFM acquisition. MVs were then washed with MilliQ and dried under a gentle stream of nitrogen. AFM analysis was performed in air at RT, using the semicontact mode of a commercial instrument (Solver Pro, NT-MDT, RU). Silicon tips (NSC36/CR-AU, MikroMash, USA) with a typical force constant of 0.6 nN/nm and a resonance frequency of about 65 kHz. Topographic height and phase images were recorded at 512 × 512 pixels at a scan rate of 0.5 Hz. Image processing was performed using Gwyddion freeware AFM analysis software, version 2.40.

The concentration of MVs delivered to NPCs has been quantified by nanoparticles tracking analysis (NTA) measurements, performed on a NanoSight LM10 system (Malvern) using approximately 500 μL of MVs, previously isolated from astrocytes FBS-free culture medium and diluited 1:10 in MilliQ H2O. Individual videos of 60 seconds for each sample were acquired using the maximum camera gain and analyzed by the NanoSight particle tracking software to calculate vesicle concentration.

fNPCs exposure to glia-derived MVs

The pellet obtained from differential centrifugations of astrocytes culture medium was resuspended in 300 μL of fresh fNPCs culture medium, with a concentration of

approximately 6.27 ± 108 vesicles/mL. A 100 µL volume was then added to each fNPCs culture at DIV 4, 8 and 12. Negative control experimental groups were treated at the same time intervals with the same volume of supernatant obtained from the second centrifugation and virtually depleted of MVs or with fresh fNPCs culture medium. Electrophysiological experiments were performed at DIV 15-17.

Electrophysiology

Patch-clamp, whole cell recordings were performed with glass micropipettes with a resistance of 5 to 8 MΩ. The intracellular pipette solution was composed as following (mM): 120 K gluconate, 20 KCl, 10 HEPES, 10 EGTA, 2 MgCl2, 2 Na2 ATP and 0.1 QX 314, pH 7.3. The external standard saline solution contained (mM): 150 NaCl, 4KCl, 1 MgCl2, 2 CaCl2, 10 HEPES, 10 glucose, pH 7.4. All recordings were performed at RT in continuous perfusion (2 mL/min). Cells were voltage clamped at a holding potential set at −56 mV (not corrected for the liquid junction potential, calculated to be 13.7 mV at 20 °C) and registered for spontaneous activity at least for 10 min. Recordings in mixed cultures were performed thanks to a simple HBO lamp that allowed to selectively choose eGFP+ cells in epifluorescence. Pharmacological experiments were performed by adding 10 µM Bicuculline (Sigma-Aldrich 14343) directly in the extracellular solution. After 5 min, spontaneous activity was recorder for 10 more min. Data were collected using a Multiclamp 700A Amplifier (Molecular Devices, US), and analyzed using either Clampfit 10.3 (Molecular Devices) or Axograph (Axograph Scientific). Glutamate AMPA-receptor and GABAA -receptor mediated post synaptic currents (PSCs) were isolated offline by building two templates with different kinetic parameters: 0.1 ms rise-time; 3 and 30 ms decay time constant (τ) respectively. Previous work (Pampaloni et al., 2018) indicates that in our experimental conditions, fast-decaying ($\tau < 5$ ms) PSCs are mediated by the glutamate AMPA-receptor type; while the slow-decaying ($\tau > 20$ ms) PSCs are mediated by the GABAA-receptor type. The two classes of PSCs were obtained from the average of ~ 300 events for every cell and organized in terms of amplitude, rise time and decay time.

Pair recordings were performed by patching two neurons simultaneously visualized in the same 40x field. The firing neuron, in current clamp mode, was hold at -70 mV and stimulated (2 nA; 5 ms) 15 times, with an interval of 1 s between every sweep. The response in the post-synaptic neuron was obtained by averaging the 15 evoked events, and evaluated in terms of delay, amplitude, decay time.

Immunofluorescence

Cultures were fixed in 4 % formaldehyde (prepared from fresh paraformaldehyde) in PBS for 20 min and 1 % glutaraldehyde for GABA staining as reported (Furlan et al., 2007), permeabilized in Triton X-100 and subsequently incubated with primary antibodies for 40 min at RT. To visualize a fourth channel, we did an intermediate step by using a donkey anti-mouse (SIGMA SAB3701110,1:300 dilution) or anti-rabbit (SIGMA SAB3700930, 1:300 dilution) biotinylated antibody. After washing in PBS, samples were finally incubated with secondary antibodies for 40 min. Cultures were then mounted with the Fluoromont (Sigma-Aldrich F4680) on 1 mm thick microscope glass slides. To visualize neurons and astrocytes we used the following: rabbit anti- β-tubulin III primary antibody (Sigma T2200, 1:500 dilution), mouse anti-GFAP primary antibody (Sigma G3893, 1:500 dilution). For GABA immunostaining we used: mouse anti- β-tubulin III (Sigma T8535, 1:500 dilution) and rabbit anti-GABA (Sigma SAB420721, 1:300 dilution). Secondary antibodies used were: Streptavidine 647 (Life technologies S21374, 1:300 dilution), Alexa 594 goat anti rabbit (Life technologies A11037, 1:500 dilution); Alexa 594 goat anti mouse (Life technologies A11032, 1:500 dilution) and DAPI to visualize nuclei (Invitrogen, 1:500 dilution). Finally, samples were mounted on 1 mm thick glass coverslips using Vectashield mounting medium (Vector Laboratories).

For the neurospheres experiments, the labeling was performed in suspension. Briefly, neurospheres were centrifuged and fixed as previously reported. Every wash was performed by consecutive centrifugation. Primary antibodies (rabbit anti-nestin, 1:100) was used at 4°C overnight and secondary antibodies as already described.

For BrdU experiments, cultures were incubated with BrdU (Thermo Fisher, Waltham, MA, USA) diluted in the culture medium at a final concentration of 10 μM for 24h at DIV 2, 4, 6. Cells were then washed with PBS and fixed by 4% formaldehyde. Free aldehyde groups were quenched in 0.1 M glycine in PBS for 5 min. Cells were then incubated with HCl 1 M for 1 min on ice and with HCl 2 M for 15 min at 37°C. Acid was then neutralized with boric acid 0.1 M for 10 min at RT. Samples were then blocked and permeabilized in 3% FBS and 0.3% Triton-X 100 in PBS for 1 h at RT. Primary antibody was used at 4°C overnight (mouse monoclonal anti-BrdU, 1:200).

All images were acquired using an inverted Nikon C2 Confocal microscopy, equipped with Ar/Kr, He/Ne and UV lasers, using a 40x (1.4 NA). oil objective (using oil mounting medium, 1.515 refractive index). Confocal sections were acquired every 300 nm and the total Z-stack thickness (3 μm) was set such that all emitted fluorescence was collected

from the sample. Fluorescence signals were quantified using ImageJ software (http://rsb.info.nih.gov/ij/).

Data analysis and statistics

All values from samples subjected to the same experimental protocols were pooled together and expressed as mean ± SEM with n = number of cells (unless otherwise indicated). A statistically significant difference between data sets was assessed by one-way ANOVA followed by Tukey's multiple comparison test or Kruskal-Wallis test followed by Dunn's multiple comparison test, depending on normality tests results. In cases of comparing just two data groups, Unpaired t test or Mann Whitney test was used, depending on normality tests results. Statistical significance was determined at $P < 0.05$, unless otherwise indicated.

Figure and figure legends

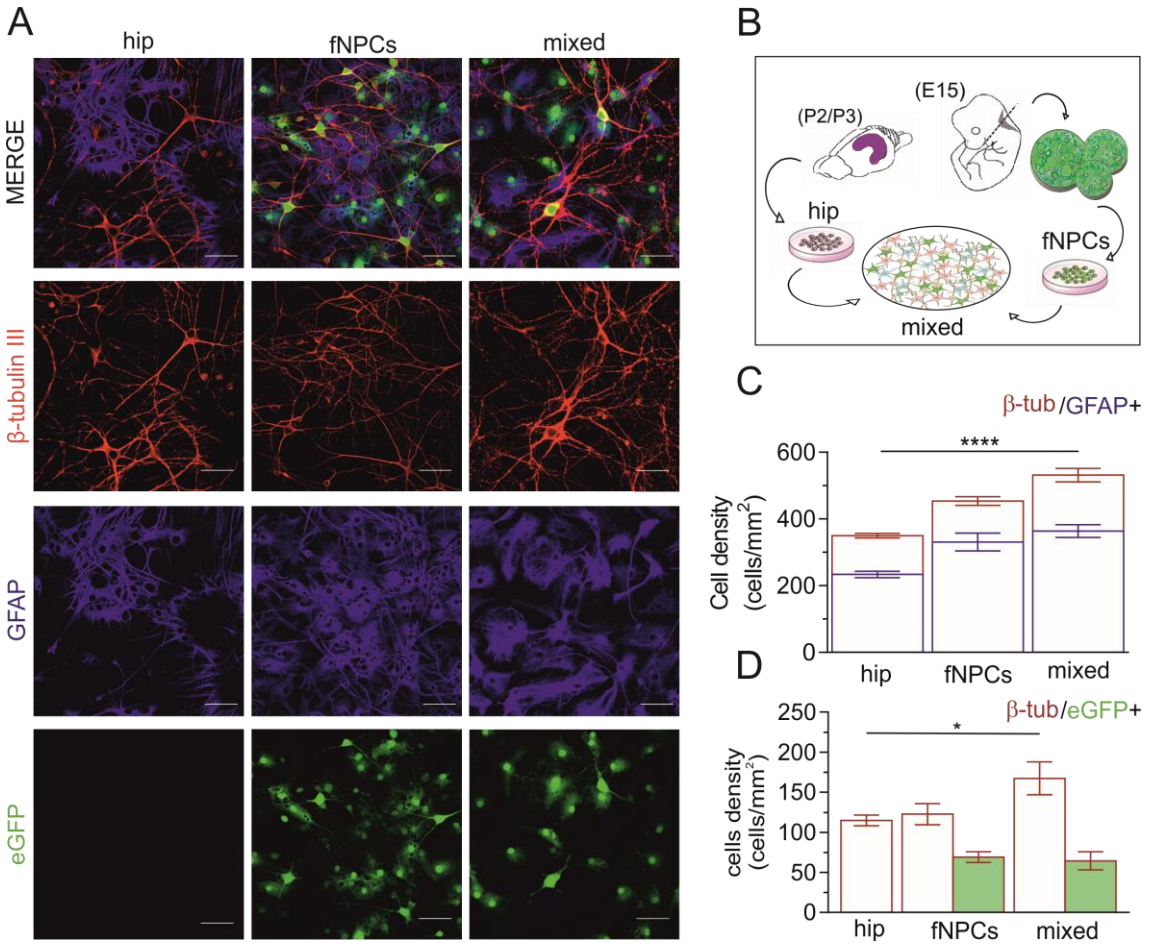

Figure 1. fNPCs grafted to hippocampal networks differentiate into neurons and astrocytes. (A) Representative immunofluorescence micrographs of the three conditions at 15-17 DIV: hippocampal neurons (hip), fetal neuronal progenitor cells (fNPCs) and mixed cultures (mixed) labeled for neurons (β-tubulin III in red), astrocytes (GFAP in blu) and eGFP expressing cells (only fNPCs, in green). Scale bars: 50 µm. (B) Sketch of the experimental setting. (C) Bar plots summarize the β-tubulin III and GFAP relative positive-cell densities in the three conditions and in (D) the density of β-tubulin III positive cells is reported in respect to eGFP-positive cells for the same groups. *P<0.05, ****P<0.0001, ANOVA.

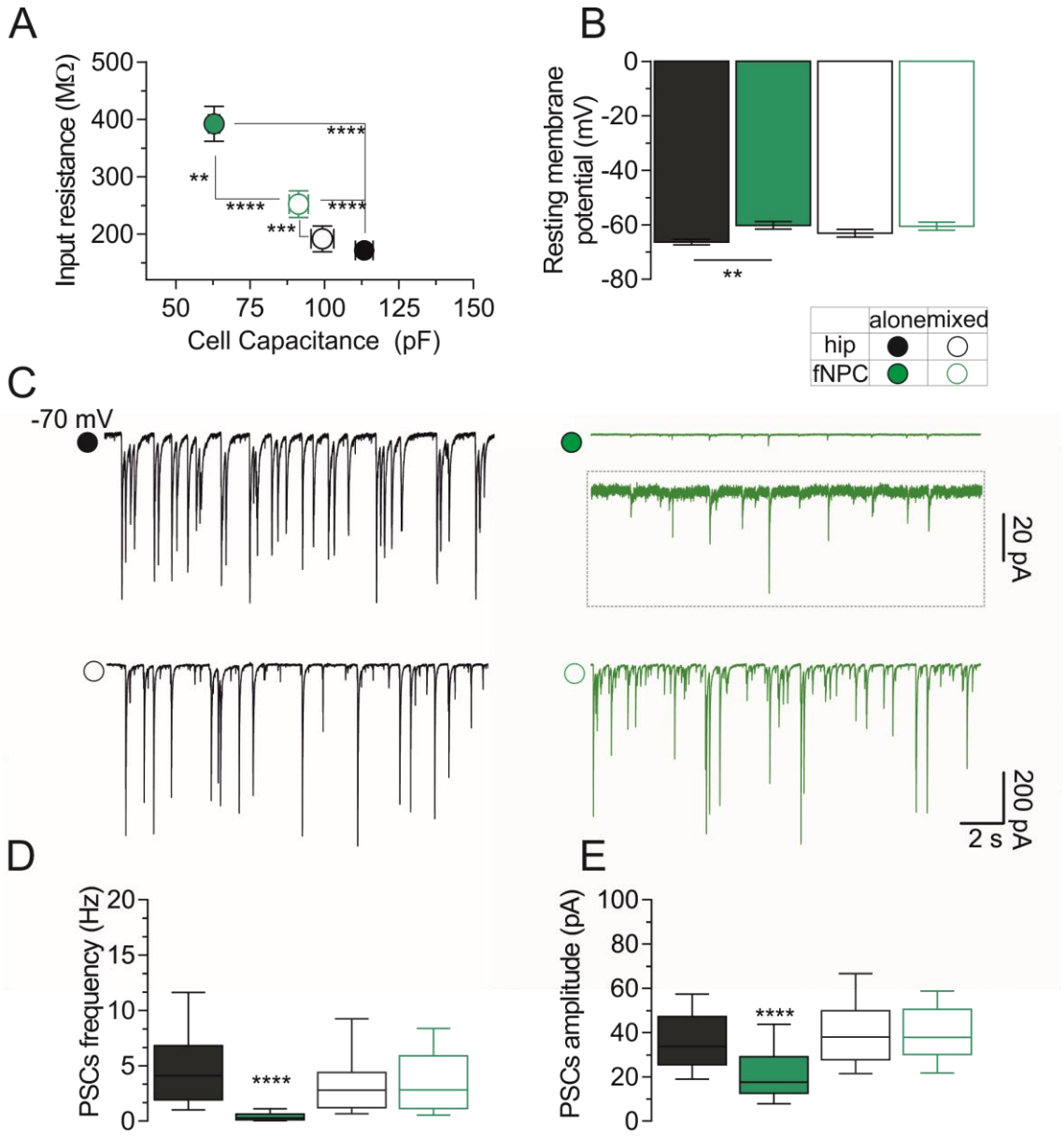

Figure 2. fNPCs neurons grafted to hippocampal networks: electrophysiological characterization. (A) Average values for neuronal cell input resistance are plotted against cell capacitance and compared in the three culture groups. (B) Bar plots report average values of the resting membrane potential recorded in the three culture groups. In the inset, the symbols for hippocampal (hip, black) and fNPCs (in green) neurons when cultured alone (filled circle) or when co-cultured (open circle) is sketched. (C) Representative traces of PSCs recorded from a hippocampal neuron (in black) or a fNPC (in green, note inset with different calibration) when cultured alone (top row) and in mixed cultures (bottom row). The box plots summarize the frequencies (D) and amplitude (E) values for all types of events in all tested conditions. **P<0.01, ***P<0.001, ****P<0.0001, Kruskal-Wallis.

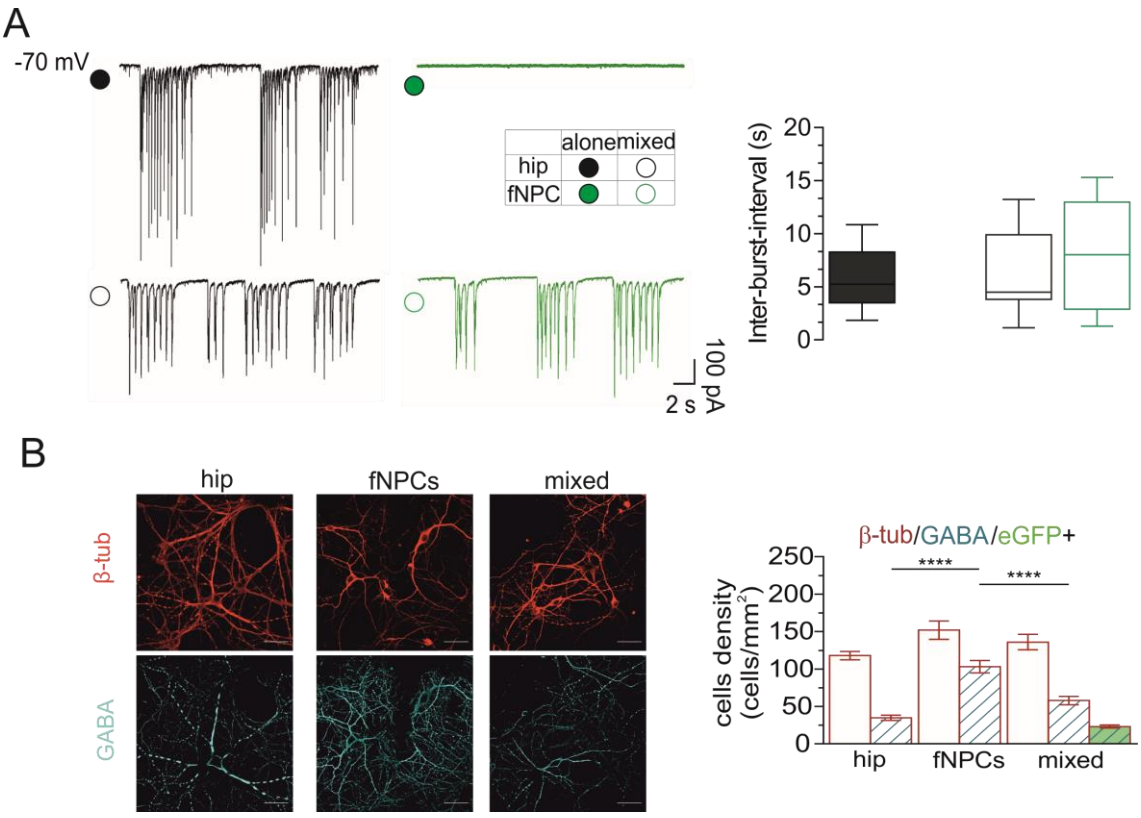

Figure 3. Bicuculline effects in fNPCs, hippocampal and mixed synaptic networks. (A) Representative recordings of PSCs in presence of 10 μM bicuculline. Note the appearance in hippocampal and mixed cultures of synchronized patterned activity organized in long bursts recorded in all neurons. Burst inter event intervals are depicted in the box plots. Conversely, bicuculline application in fNPCs virtually removed all PSCs. (B) β-tubulin positive (in red) neurons and GABA positive (in cyan) ones are shown for the three culturing conditions. Scale bar 50 μm. The bar plots summarize the densities of β-tubulin positive cells, β-tubulin and GABA double positive cells, and β-tubulin, GABA and eGFP triple positive cells. The percentage of double positive neurons was 31 % in hippocampal cells; 68 % in fNPCs and 42% in mixed cultures. In mixed cultures, GABAergic neurons were 48 % of the total β-tubulin and eGFP-positive cells. ****P<0.0001, Kruskal-Wallis.

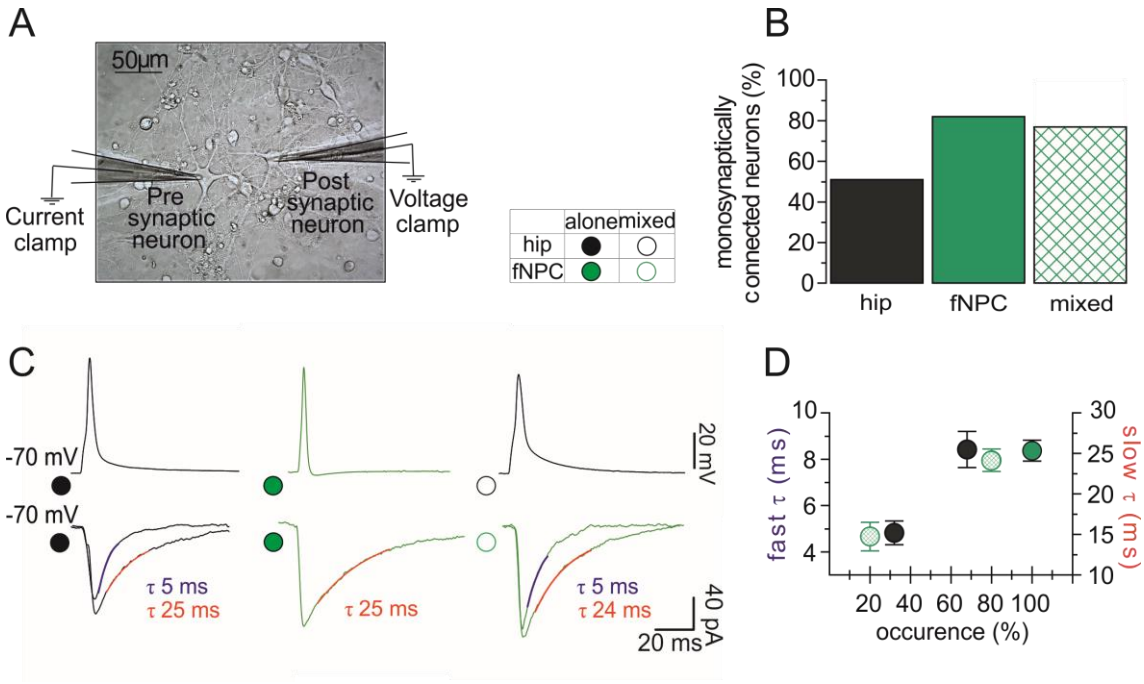

Figure 4. Synaptic characterization by pair recordings: uPSCs in hippocampal, fNPCs and mixed cultures. (A) Bright field image and experimental sketch of pair recordings. (B) Bar plot reporting probability (expressed as percentage) of finding mono-synaptically connected pairs in the three conditions. (C) Representative traces of induced pre-synaptic action potentials (top) and evoked post-synaptic responses (bottom) with relative symbol legend identifying hippocampal neurons (hip, black) and fNPCs (in green), when cultured alone (filled circle) or when co-cultured (open circle). In hippocampal neurons pairs, post-synaptic responses were represented by both slow and fast τPSCs (fast τ is highlighted in blue and slow τ is highlighted in red with corresponded value in ms). In fNPCs pairs, 100% of responses were represented by slow τPSCs. When recorded in mixed cultures, post-synaptic responses in eGFP-positive cells exhibited both τPSCs (both slow and fast are shown). (D) Percentage of occurrence of fast and slow τPSCs and relative duration in time is summarized in the plot.

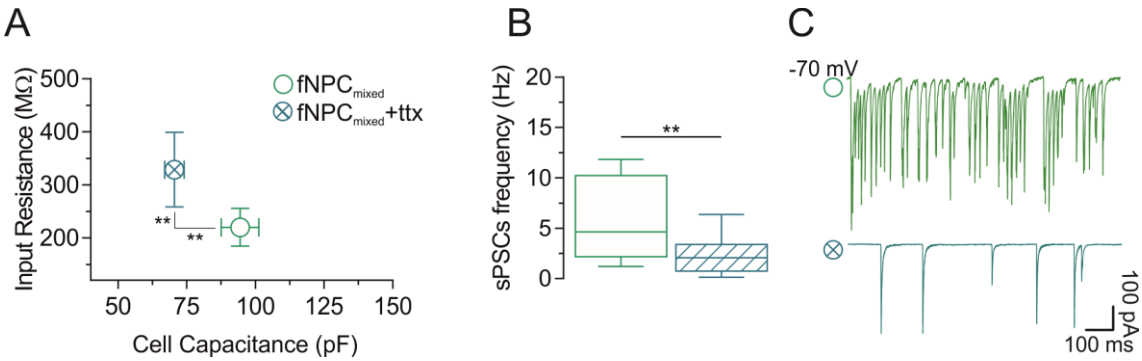

Figure 5. fNPCs feature in mixed cultures when developed in the absence of neuronal firing. (A) Plot summarizing membrane passive properties in fNPCs in mixed cultures (fNPCs$_{mixed}$; open green circle) and in fNPCs developed in TTX treatment (fNPCs$_{mixed}$ + ttx; crossed darker green open circle). (B) Boxplot quantifying PSCs frequency and relative representative traces (C). **P<0.01, Mann Whitney test.

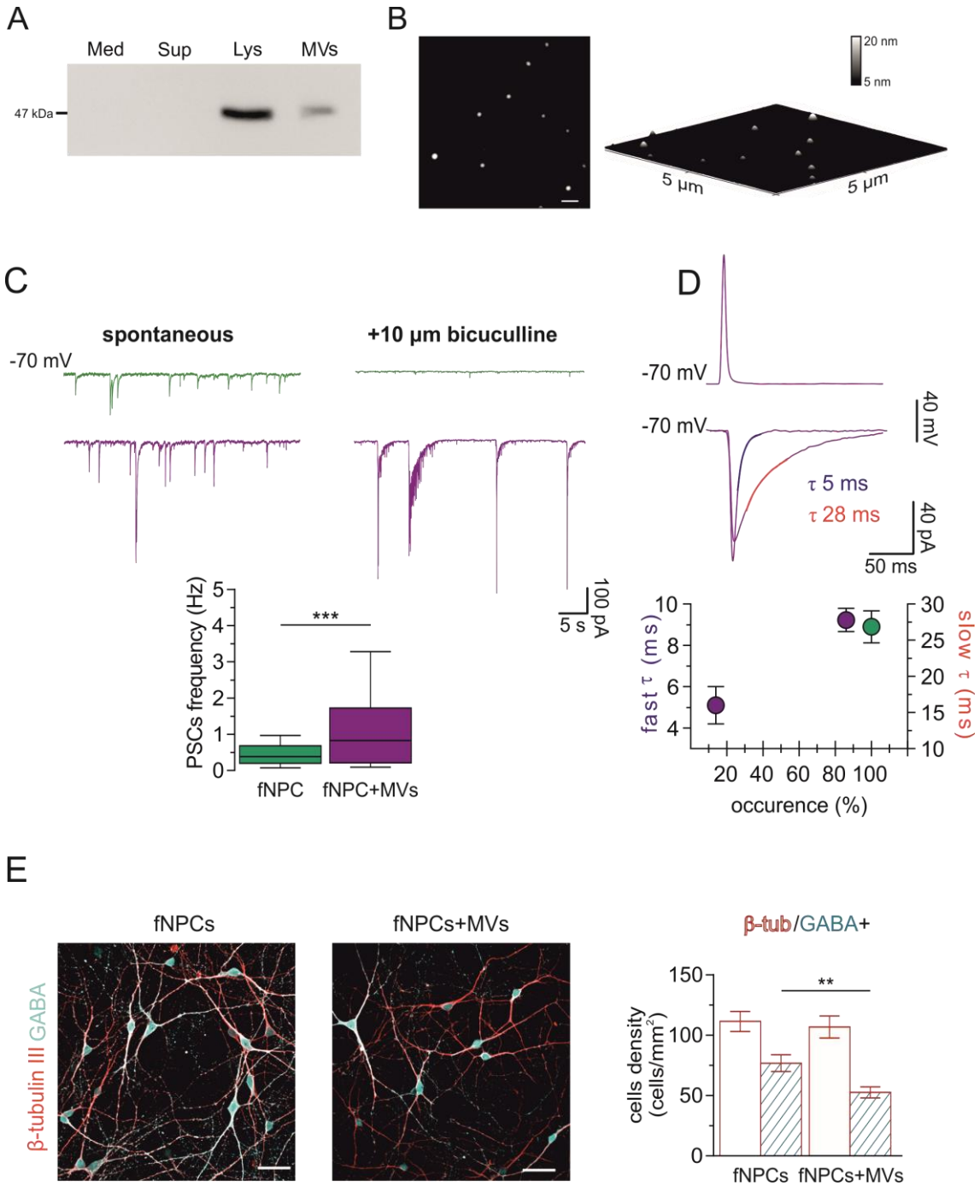

Figure 6. fNPCs network changed synaptic features when incubated with MVs released by cultured astrocytes. (A) Western blot analysis for biomarker flotillin-1, expressed on cell membrane as showed by the band corresponding to glial cell lysate (Lys). MVs presence is demonstrated by the band corresponding to the pellet isolated from glial culture medium (MVs). Any presence of MVs were found neither in the supernatant obtained during the second centrifugation (Sup) nor in the fresh glial culture medium (Med). (B) AFM images of fixed MVs deposited on mica surface and represented in 2D (left) and 3D (right) where the differences in color are representative of height

differences (brighter means higher). Scale bar: 500 nm. (C) Representative tracings in standard saline solution and in bicuculline; fNPCs in green, fNPCs treated by MVs in purple. Bottom: box plots summarize PSCs frequency values in the two conditions. (D) Representative pair recordings from both culture groups. Bottom: probability of finding (expressed as percentage) fast and slow τ PSCs plotted against τ values; (E). Immunofluorescence micrographs of the two conditions labeled for neurons (β-tubulin III in red) and GABA (GABA in cyan). Scale bar 50μm. Bar plots quantify the neurons density in the two conditions and the relative GABAergic (double positive) cells. *P<0.05, **P<0.01, ***P<0.001 Mann Whitney test.

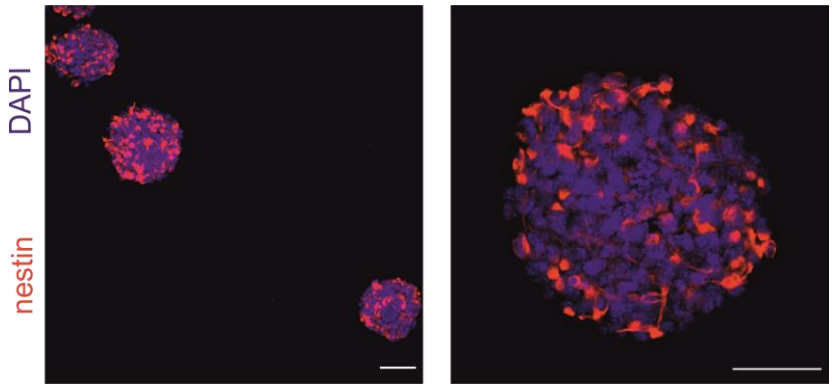

Supplementary figure 1. fNPCs proliferating as neurospheres.
Representative immunofluorescence micrographs of fNPCs assembled in proliferating neurospheres at DIV 3 post dissection, labeled for early proliferation marker (nestin in red) and nuclei (DAPI in blue). Scale bars: 50 μm.

Competing interests

The authors declare no financial competing interest.

References

Al-Nedawi, K., Meehan, B., and Rak, J. (2009). Microvesicles: Messengers and mediators of tumor progression. Cell Cycle 8, 2014–2018. doi:10.4161/cc.8.13.8988.

Angulo, M. C., Rossier, J., and Audinat, E. (1999). Postsynaptic Glutamate Receptors and Integrative Properties of Fast-Spiking Interneurons in the Rat Neocortex. J. Neurophysiol. 82, 1295–1302. doi:10.1152/jn.1999.82.3.1295.

Antonov, S. A., Novosadova, E. V., Kobylyansky, A. G., Illarioshkin, S. N., Tarantul, V. Z., and Grivennikov, I. A. (2019). Expression and Functional Properties of NMDA and GABAA

Receptors during Differentiation of Human Induced Pluripotent Stem Cells into Ventral Mesencephalic Neurons. Biochem. 84, 310–320. doi:10.1134/S0006297919030131.

Aurand, E. R., Wagner, J. L., Shandas, R., and Bjugstad, K. B. (2014). Hydrogel formulation determines cell fate of fetal and adult neural progenitor cells. Stem Cell Res. 12, 11–23. doi:10.1016/J.SCR.2013.09.013.

Avaliani, N., Sørensen, A. T., Ledri, M., Bengzon, J., Koch, P., Brüstle, O., et al. (2014). Optogenetics reveal delayed afferent synaptogenesis on grafted human-induced pluripotent stem cell-derived neural progenitors. Stem Cells 32, 3088–98. doi:10.1002/stem.1823.

Banks, M. I., and Pearce, R. A. (2000). Kinetic differences between synaptic and extrasynaptic GABA(A) receptors in CA1 pyramidal cells. J. Neurosci. 20, 937–48. doi:10.1523/JNEUROSCI.20-03-00937.2000.

Benson, D. L., Watkins, F. H., Steward, O., and Banker, G. (1994). Characterization of GABAergic neurons in hippocampal cell cultures. J. Neurocytol. 23, 279–95. Available at: http://www.ncbi.nlm.nih.gov/pubmed/8089704 [Accessed January 13, 2019].

Calegari, F., Coco, S., Taverna, E., Bassetti, M., Verderio, C., Corradi, N., et al. (1999). A regulated secretory pathway in cultured hippocampal astrocytes. J. Biol. Chem. 274, 22539–47. doi:10.1074/JBC.274.32.22539.

Cellot, G., Toma, F. M., Varley, Z. K., Laishram, J., Villari, A., Quintana, M., et al. (2011). Carbon Nanotube Scaffolds Tune Synaptic Strength in Cultured Neural Circuits: Novel Frontiers in Nanomaterial–Tissue Interactions. J. Neurosci. 31, 12945–12953. doi:10.1523/JNEUROSCI.1332-11.2011.

Conde, I. del, Shrimpton, C. N., Thiagarajan, P., and López, J. A. (2005). Tissue-factor–bearing microvesicles arise from lipid rafts and fuse with activated platelets to initiate coagulation. Blood 106, 1604–1611. doi:10.1182/BLOOD-2004-03-1095.

Deisseroth, K., Singla, S., Toda, H., Monje, M., Palmer, T. D., and Malenka, R. C. (2004). Excitation-Neurogenesis Coupling in Adult Neural Stem/Progenitor Cells. Neuron 42, 535–552. doi:10.1016/S0896-6273(04)00266-1.

Eisenman, L. N., Emnett, C. M., Mohan, J., Zorumski, C. F., and Mennerick, S. (2015). Quantification of bursting and synchrony in cultured hippocampal neurons. J. Neurophysiol. 114, 1059–1071. doi:10.1152/jn.00079.2015.

Fricker, R. A., Carpenter, M. K., Winkler, C., Greco, C., Gates, M. A., and Björklund, A. (1999). Site-specific migration and neuronal differentiation of human neural progenitor cells after transplantation in the adult rat brain. J. Neurosci. 19, 5990–6005. doi:10.1523/JNEUROSCI.19-14-05990.1999.

Furlan, F., Taccola, G., Grandolfo, M., Guasti, L., Arcangeli, A., Nistri, A., et al. (2007). ERG Conductance Expression Modulates the Excitability of Ventral Horn GABAergic Interneurons

That Control Rhythmic Oscillations in the Developing Mouse Spinal Cord. J. Neurosci. 27, 919–928. doi:10.1523/JNEUROSCI.4035-06.2007.

Gao, P., Postiglione, M. P., Krieger, T. G., Hernandez, L., Wang, C., Han, Z., et al. (2014). Deterministic Progenitor Behavior and Unitary Production of Neurons in the Neocortex. Cell 159, 775–788. doi:10.1016/J.CELL.2014.10.027.

Heikkilä, T. J., Ylä-Outinen, L., Tanskanen, J. M. A., Lappalainen, R. S., Skottman, H., Suuronen, R., et al. (2009). Human embryonic stem cell-derived neuronal cells form spontaneously active neuronal networks in vitro. Exp. Neurol. 218, 109–116. doi:10.1016/j.expneurol.2009.04.011.

Kopach, O., Rybachuk, O., Krotov, V., Kyryk, V., Voitenko, N., and Pivneva, T. (2018). Maturation of neural stem cells and integration into hippocampal circuits - a functional study in an in situ model of cerebral ischemia. J. Cell Sci. 131, jcs210989. doi:10.1242/jcs.210989.

le Magueresse, C., Alfonso, J., Khodosevich, K., Martín, Á. A. A., Bark, C., and Monyer, H. (2011). "Small axonless neurons": Postnatally generated neocortical interneurons with delayed functional maturation. J. Neurosci. 31, 16731–16747. doi:10.1523/JNEUROSCI.4273-11.2011.

Lepski, G., Jannes, C. E., Nikkhah, G., and Bischofberger, J. (2013). cAMP promotes the differentiation of neural progenitor cells in vitro via modulation of voltage-gated calcium channels. Front. Cell. Neurosci. 7. doi:10.3389/fncel.2013.00155.

Lovat, V., Pantarotto, D., Lagostena, L., Cacciari, B., Grandolfo, M., Righi, M., et al. (2005). Carbon Nanotube Substrates Boost Neuronal Electrical Signaling. Nano Lett. 5, 1107–1110. doi:10.1021/nl050637m.

Marzesco, A.-M., Janich, P., Wilsch-Bräuninger, M., Dubreuil, V., Langenfeld, K., Corbeil, D., et al. (2005). Release of extracellular membrane particles carrying the stem cell marker prominin-1 (CD133) from neural progenitors and other epithelial cells. J. Cell Sci. 118, 2849–2858. doi:10.1242/jcs.02439.

Miskinyte, G., Devaraju, K., Grønning Hansen, M., Monni, E., Tornero, D., Woods, N. B., et al. (2017). Direct conversion of human fibroblasts to functional excitatory cortical neurons integrating into human neural networks. Stem Cell Res. Ther. 8, 207. doi:10.1186/s13287-017-0658-3.

Muth-Köhne, E., Terhag, J., Pahl, S., Werner, M., Joshi, I., and Hollmann, M. (2010). Functional excitatory GABAA receptors precede ionotropic glutamate receptors in radial glia-like neural stem cells. Mol. Cell. Neurosci. 43, 209–221. doi:10.1016/j.mcn.2009.11.002.

Pampaloni, N. P., Lottner, M., Giugliano, M., Matruglio, A., D'Amico, F., Prato, M., et al. (2018). Single-layer graphene modulates neuronal communication and augments membrane ion currents. Nat. Nanotechnol. 13, 755–764. doi:10.1038/s41565-018-0163-6.

Raposo, G., and Stoorvogel, W. (2013). Extracellular vesicles: Exosomes, microvesicles, and friends. J. Cell Biol. 200, 373–383. doi:10.1083/jcb.201211138.

Rauti, R., Lozano, N., León, V., Scaini, D., Musto, M., Rago, I., et al. (2016). Graphene Oxide Nanosheets Reshape Synaptic Function in Cultured Brain Networks. ACS Nano 10, 4459–4471. doi:10.1021/acsnano.6b00130.

Ruschenschmidt, C., Koch, P. G., Brustle, O., and Beck, H. (2005). Functional Properties of ES Cell-Derived Neurons Engrafted into the Hippocampus of Adult Normal and Chronically Epileptic Rats. Epilepsia 46, 174–183. doi:10.1111/j.1528-1167.2005.01028.x.

Théry, C., Zitvogel, L., and Amigorena, S. (2002). Exosomes: composition, biogenesis and function. Nat. Rev. Immunol. 2, 569–579. doi:10.1038/nri855.

Upadhya, D., Hattiangady, B., Castro, O. W., Shuai, B., Kodali, M., Attaluri, S., et al. (2019). Human induced pluripotent stem cell-derived MGE cell grafting after status epilepticus attenuates chronic epilepsy and comorbidities via synaptic integration. Proc. Natl. Acad. Sci. U. S. A. 116, 287–296. doi:10.1073/pnas.1814185115.

Widera, D., Grimm, W.-D., Moebius, J. M., Mikenberg, I., Piechaczek, C., Gassmann, G., et al. (2007). Highly Efficient Neural Differentiation of Human Somatic Stem Cells, Isolated by Minimally Invasive Periodontal Surgery. Stem Cells Dev. 16, 447–460. doi:10.1089/scd.2006.0068.

Wu, Y., Chen, Q., Peng, H., Dou, H., Zhou, Y., Huang, Y., et al. (2012). Directed migration of human neural progenitor cells to interleukin-1β is promoted by chemokines stromal cell-derived factor-1 and monocyte chemotactic factor-1 in mouse brains. Transl. Neurodegener. 1, 15. doi:10.1186/2047-9158-1-15.

Xu, W., Lakshman, N., and Morshead, C. M. (2017). Building a central nervous system: The neural stem cell lineage revealed. Neurogenes. (Austin, Tex.) 4, e1300037. doi:10.1080/23262133.2017.1300037.

Yin, X., Xu, J.-C., Cho, G.-S., Kwon, C., Dawson, T. M., and Dawson, V. L. (2019). Neurons Derived from Human Induced Pluripotent Stem Cells Integrate into Rat Brain Circuits and Maintain Both Excitatory and Inhibitory Synaptic Activities. eNeuro 6. doi:10.1523/ENEURO.0148-19.2019.

Yizhar, O., Fenno, L. E., Prigge, M., Schneider, F., Davidson, T. J., O'Shea, D. J., et al. (2011). Neocortical excitation/inhibition balance in information processing and social dysfunction. Nature 477, 171–178. doi:10.1038/nature10360.

4.2 Fetal neural progenitors contribute to postnatal circuits formation *ex vivo*: an electrophysiological investigation

Matteo Manzati [(1, *)], Teresa Sorbo [(1, *)], Michele Giugliano [(2-3, #)], Laura Ballerini [(1, #)]

(1)Neuron Physiology and Technology Lab, International School for Advanced Studies (SISSA), Neuroscience, I-34136 Trieste, Italy

(2) Neuronal Dynamics Lab, International School for Advanced Studies (SISSA), Neuroscience, I-34136 Trieste, Italy

(3)Department of Biomedical Sciences and Institute Born-Bunge, Universiteit Antwerpen, B-2610 Wilrijk, Belgium

(*) Equally contributing authors

[#]Corresponding authors
laura.ballerini@sissa.it
Laura Ballerini
International School for Advanced Studies (SISSA), Neuroscience
Via Bonomea 265, I-34136 Trieste, Italy

michele.giugliano@sissa.it
Michele Giugliano
International School for Advanced Studies (SISSA), Neuroscience
Via Bonomea 265, I-34136 Trieste, Italy

Abstract

Neuronal progenitor cells (NPC) play an essential role in homeostasis of the central nervous system (CNS). Considering their ability to differentiate into specific lineages, their manipulation and control could have a major impact on future therapeutic approaches for those CNS injuries or degenerative diseases characterized by neuronal cell loss. In this work, we established an *in vitro* co-culture and tested the ability of foetal NPC (fNPC) to integrate among post-mitotic hippocampal neurons and contribute to the electrical activity of the resulting networks. We performed extracellular electrophysiological recordings of the activity of neuronal networks and compared the properties of the emerging spontaneous spiking in hippocampal, fNPC, and mixed circuitries *ex vivo*. We further employed patch-clamp intracellular recordings to examine single-cell excitability. Our results describe overall the capability of fNPC to mature when combined to hippocampal neurons, shaping the profile of network activity, a result suggestive of newly formed connectivity *ex vivo*.

Keywords: Microelectrode arrays, cell electrophysiology, neuronal networks, neuronal progenitor cells, hippocampus.

Introduction

During the last decade, neuronal replacement therapy (NBT) has come to the forefront of experimental research in neurodegenerative diseases. Alternative to those interventions aimed at slowing down cell loss or at a refined rehabilitation, NBT directly addresses neurodegeneration by replacing dead cells with healthy new ones in order to restore compromised brain functions. Such perspectives have become within our reach thanks to our progress in understanding the functional homeostasis (Grade and Götz, 2017) of the mammalian central nervous system (CNS), despite CNS's inherent lack of tissue regeneration. Among the candidates for NBT, multipotent neural stem cells derived from embryonic tissue are the most promising. They are well known to differentiate into neuronal and glial cells, under the appropriate manipulations (Snyder et al., 1997), and their protective effects against the host's dysfunctional neurons has been demonstrated in rodents (Ourednik et al., 2002). However, the mechanisms underlying the functional CNSimprovements by NBT have not yet been completely understood (Grade and Götz, 2017). For this reason, we decided to focus on foetal neural progenitor cells (fNPC) as a reservoir of proliferating cells, and we defined a new *in vitro* experimental model. This consisted of a mixed population of fNPC and of cultured neurons dissociated from the rat hippocampus, reorganizing *ex vivo* into functional circuits. This coculture system was then coupled to the surface of an array of substrate-integrated microelectrodes (MEAs), which allowed us to monitor over time and non-invasively the simultaneous electrical activity of cells from up to 60 spatial locations. Our MEA coculture system revealed to be a powerful *in vitro* assay for the systematic dissection of cellular and circuits correlates of NBT.

Material and methods

Cultures preparation. Primary cultures of hippocampal cells were obtained from Wistar rats at postnatal days 2-3 (P2-3), as reported (Bosi et al., 2015). Foetal neural progenitor cells (fNPC) were instead isolated from (E15) embryos, as already described (Aurand et al., 2014). fNPC were next tagged by a reporter fluorescent protein (eGFP), upon

transduction with Lentiviral vectors and under the PGK promoter. All experimental conditions shared identical plating and culture conditions, with the culture medium containing Neurobasal A Medium, 2% B-27 Supplement, 1% GlutaMAX Supplement, and 0.05% gentamicin (50mg/mL). Mixed cultures were obtained by adding fNPC to hippocampal cultures (1:1 ratio) and then compared to cultures of fNPC or hippocampal cells. Cells were plated at a density of ~420 cells/mm^2 on 0.01% poly-L-ornithine solution-coated glass coverslips (Orsatec GmbH, Bobingen, Germany) in a 144 mm^2 medium droplet, for single-cell intracellular electrophysiology. Cells were instead plated at a density of ~3000 cells/mm^2 on the inner area of MicroElectrode Arrays (MEA) (Multi Channel System GmBH, Reutlingen, Germany). Prior to plating, each MEA was plasma-cleaned (PDC-32G, Harrick Plasma, Ithaca, USA; 80s at medium power) and later coated with a 0.1% polyethylene-imine (03880, Sigma-Aldrich) solution, rinsed with sterile milliQ water. Cover slips and MEAs were incubated at 37 °C, 5% CO_2 for 15-17 days *in vitro* (DIV), with MEAs sealed with polydimethylsiloxane (PDMS) caps (Sylgard 184, Dow Corning, Midland, USA) (Blau *et al.*, 2009), preventing contamination and reducing osmotic drift. All chemicals and reagents were obtained from Thermo Fisher Scientific (Monza, Italy), or Sigma-Aldrich (Milan, Italy).

Single-cell electrophysiology. Intracellular recordings were performed by patch-clamp in the whole-cell configuration, at room temperature (20-22 °C). Glass micropipette electrodes were fabricated on a horizontal puller (P-10, Sutter, Novato, USA) and had a resistance of 5-8 MΩ when filled with an intracellular solution, containing (in mM) 120 K gluconate, 20 KCl, 10 HEPES, 10 EGTA, 2 $MgCl_2$, 2 Na_2ATP, pH adjusted to 7.3. All recordings were performed under continuous perfusion (2 mL/min) of an extracellular solution containing (in mM) 150 NaCl, 4 KCl, 1 $MgCl_2$, 2 $CaCl_2$, 10 HEPES, 10 glucose, pH adjusted to 7.4. As fNPC were GFP-tagged, discriminating between progenitors and hippocampal cells in mixed cultures was possible by meansof epifluorescence videomicroscopy. Raw membrane potential traces were recorded in current-clamp (after bridge balance compensation) using a Multiclamp 700A Amplifier (Molecular Devices, US), sampled (10 kHz) and digitized with pClamp 10 (Molecular Devices), analyzed by Clampfit 10.3 (Molecular Devices), and stored on disk for further analysis. The liquid junction potential was left uncorrected (estimated as 13.7 mV at 22°C). The membrane passive electrical properties (i.e. the apparent input resistance and the capacitance) were estimated using pClamp, analyzing the cell electrical response to short pulse stimuli,

delivered in voltage clamp and holding the cells at -56 mV. Action potentials were evoked in current clamp upon delivering repeated brief depolarizing current steps (4 nA, 5 ms, 15 times, 1 Hz), holding the cells at -70 mV by injection of a very small negative current.

Network electrophysiology. Multisite extracellular recordings were carried out by MEAs, featuring an 8 x 8 regular layout of 60 substrate-integrated TiN microelectrodes (30 μm diameter, 200 μm inter-electrode distance). Individual MEAs were alternatively connected to a multichannel amplifier (MEA1060-Inv-BC, MultiChannel Systems). The raw voltage signals, detected simultaneously from each of the 60 microelectrodes of a MEA, were amplified (1000x), sampled (10 kHz), digitized (16 bits) with an A/D acquisition card (MCCard, MultiChannel Systems), and stored on disk by using MCRack (MultiChannel Systems). Recordings were performed, at 37 °C, in the presence of cell culture medium, and consisted first of a 1) 30 min session, initially monitoring the spontaneous activity; then of a 2) 30 min session, monitoring the activity in the presence of bicuculline (10 μM), a $GABA_A$ synaptic receptors blocker; and finally of a 3) 5 min session, validating the biological signal detection upon the presence of tetrodotoxin (1 μM), a Na-ion channels blocker (Latoxan, Portes les valence, France).

Immunofluorescence. Cells were fixed by exposing them to 4% formaldehyde (obtained from fresh paraformaldehyde) in PBS, for 20 min. Neurons were visualized by the rabbit anti- β-tubulin III primary antibody (Sigma T2200, 1:500 dilution) and Alexa 594 goat anti rabbit (Life technologies A11037, 1:500 dilution) as secondary antibody, while DAPI (Invitrogen, 1:500 dilution) was employed to visualize the cell nuclei. All antibodies were dissolved in a blocking solution, composed by 5% FBS and 3% TritonX. Images were digitally acquired on an inverted Nikon eclipse T*i*2 confocal microscope, equipped with lasers (405, 488, 560 nm), using 10x/0.45λ or 20x/0.75λ objectives, while collecting sections every 0.5 μm. Collapsed stacks were later imported into ImageJ® software (National Institutes of Health—NIH, Bethesda, MD) and merged together with an image of the plane containing the MEA microelectrodes, acquired under transmitted light.

Data analysis. Unless otherwise specified, samples subjected to the same experimental conditions were pooled together and their data expressed as mean, standard error of the mean, median values (i.e. upon testing for normality - D'Agostino & Pearson omnibus normality test), and cell numerosity. Statistically significant differences (at $p < 0.05$)

between data sets were assessed by Kruskal-Wallis test followed by Dunn's multiple comparison test. Raw MEA data were analyzed offline using QSpike Tools (Mahmud *et al.*, 2014) and statistical analysis performed using GraphPad Prism 6 (GraphPad Software, San Diego, USA), using unpaired Mann-Whitney and Kruskal-Wallis tests.

Results

To investigate the functional integration of fNPC into postnatal hippocampal circuitry and explore their impact, we developed and compared three culturing conditions: hippocampal cultures (n = 8), fNPC cultures (n = 8), and mixed ones, constituted by both hippocampal and fNPC (n = 8). All cultures were seeded and grown on substrate-integrated microelectrode arrays (MEAs), bathed by the standard culture medium (see the Methods). Hippocampal cells and fNPC, visualized by eGFP (see the Methods), reorganized *ex vivo* into interconnected networks (Fig. 1A). As for the hippocampal cultures, mixed networks cultured on MEAs showed prominent spontaneous extracellular electrical activity at 14-15 days *in vitro* (DIVs). The activity was organized in bursts of action potentials (i.e. spikes), occurring synchronously (see below) in cells across the network and detected by distinct MEA microelectrodes (Fig. 1B and plots in Fig. 2 A-E**)**. These bursts are known to emerge and terminate by means of an interplay between excitatory and inhibitory synaptic transmission, as well as intrinsic cell electrical properties (Giugliano et al., 2004). In fact, as we pharmacologically blocked the inhibitory $GABA_A$ receptors by bicuculline (10 μM, 20 min; Fig. 1C and plots in Fig. B-F), the network activity patterns became altered. When fNPC were cultured alone, they displayed rare or no spiking activity, even under pharmacological disinhibition (Fig. 1 B-C and plots in Fig. 2 A-F).

The number of microelectrodes detecting repeated extracellular action potentials was then taken, for each MEA, as a measure of synaptic and neuronal activity, across the network or locally (Fig. 2A). When quantified systematically, we observed a much higher number of active electrodes in mixed cultures (45.0 ± 4.69; median = 41.5; n = 8) and hippocampal control cultures (38.5 ± 2.83; median = 44.5; n = 8) than in fNPC control cultures (5.00 ± 1.95; median = 3.5; n = 8). Similarly, upon exposure to bicuculline (Fig. 2B), we still found that the number of active electrodes was higher in mixed cultures (46.6 ± 3.26; median = 45; n = 8) and hippocampal control cultures (40.9 ± 5.27; median = 43; n = 8) than in fNPC control cultures (5.63 ± 1.82; median = 4.5; n = 8). Next, we investigated and quantified the frequency of occurrence of spontaneous action potentials (i.e. spikes)

for every culture (Fig. 2C). We observed that the spontaneous spike frequency differed, although not significantly, comparing hippocampal cultures (76.7 ± 22.6 Hz; median = 48.3 Hz; n = 8) and mixed cultures (151 ± 32.2 Hz; median = 114 Hz; n = 8). Instead the difference was significant both with hippocampal cultures ($p < 0.05$) and mixed cultures ($p < 0.001$), compared to fNPC control cultures (2.66 ± 1.44 Hz; median = 0.724 Hz; n = 8). A similar scenario was observed under bicuculline application too, so that the spike frequency in mixed cultures (190 ± 40.8 Hz; median = 164 Hz; n = 7) was higher, although not significantly, than in hippocampal cultures (144 ± 44.4 Hz; 99.1; n = 8), and both were significantly different (Fig. 2D) than fNPC control cultures (1.38 ± 0.565 Hz; median = 0.723 Hz; n = 8) (respectively, $p < 0.01$ and $p < 0.001$).

Finally, the emergence of episodic synchronization of action potentials, a well-known correlate of synaptogenesis (Kamioka et al., 1996; Marom and Shahaf, 2002), was studied. This was achieved upon analysing the frequency of co-occurrence of burst of action potential, across the microelectrodes of the same MEA (Fig. 2E). Interestingly, fNPC control cultures never displayed bursting behaviour. Burst frequency was significantly higher ($p < 0.5$) in mixed cultures (0.547 ± 0.131 Hz; median = 0.484 Hz; n = 8) than hippocampal control cultures (0.163 ± 0.063 Hz; median = 0.113; n = 8). Repeating the same analysis, in the presence of bicuculline, revealed that the pharmacological disinhibition did not ignite any bursting in fNPC control cultures (Fig. 2F), while induced a very similar degree of episodic synchronization in mixed cultures (0.615 ± 0.094 Hz; median = 0.640; n = 7) and hippocampal control cultures (0.410 ± 0.109 Hz; median = 0.378; n = 8).

In order to dissect within each culture groups network from single-cell contributions in generating basal activity, we asked whether passive or active electrical properties of single neuronal membranes significantly differed. We thus complemented the above analysis with single-cell intracellular electrical recordings, comparing GFP-tagged and GFP-negative neurons (see the Methods) across our experimental conditions. The values of input resistance (318.6 ± 22.6 MΩ; n = 65) were significantly higher in fNPC when cultured alone and compared to hippocampal neurons (207.2 ± 14.8 MΩ; n = 56), under control conditions. Instead, fNPC in mixed cultured displayed no differences (298.9 ± 25.9 MΩ; n = 44) when compared to hippocampal neurons (235.2 ± 23.7 MΩ; n = 37) in the same cultures, however a slight increase in input resistance when compared to control was detected in all mixed neurons recorded (Fig. 3B). The cell capacitance in fNPC (65.1 ± 2.5 pF; n = 65) displayed significative differences when compared to hippocampal

neurons (109 ± 4.7 pF; n = 56) in control condition, and significant differences when compared to fNPC grown in mixed cultures (101.2 ± 5.4 pF; n = 45), as shown in Fig. 3A. Finally, we probed the active membrane properties upon the injection of a current pulse waveform, while monitoring the membrane electrical potential. Representative traces in Fig. 3D show that all cell types responded with an action potential upon current injection. However, despite similar peak amplitudes (average 100.8 ± 1.8 mV), the rise time was significantly faster in fNPC (2.1 ± 0.1 ms; n = 63) than among all the other experimental conditions (Fig. 3C). Comparing these values to those obtained in more mature hippocampal neurons (2.8 ± 0.1 ms; n = 53), a significative different degree of maturation could be observed, comparing these values to fNPC in mixed cultures (2.6 ± 0.1 ms; n = 44).

Discussion

The deep understanding of fNPC's development will have an enormous impact on future therapeutic approaches (Silver and Miller, 2004; Widera et al., 2007). As we evaluated whether these cells could integrate among and communicate with post-mitotic hippocampal neurons, we established a novel *in vitro* co-culture system and electrophysiological assay. Our MEAs recordings suggests that the formation of functional hybrid networks differs from control cultures, in terms of their electrophysiological characteristics, resulting in qualitatively and quantitatively different emerging spontaneous episodic synchronization.

Recordings in voltage clamp indicated a significant alteration of their membrane electrical passive properties, when fNPC grown in mixed cultures compared to control cultures. We specifically observed an increase in capacitance and a decrease of input resistance, implying overall a maturation through a significant increase in cell size and in the number of ion channels of the cell membranes. Current-clamp experiments further suggests cellular maturation, as fNPC's excitability was examined in response to a depolarizing stimulus.

Conclusions

Overall our data show that, when growing together, fNPC and hippocampal neurons form electrically active hybrid networks, where single-cell and network electrophysiological correlates *ex vivo* differ significantly than fNPC control cultures. Despite obvious limitations of any *in vitro* study, our results convincingly suggest that fNPC develop into

a more mature electrical phenotype when co-cultured with hippocampal neurons. This appears to be the first step towards a complete experimental manipulation of the electrophysiological properties of fNPC, for the perspectives of integrating these cells into neuronal microcircuits *in vivo.*

Formatting of funding sources

This work was supported by the Flemish Research Foundation (grants n. G0F1517N and n. K201619N to MG) and the Scuola Internazionale Superiore di Studi Avanzati ("Collaborazione di Eccellenza 2018" to MG). The funders had no role in study design, data collection and analysis, decision to publish, or preparation of the manuscript.

Reference

Aurand, E. R., Wagner, J. L., Shandas, R., and Bjugstad, K. B. (2014). Hydrogel formulation determines cell fate of fetal and adult neural progenitor cells. *Stem Cell Res.* 12, 11–23. doi:10.1016/J.SCR.2013.09.013.

Bosi, S., Rauti, R., Laishram, J., Turco, A., Lonardoni, D., Nieus, T., et al. (2015). From 2D to 3D: novel nanostructured scaffolds to investigate signalling in reconstructed neuronal networks. *Sci. Rep.* 5, 9562. doi:10.1038/srep09562.

Giugliano, M., Darbon, P., Arsiero, M., Lüscher, H.-R., and Streit, J. (2004). Single-neuron discharge properties and network activity in dissociated cultures of neocortex. *J. Neurophysiol.* 92, 977–96. doi:10.1152/jn.00067.2004.

Grade, S., and Götz, M. (2017). Neuronal replacement therapy: previous achievements and challenges ahead. *npj Regen. Med.* 2, 29. doi:10.1038/s41536-017-0033-0.

Kamioka, H., Maeda, E., Jimbo, Y., Robinson, H. P. C., and Kawana, A. (1996). Spontaneous periodic synchronized bursting during formation of mature patterns of connections in cortical cultures. *Neurosci. Lett.* 206, 109–112. doi:10.1016/S0304-3940(96)12448-4.

Marom, S., and Shahaf, G. (2002). Development, learning and memory in large random networks of cortical neurons: Lessons beyond anatomy. *Q. Rev. Biophys.* 35, 63–87. doi:10.1017/S0033583501003742.

Ourednik, J., Ourednik, V., Lynch, W. P., Schachner, M., and Snyder, E. Y. (2002). Neural stem cells display an inherent mechanism for rescuing dysfunctional neurons. *Nat. Biotechnol.* 20, 1103–1110. doi:10.1038/nbt750.

Silver, J., and Miller, J. H. (2004). Regeneration beyond the glial scar. *Nat. Rev. Neurosci.* 5, 146–156. doi:10.1038/nrn1326.

Snyder, E. Y., Yoon, C., Flax, J. D., and Macklis, J. D. (1997). Multipotent neural precursors can differentiate toward replacement of neurons undergoing targeted apoptotic degeneration in adult mouse neocortex. *Proc. Natl. Acad. Sci. U. S. A.* 94, 11663–8. doi:10.1073/pnas.94.21.11663.

Widera, D., Grimm, W.-D., Moebius, J. M., Mikenberg, I., Piechaczek, C., Gassmann, G., et al. (2007). Highly Efficient Neural Differentiation of Human Somatic Stem Cells, Isolated by Minimally Invasive Periodontal Surgery. *Stem Cells Dev.* 16, 447–460. doi:10.1089/scd.2006.0068.

Figures and Figures Legends

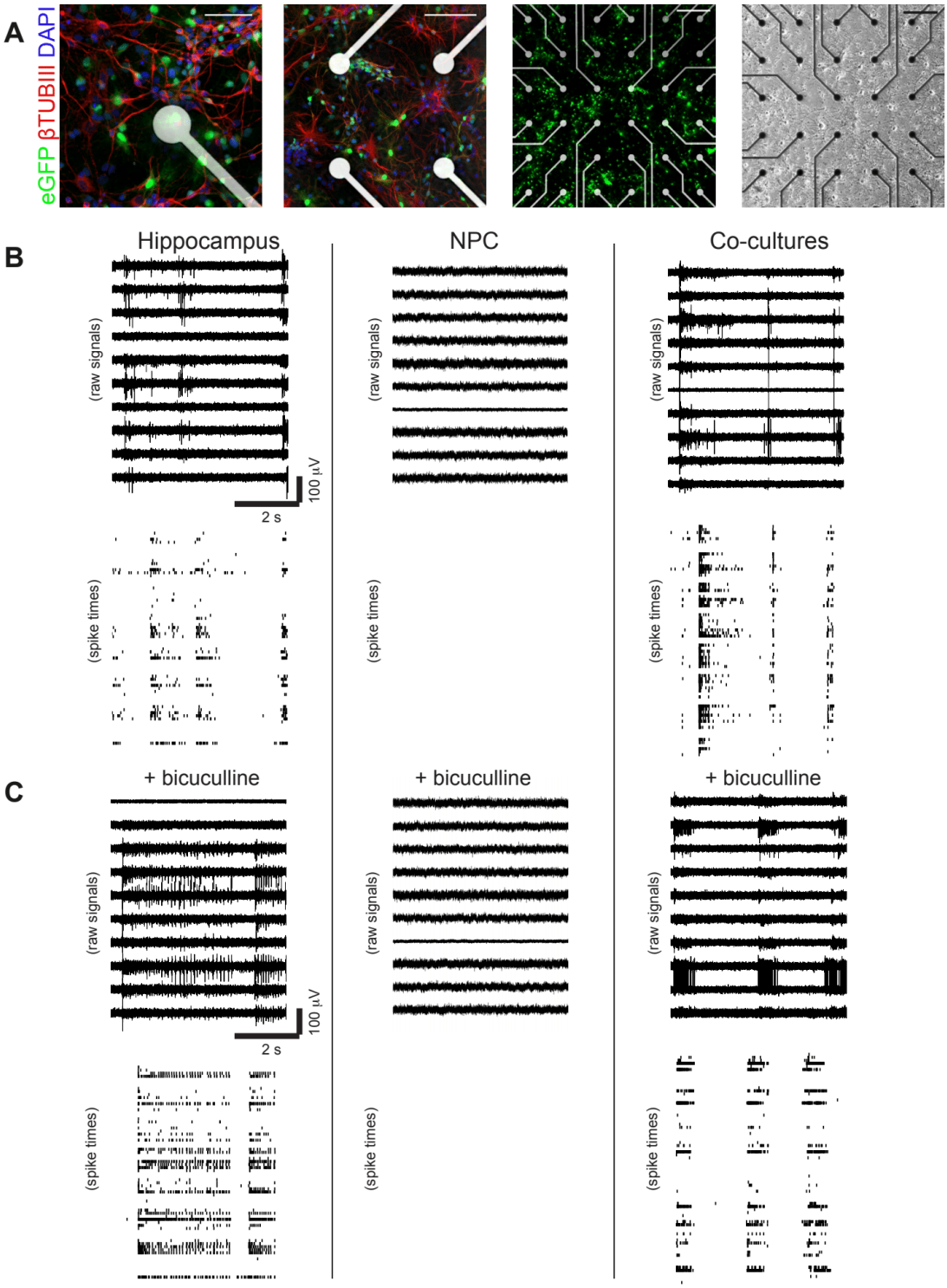

***Figure 1*: Extracellular electrical recordings reveal heterogeneity of the electrophysiological phenotype, across cell culture conditions. (A)** Representative pictures of mixed cultures obtained by phase contrast and confocal microscopy (respectively left and right top images, scale bar = 200 µm); bottom images display

increasing details of β tubulin III$^+$ neurons in red, eGFP$^+$ neurons in green and cells nuclei in blue surrounding electrodes (scale bars = 100 and 50 µm). Sample recordings of the raw extracellular electrical voltages, detected at single sites of three distinct MEAs representative of our experimental conditions, under control conditions and upon pharmacological disinhibition **(B)**.

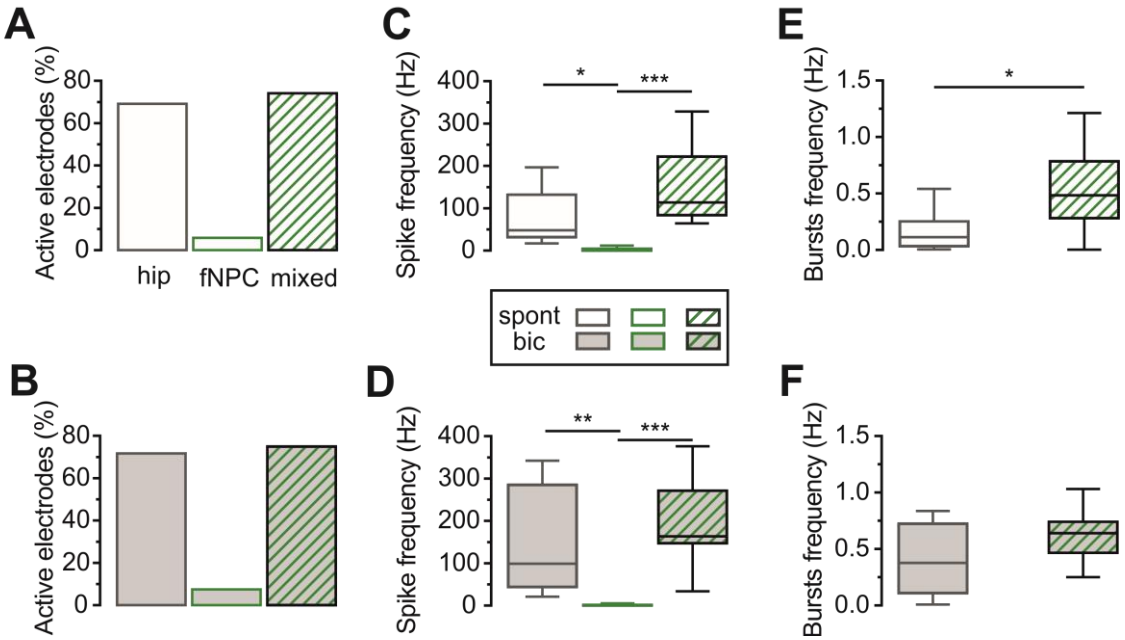

Figure 2: **Extracellular electrical recordings reveal heterogeneity of the electrophysiological phenotype, across cell culture conditions. (A-F)** Population summary over all our MEAs experiments: under both control conditions and disinhibition, hippocampal control cultures and hippocampal + fNPC mixed cultures, but not fNPC control cultures, detected spiking activity from the largest majority of MEA microelectrodes **(A,B)**, with high rate of occurrence **(C,D)** and synchronization **(E,F)**. **P<0.01, ***P<0.001, Mann-Whitney U test.

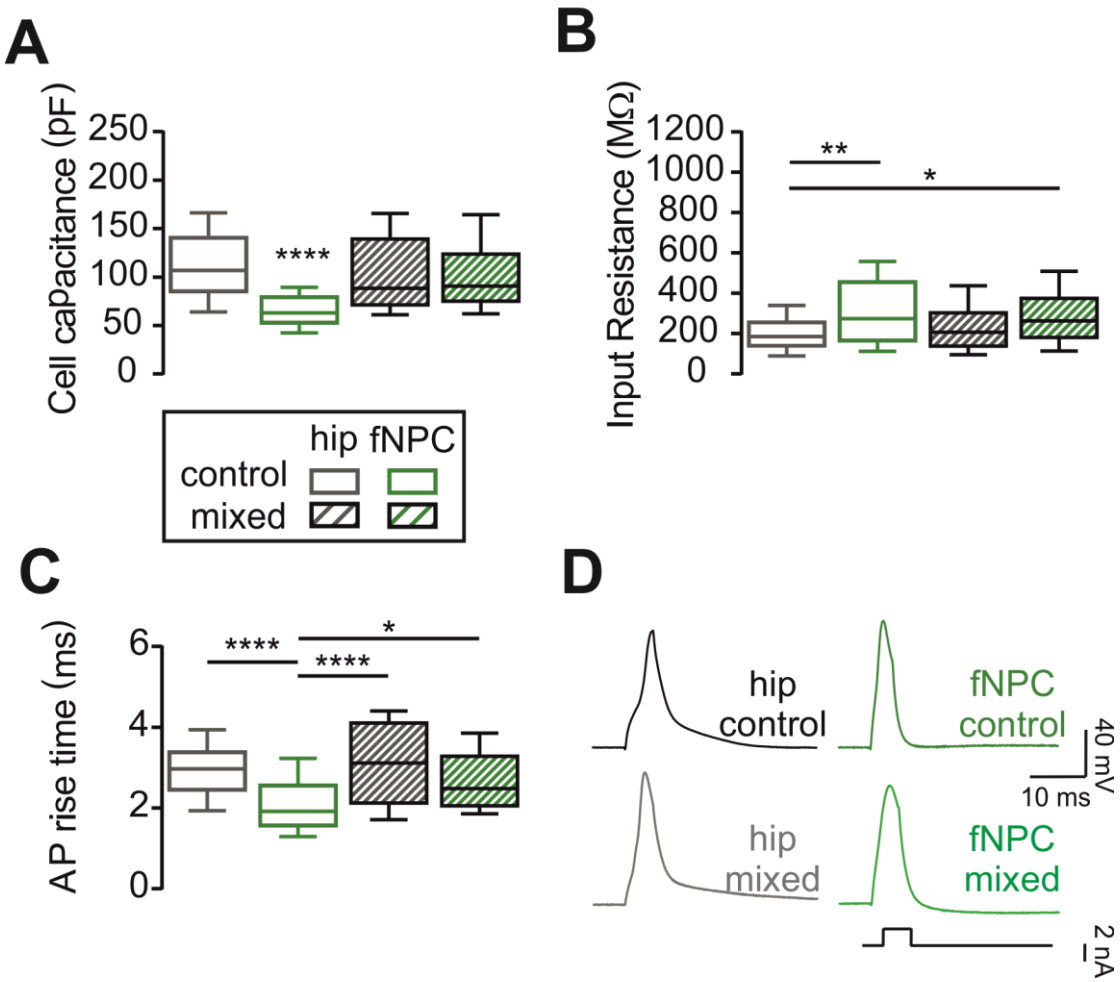

***Figure 3*: Passive and active electrical cells' properties reveal a distinct electrophysiological phenotype of fNPC in mixed cultures.** Representative recordings of induced action potentials in all conditions after injection of 4 nA (B), controls on the top and mixed cells on the bottom. Relative calculated action potentials rise times are displayed by the boxplot in A. Membrane passive properties in terms of input resistance and cell capacitance are summarized by the boxplots C and D. Note the inset explaining the legend. *P<0.05, **P<0.01, ***P<0.001, ****P<0.0001, Kruskal-Wallis.

5 APPENDIX

5.1 Exploit early activity to evaluate integration rate

In order to determine when fetal neural progenitor cells (fNPCs) characteristics initiate to change when growing in mixed hippocampal-fNPC cultures, we investigated a premature (rather than 14-17 DIV) time point of *in vitro* growth, namely 9-11 DIV. Hence, cell membrane passive properties and network activity has been studied after one week of growth *in vitro.*

Materials and Methods

For cell cultures preparation see methods at pag. 3324. Electrophysiological recordings were performed as described at pag. 33, except that in vitro growth time was evaluated between 9-11 DIV.

Results and discussions

At 9-11 DIV the electrophysiological characteristics of fNPCs were significantly different from hippocampal neurons ones, both in terms of passive membrane properties and spontaneous PSCs frequency. In fact, data obtained from fNPCs in mixed cultures ($fNPCs_{mixed}$, n = 33) remained very similar to their control cells (fNPCs plated alone, n = 25) in terms of cell capacitance (54 pF and 45 pF rispectively) and input resistance (688 MΩ and 539 MΩ rispectively) as shown in Figure 8A. The same plot dispalys that also hippocampal neurons in mixed cultures (H_{mixed}, n = 30) almost retained the same phenotipe (78 pF and 359 MΩ) of their control cells (hippocampal neurons plated alone, 73 pF and 271 MΩ, n = 50). However, regarding spontaneous activity it is already present a considerable increase in spontanoues PSCs frequency for $fNPCs_{mixed}$ (from 0.3 Hz in control condition to 1.3 Hz in mixed cultures) as depicted form representative green traces in Figure 8C (control conditions on the top and mixed cells on the bottom) and the boxplot in Figure 8B. Therefore, as fNPCs display a spontaneous PSCs frequency significative higher if compared to their control, this may indicate that the co-presence of post mitotic neuons in the plate has a non negligible effect on the formation of the new hybrid network. These results may indicate the formation of a new network that shows already, at early stages, different characteristics from the ones observed in mono-cultures, despite no changes in terms of single cells passive properties were evident.

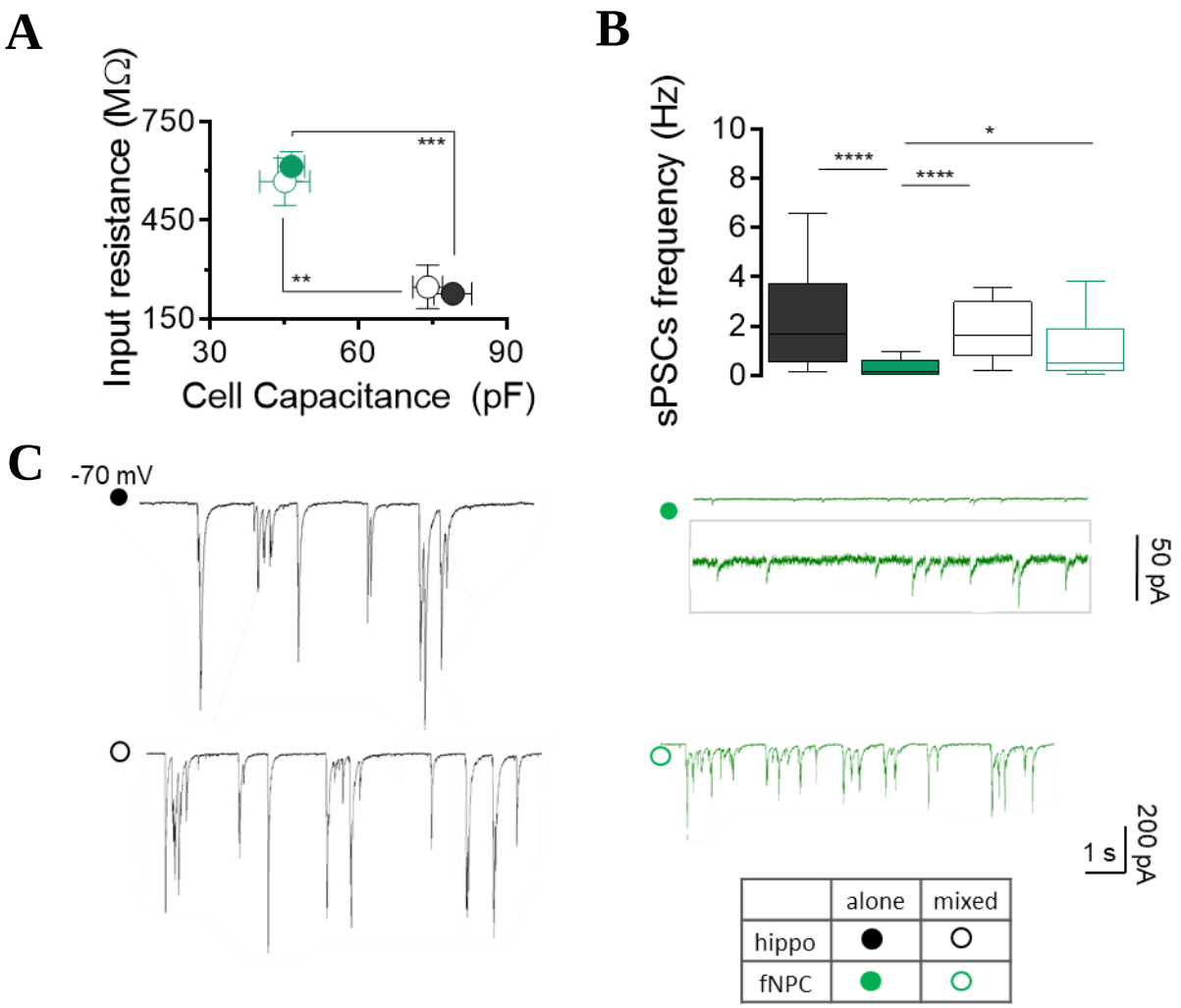

Figure 8. Exploit early activity to evaluate integration rate

On the bottom right, a **s**ketch representative of the symbol legend identifying hippocampal neurons and fNPCs, when cultured alone or when co-cultured. A) The plot indicates cells membrane passive properties. B) The box plots summarizes the frequencies values in all tested conditions. C) Representative traces of spontaneous PSCs recorded from all conditions: monocultures on the top and mixed cultures on the bottom. Note the inset with different scale to highlight fNPCs activity. *P<0.05, **P<0.01, ****P<0.0001, Kruskal-Wallis.

5.2 The impact of conditioned media on fNPCs development

In the study of co-cultures, there are several factors that could have a fundamental role on fNPCs development. Among them we investigated in details: (1) growth time, expressed as weeks of *in vitro* growth (pag. 60), (2) the neuronal activity, refferred as action potentials generation, (3) the role of astrocytes as feeding and supporting cells, (4) the level of contact between co-cultured cells. Concerning the last point, when neurons are forced to grow in narrow contact, they may develop functional synapses which of course play a fundamental role on network evolution. However, similarly, they could release paracrine factors which may be ultimately relevant. Cells producing paracrine factors secrete them right into the immediate extracellular environment, traveling to nearby cells in which the gradient of factor received determines the outcome. Different experiments were designed to gain insights about the boost of fNPCs develompment in co-cultures considering the hippocampal neurons and astrocytes soluble components as major player. Since the exact distance that paracrine factors can travel is not certain, the use of cell culture medium conditioned by hippocampal neurons and astrocytes, appears to be an ideal manner to approach this issue. By definition, conditioned medium is spent media harvested from cultured cells. It contains metabolites, growth factors, and extracellular matrix proteins secreted into the medium by the previously cultured cells. Examples of each might include: metabolites such as glucose, amino acids, and nucleosides; growth factors such as interleukins, EGF (epidermal growth factor), and PDGF (platelet-derived growth factor); and matrix proteins such as collagen, fibronectin, and various proteoglycans. Numerous studies demonstrates the advantages of diverse conditioned media on fNPCs maturation (Moon et al., 2019)(Matsui and Mori, 2018).

Methods

Cultures of dissociated hippocampal neurons and fNPCs were prepared as already explained (pag. 60). Primary brain glial cultures were obtained as described at pag x.

Culture medium from hippocampal neurons and from astrocytes samples was collected after one week of conditioning and administrate to newly plated fNPCs samples in 1:1 ratio with fresh medium. fNPCs conditioned and non-conditioned samples were grown, at 37 °C, in a humidified atmosphere with 5% CO_2 for 2 weeks and then tested by electrophysiological experiments performed as previously descrived (pag. 3360). Immunofluorescence experiments were perfomed as described above (pag. 33).

Results and discussions

Electrophysiological data showed significative difference between fNPCs grown in hippocampal neurons conditioned medium if compared to their control. Membrane passive properties of treated cells (n = 73) displayed a decrease in input resistance values from 379 MΩ to 222 MΩ if compared to fNPCs grown in control conditions (n = 94); this was associated with a parallel increase in cell capacitance values from 61 pF to 69 pF respectively. Also resting membrane potential value of conditioned cells (-58 mV) was significativly different if compared to control (-48 mV). These results seem to indicate the presence, in the conditioned medium, of soluble factors released by post mitotic neurons which largely impacted single cells development. Concerning spontaneous activity, it is present a considerable increase in sontaneous PSCs frequency from 0.2 Hz to 0.8 Hz (Figure 9).

Taken together this data show a different development of fNPC grown in conditioned medium both in terms of single cell properties and network activity, depicting a precise phenotype similar to the one obtained from fNPCs directly co-cultured with hippocampal neurons (pag. 60). However, differently from fNPCs totally integrated in muxed cultures, in this case single cells and network values tend to reseamble more fNPCs characteristics found in control conditions, rather than hippocampal neurons ones. Such fNPCs improvement in the maturation rate suggests that enriched culture media contained biologically active components, released from previously cultured hippocampal neurons, that have a fundamental role in affecting certain cell functions. Trying to assess if the soluble component was majorly produced by neurons or astrocytes, we also incubated fNPCs with conditioned medium purerly obtained by astrocytes. In this case no electrophysiological experiments were performed because, as shown by the immunofluorescence data in Figure 10, the totality of plated cells converted into astrocytes within hours after the conditioning. Aware of serum well-known effect on stem-like cells, FBS-free conditioned medium from astrocytes cultures was administrate to fNPCs, but the same phenomenon was observed (data not showed).

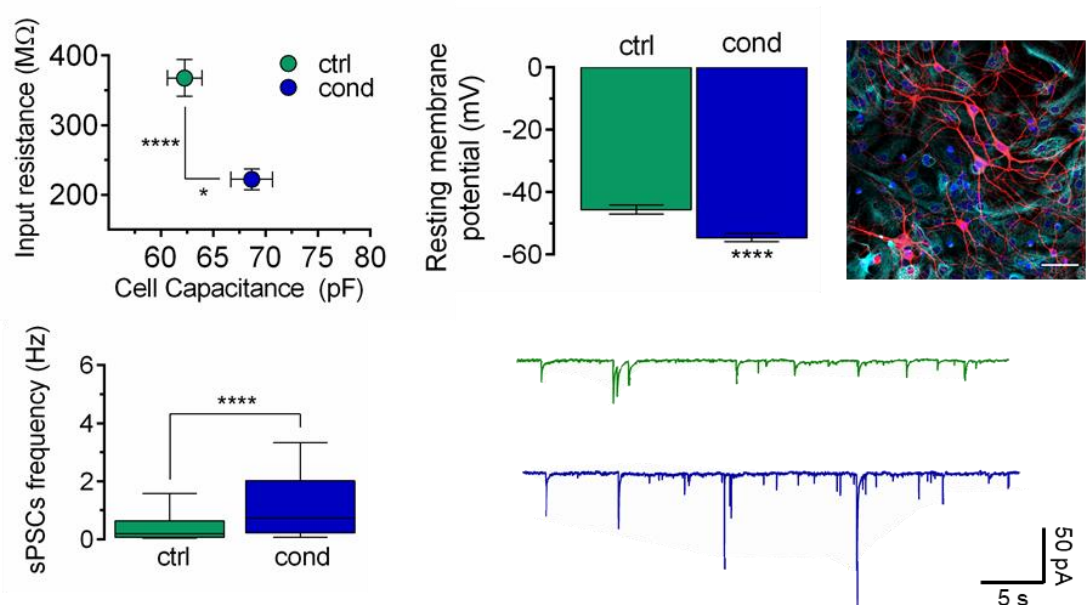

Figure 9. The impact of conditioned media

The plots on the top compare membrane passive properties of fNPCs grown in control conditions and treated with the hippocampal neurons conditioned medium in terms of cell capacitance, input resistance and resting potential (histograms). Top on the right is shown a representative immunofluorescent picture of the treated culture (β-tubulin III in red, GFAP in cyan, DAPI in blue; scale bar 50 µm). The box plot on the bottom displays a significative increase in frequency for the treated cultures. Representative traces recorded from control (green) and conditioned fNPCs (blue) are shown. *P<0.05, ****P<0.0001, Mann Whitney test.

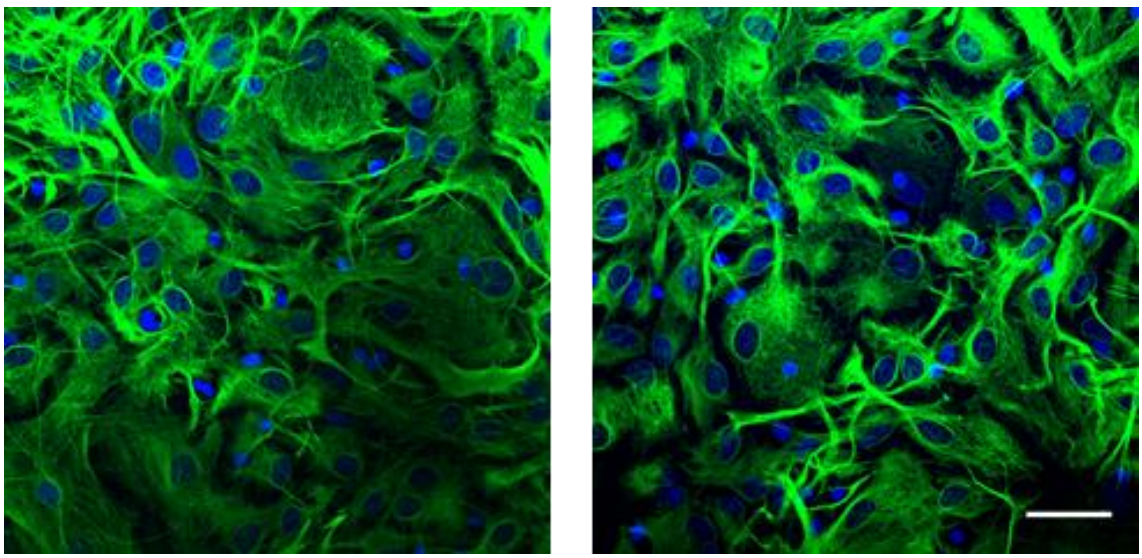

Figure 10. The impact of astrocytes

Representative immunofluorescent images of astrocytes-conditioned fNPCs cultures (β-tubulin III in red, GFAP in green, DAPI in blue; scale bar 50 µm) 24 hours (left) and 7 (right) days after plating.

5.3 Pair pulse ratio

The study of synapses has been a fundamental point in the whole study. Recording from mix pairs in mixed cultures allowed evaluation of several synapses parameters at many levels. For instance, synapses exhibit several forms of short-term plasticity that play several computational roles. Short-term depression suppresses neurotransmitter release for hundreds of milliseconds to tens of seconds; facilitation and post-tetanic potentiation lead to synaptic enhancement lasting hundreds of milliseconds to minutes (Fioravante and Regehr, 2011). Hence, short-term synaptic plasticity has been an additional parameter evaluated by performing paired pulse experiments. Paired pulse ratio (PPR) reflects the release probability of the presynaptic cell: if the presynaptic cell has high release probability, then the first pulse will deplete the available transmitter, and the second pulse will cause less transmitter to be release, leading to paired pulse depression a (PPD). If the presynaptic cell has a low release probability, then the first spike will cause a small postsynaptic response, but the build-up of calcium in the presynaptic terminal will lead to an increased release probability on the second spike and as a result, greater transmitter release and a greater postsynaptic response, and a paired pulse facilitation (PPF).

Methods

Cultures of dissociated hippocampal neurons and fNPCs were prepared as already explained (pag. 33). Electrophysiological recordings were performed as described at pag 33, as well as the pair recording studies. To evaluate PPR, the stimulation protocol was set at 20 Hz firing frequency into the pre-synaptic neurons while post-synaptic currents were evaluated in terms of ampliude.

Results and discussions

Pair pulse facilitation (or depression) is a form of short-term synaptic plasticity studied by evoking two presynaptic spikes in close succession and by measuring the responses of the postsynaptic cell in terms of PPR which measures the postsynaptic response to the second presynaptic spike over the response to the first one. In this study, by investigating synpasis we found, as first result already discussed above (pag. 25), higher number of mono-synaptically connected neurons recalled in the histograms in Figure 11. In hippocampal neurons, among 16 paired neuorons, PPD was mainly observed (69% as indicated by the black symbol in the plot in Figure 11) with an average ratio value of 0.79 ± 0.05 (also indicated as 21% of depression after the first PSC). The remaining 31% of

PPF show 14% of facilitation, also summarized by the black symbol in the plot in Figure 11. To reveal any specific link between the kind of synapsis and the relavite plasticity, further analysis was performed by classifing the τPSC in relation to the consequent short term plasticity. In hippocampal neurons, slow τPSC were involved in the same way in PPF and PPD (31% and 38% rispectively), while all fast τPSC were involved in phonomena of short term depression. Concerning fNPCs, as none fast τPSC was ever recorded in the study of synapses as already descrived above (pag. X), all recorded values for short term plasticity originated from slow τPSC in a majority of PPD (74%). In mixed cultures, the highest rate of PPF has been found (40%) and, as in the case of hippocampal neurons, slow τPSC were involved in the same way in PPF and PPD (40% and 45% rispectively). Average value of short term plasticity were 22% of depression and 17% facilitation (summarized by the empy green symbol in the plot in Figure 11). It was needed to investigate this feature due to the fact that our system is completely new, even if no significative difference were found between the three groups in this case.

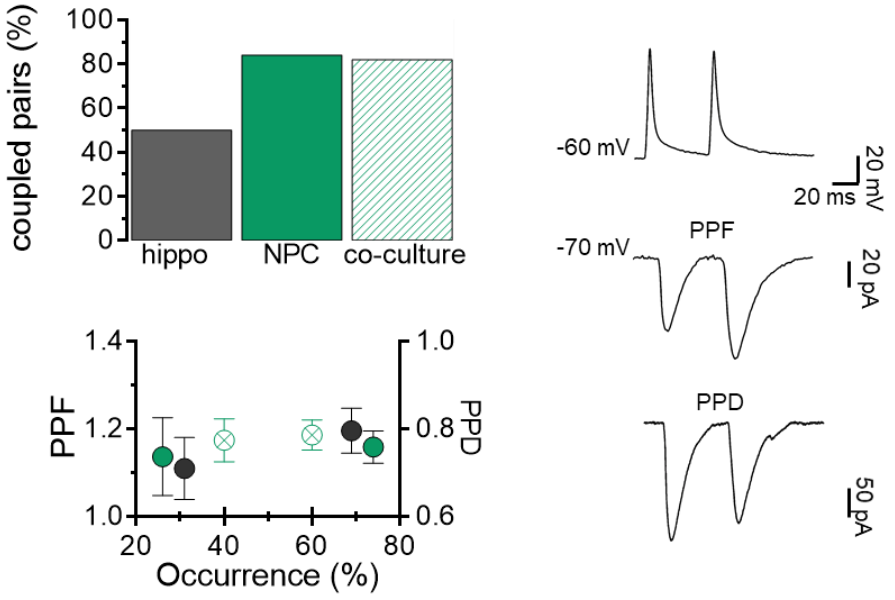

Figure 11. Pair pulse ratio

Representative traces of evoked PPF and PPD on the right. The histograms on the top represent the percentage of the mono-synaptically connected neurons found in the three conditions. The plot on the bottom display the occurrence in percentage of PPF and PPD among the recorded paired neurons; on the Y axes the relative mean value of each ratio (symbol legend: black for hippocampal neurons, green for fNPCs and empty green for mixed pairs).

5.4 Dopaminergic neurons and fNPCs

The idea to evaluate fNPCs' capability to differentiate and integrate among post-natal cells was extended by using cultures obtained from different brain regions. Besides the hippocampus, also neurons derived from Substatia Nigra Compacta (SNc) and Ventral Tegmental Area (VTA) were studied as possible host cells as they offer unique features detectable as new variables *in vitro*.

Methods

Primary cultures of SNc and VTA neurons were obtained from neonatal rat pups (Wistar). Briefly, SNc-VTA area was dissected from midbrain slices and dissociated by following a threee steps enzimatic procedure: (1) coarse pieces of SNc-VTA region were first digested in presence of trypsin (Sigma-Aldrich T1005) and deoxyribonuclease (DNAse - Sigma-Aldrich D5025-150KU) for 5 minutes at 37°C; (2) coarse pieces of SNc-VTA region were then treated with trypsin inhibitor (Sigma-Aldrich T9003) for 10 minutes at 4°C; (3) final mechanical dissociation was performed in presence of DNAse. Cells were then filtered (0.7 µm), centrifuged (100 *g* for 5 m) and resuspended in culture medium. Culture medium was composed of Neurobasal™-A Medium (Gibco™ 10888022), 2% B-27™ Supplement (Gibco™ 17504044), 1% GlutaMAX™ Supplement (Gibco® 35050061) and 0.05% gentamicin (50mg/mL) (Gibco® 15710-049). Samples were prepared by plating cells on poly-L-ornithine-coated (Sigma Aldrich P4957, 0.01% solution) round glass coverslips (12 mm Ø, 0.17 mm thickness) at a density of 330 cells/mm^2 and incubated at 37 °C, 5% CO_2 for 15-17 DIV.

fNPCs mono-cultures and mixed cultures were prepared as already described (pag. X) but by using higher cell density (330 cells/mm^2) to help SNc-VTA neurons survive. Electrophysiological and immunofluorescence experiments were performed as already described (pag. 33) plus the application of anti-Tyrosine Hydroxylase (TH) antibody (Merk T2928, dilution 1:300) to reveal dopaminergic neurons.

Results and discussions

Using established protocols, we co-cultured proliferating fNPCs and cells from SNc-VTA regions in 1:1 ratio. After 15-17 DIV, immunofluorescence data were collected by identifying β-tubulin III-positive cells as neurons and TH-positive cells as dopaminergic ones (Figure 12). Cell density analysis showed significative higher number of neurons in mixed cultures (113.6 ± 10 cells/mm^2) if compared with SNc-VTA cultures (58.3 ± 4

cells/mm^2). This may be explained by considering that proliferation ability of fNPCs can be retained for 7 days after plating as confirmed by BrdU labeling experiments (data not showed). Immunofluorescence data analysis did not revealed a difference in the density of TH-positive neurons in the two conditions (histograms in Figure 12). In fact, samples from SNc-VTA cultures (n = 4 samples) showed almost the same neuronal density expressed as β-tubulin III- and TH-double positive cells (13 ± 3 cells/mm^2) than mixed cultures (15 ± 2 cells/mm^2). In these samples, also β-tubulin III- and eGFP-double positive cells have been analyzed, but none showed the dopaminergic phenotipe meaning that fNPCs did not express the capability to syntetize dopamine in these conditions.

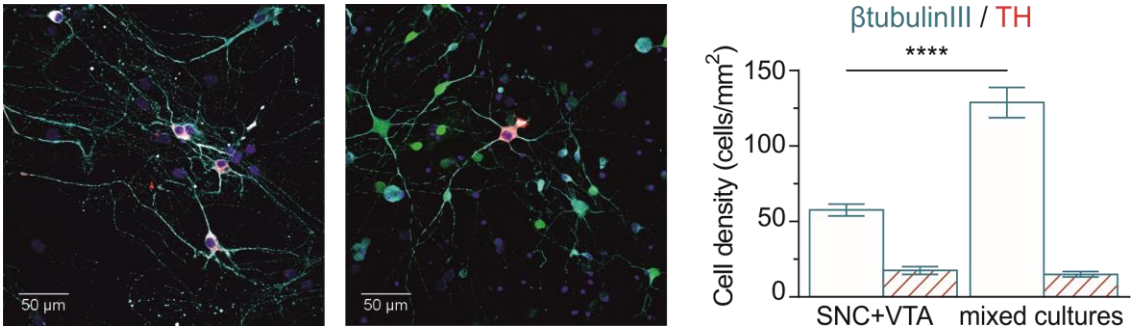

Figure 12. Dopaminergic neurons

Representative immunofluorescence micrograph of SNc-VTA sample (left) and mixed culture (right) at two weeks *in vitro*: labeled for neurons (β-tubulin III in cyan), dopamine (TH in red) and eGFP expressing cells (only fNPCs). Histograms quantifying density of neurons and relative presence of TH-positive cells (dashed red). ****P<0.0001, Student T-test

To investigate cells membrane passive properties and synaptic activity, we used whole-cell patch-clamp technique. Neurons from SNc-VTA cultures and fNPCs plated on poly-ornithine coated glass coverslips were compared in control conditions (grown alone) and in mixed cultures. fNPCs grown in mixed cultures (fNPCs$_{mixed}$) displayed values of cell capacitance and input resistance (46.1 pF and 484 MΩ rispectively, n = 24; see plot in Figure 13) similar to their control (fNPCs) (51.4 pF and 483.1 MΩ respectively, n = 23). Surprisingly, neurons from SNC-VTA recorded in mixed cultures (SNc-VTA$_{mixed}$) show a slight increase in terms of input resistance (458.7 MΩ, n = 23) if compared to their control (321.5 MΩ, n = 49) and a significative higher value of cell capacitance (59.8 pF) in relation to fNPCs$_{mixed}$. Resting membrane potential values (Figure 13) confirm a considerable change in term of membrane passive properties for cells grown in mixed cultures if compared to their control.

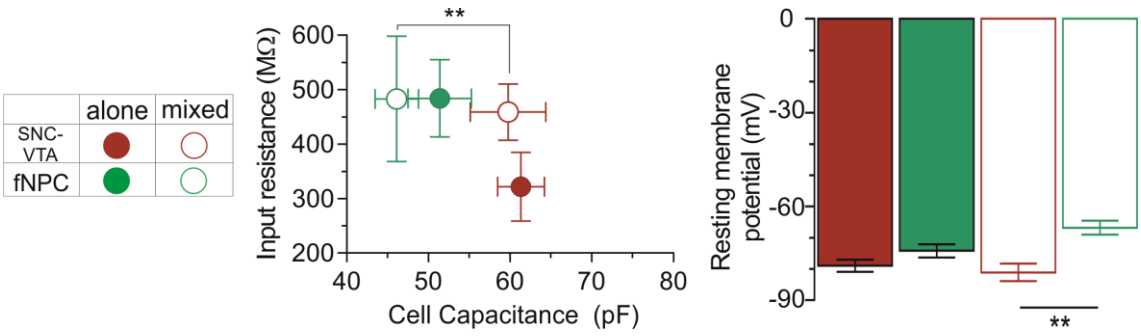

Figure 13. SNc-VTA neurons' passive membrane properties

Sketch representative of the symbol legend identifying SNC-VTA neurons (red) and fNPCs (in green), when cultured alone (filled circle) or when co-cultured (open circle). The plot summarizes the SNc-VTA neurons and fNPCs passive membrane properties. Histograms quantifying resting membrane potential values. ** P<0.001 Kruskal-Wallis test

To investigate fNPCs integration in the neural network, we monitored the occurrence of spontaneous postsynaptic currents (PSCs) as clear evidence of functional synapse formation and index of network efficacy. Spontaneous synaptic activity in our recording conditions was manifested by inward currents made up by a mixed population of inhibitory ($GABA_A$-receptor mediated) and excitatory (glutamate AMPA-receptor mediated) PSCs, characterized by different kinetics properties (overlapped currents showed in Figure 14).

The activity recorded from SNc-VTA neurons (n = 36) was represented by inward currents of variable amplitude (representative traces are shown in red in Figure 14) occurring at a frequency of 1.6 Hz (boxplot in Figure 14). fNPCs displayed a significant lower frequency (0.46 Hz) of sPSCs, compared to SNc-VTA neurons. On the other hand, no significant differences were detected in the average amplitude values of the recorded sPSCs between the two groups (34.8 pA evarage value, n = 48). To gain insights about the synaptic activity in the neural network, we performed offline differential analysis of sPSCs kinetic, in particular of their decay (Lovat et al., 2005). Based on their kinetic, we identified slow decaying PSCs (τ = 23.7 ± 1.5 ms) corresponding to $GABA_A$-receptor mediated events from fast decaying (τ = 3.1 ± 0.3 ms) events usually corresponding to AMPA-receptor mediated currents. The frequency of both currents occurred with some differences in the two cultures types: SNC-VTA neurons displayed most of glutamatergic currents (~90%) while in fNPCs we find a majority of GABAergic ones (~84%).

Electrophysiological recordings in mixed cultures were performed on eGFP-positive ($fNPCs_{mixed}$) and non-positive neurons. In this condition, both eGFP-non-positive cells (n = 20) and $fNPCs_{mixed}$ (n =20) showed a significative change in terms of sPSCs frequency that rise up to 2.6 and 2.3 Hz respectivly (Figure 14), in parallel with changes in occurrence of glutamatergic currents for $fNPCs_{mixed}$ that reach the 82% of the total sPSCs. Such a change may indicate, beside the integration and different maturation of $fNPCs_{mixed}$ among SNc-VTA neurons, the formation of a new neuronal network where both cell types interact in a synergic way.

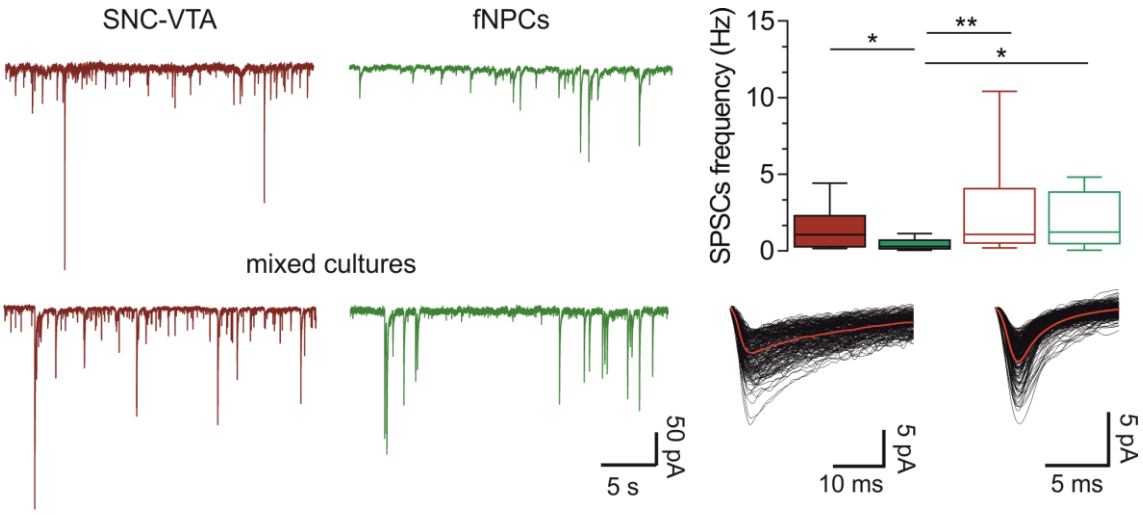

Figure 14. Spontaneous post synaptic activity in SNc-VTA cultures

Representative traces of electrophysiological recordings for SNc-VTA neurons (in red) and fNPCs (in green) when cultured alone (top) and in mixed cultures (bottom). Boxplot summarizing median frequency value of recorded sPSCs in all condition (filled box for control conditions and empty box for mixed cultures). Representative overlapped traces of different current types distinguished by the decay time.

To better study the integration between fNPCs and SNc-VTA neurons in the mixed network we investigated the synapses by performing pair recordings. By using two different patch-clamp configurations we induced an action potential in the pre-synaptic neurons (hold in current clamp mode at -70 mV) and evaluated the response in the post-synaptic one (hold in voltage clamp mode at -70 mV). The percentage of mono-synaptically connected neurons found in fNPCs cultures (n = 8 pairs) was very high (~70%) if compared to SNc-VTA neurons ones (22%, n = 9 pairs); this is a characteristic retained in mixed cultures were the percentage of mono synaptically connected neurons was doubled if compared to SNc-VTA cultures (n = 32 mix pairs, 47%) as depicted by

the plot in Figure 15. In all cases the post-synaptic response could be identified based on the decay time, as stated before (representative traces are showed in Figure 15 – slow τPSCs on the top and fast τPSCs on the bottom). fNPCs pairs displayed 100% of GABAergic synapses (τ = 30.1 ± 2.1 ms) while SNc-VTA pairs only 50% of founded synapses were GABAergic with τ = 37.7 ms. Also in this aspect, mixed cultures revealed a completely different phenotype by presenting 80% of glutamatergic synapses (τ = 4 ± 1.1 ms) in mix pairs. Percentage of mono-synaptically connected neurons and relative occurrence of slow τ responses is summarized in Figure 15 (plot top right).

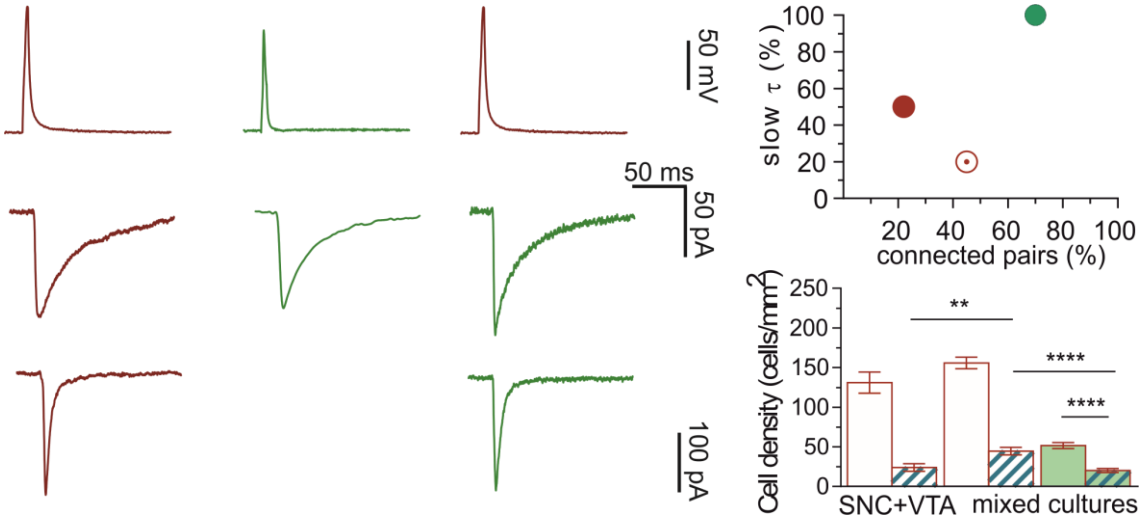

Figure 15. Pair recordings in SNc-VTA cultures

Representative traces of induced pre-synaptic action potentials (top) and evoked post-synaptic responses (bottom). Holding potential = -70 mV. Different colors identify SNc-VTA neurons (red) and fNPCs (green), when recorded alone or when recorded in mixed cultures. In SNc-VTA and mixed pairs, post-synaptic responses were represented by both slow and fast τPSCs (top and bottom respectively). Plot (top right) indicates the percentage of mono-synaptically connected couples found in the three condition and the relative percentage of slow τPSCs. Histograms (bottom right) quantify the % of double βtubIII (red) and GABA-positive (cyan internal pattern) neurons. Also, the % of triple positive βtubIII-GABA-eGFP neurons is highlighted in green in mixed cultures. **P<0.01, ****P<0.0001, Kruskal-Wallis.

To have a deeper understanding about this phenomenon, we also performed specific immunostainings by labeling cells with anti-β-tubulin III and anti-GABA antibodies. We found a significative different phenotype among the two conditions (histograms in Figure 15): in SNc-VTA samples (n = 8 samples), double β-tubulin III- and GABA-positive cells density is 24 ± 5 cells/mm^2 and in mixed culture (n = 9 samples) the value is 45 ± 5

cells/mm^2. Also, the density of triple β-tubulin III-GABA-eGFP-positive cells in mixed culture is highlighted in green (20 ± 2 cells/mm^2 on a total of 52 ± 4 cells/mm^2 β-tubulin III-eGFP positive ones), indicating that the fNPCs changed the usual GABAergic phenotype described above (pag.25). To sum up, the hybrid network found in mixed cultures shows very different features if compared to its relative components grown in mono-cultures. In tems of single cells maturation, the mixed culture doesn't represent an environment promoting membrane passive properties development while, looking at voltage-clamp recordings, we found significative difference in PCSs type and spontaneous frequency. At the level of the synapses, into the investigated ones higher presence of fast τPSCs is confirmed together with a higher (almost double) contacts formation. Despite an higher PCSs frequency, the aboundancy of fast τPSCs (not found in any of the controls) indicates a different network's development. By immunolabeling, we detected a higher number of GABAergic neurons in mixed cultures if compared to SNc-VTA samples which is in contrast with the electrophysiological data. From previous studies it is known that fNPCs cultured alone display a very high level of GABA-positive cells, and this is reflected by the functional, electrophysiology, results (pag. 25). Collected data in this study suggest that fNPCs, when cultured with SNc-VTA are not entirely affected by SNc-VTA mature neurons and their influence on the emerging mixed network is not clear. Therefore, the hybrid network found in the mixed cultures deserve further investigation to understand how and where the new interactions create such changes and what is the role of such GABAergic neurons.

5.5 *Foxg1* upregulation enhances neocortical projection neuron activity.

Wendalina Tigani[1,§], Moira Pinzan Rossi[1,2,§], Osvaldo Artimagnella[1], Manuela Santo[1], Rossana Rauti[3,4], Teresa Sorbo[3], Francesco Paolo Severino Ulloa[5,6], Giovanni Provenzano[7], Manuela Allegri[8], Matteo Caleo[8], Laura Ballerini[3], Yuri Bozzi[7], Antonello Mallamaci[1,*]

Affiliations

(1) Laboratory of Cerebral Cortex Development, SISSA, Trieste, Italy

(2) *present address:* AgenTus Therapeutics, Inc., Cambridge UK

(3) Laboratory of Neurons and Nanomaterials, SISSA, Trieste, Italy

(4) *present address*: Dept. Biomedical Engineering, Tel Aviv University, Tel Aviv, Israel

(5) Laboratory of Bionanotechnologies, SISSA, Trieste, Italy

(6) *present address*: Cell Biology Dept, Duke University Medical Center, Duke University, Durham, NC-USA

(7) Laboratory of Molecular Neuropathology, Centre for Integrative Biology (CIBIO), University of Trento, Italy.

(8) CNR Neuroscience Institute, National Research Council (CNR) Pisa, Italy.

(§) equally contributing authors

(*) corresponding author

Corresponding Author

Antonello Mallamaci

Lab of Cerebral Cortex Development

SISSA

via Bonomea 265 - 34136 Trieste - Italy

phone: +39 040 3787 717

e-mail: amallama@sissa.it

Key words

Foxg1, West syndrome, neuron hyperactivity, immediate early genes

ABSTRACT

Foxg1 is an ancient transcription factor gene orchestrating a number of neurodevelopmental processes taking place in the rostral brain. In this study we investigated its impact on activity of neocortical pyramids. We found that mice overexpressing *Foxg1* in these neurons displayed an EEG with increased spike frequency and were more prone to KA-induced seizures. Consistently, primary cultures of neocortical neurons made gain-of-function for *Foxg1* were hyperactive and hypersynchronized. That reflected an unbalanced expression of key genes encoding for ion channels, GABA and glutamate receptors. It was likely exacerbated by a pronounced interneuron depletion. We also detected a transient *Foxg1* upregulation ignited by neuronal activity and mediated by immediate early genes. Based on this, we propose that even small changes of Foxg1 levels may result in a profound impact on pyramids' activity, an issue relevant to neuronal physiology and neurological aberrancies associated to *FOXG1* copy number variations.

INTRODUCTION

Foxg1 is a pleiotropic effector mastering a variety of neurodevelopmental subroutines occurring within the rostral brain. It specifies the telencephalic field (Hanashima et al. 2007), promotes subpallial programs (Manuel et al. 2010), and activates paleo- and neocortical morphogenesis (Muzio and Mallamaci 2005). Besides, *Foxg1* stimulates neural precursors self renewal (Martynoga et al. 2005) and orchestrates temporal articulation of neocorticogenesis. Stable *Foxg1* silencing paves the way to Cajal-Retzius cells generation (Hanashima et al. 2004). A short-term decline of it followed by reactivation is instrumental to birth, radial migration, proper laminar commitment and architectural maturation of later born pyramidal neurons (Martynoga et al. 2005; Miyoshi and Fishell 2012; Toma et al. 2014; Chiola et al. 2018) *FOXG1* upregulation occurring in ASD patient-specific neuro-organoids has been reported to underlie an increase of neocortical interneurons, due to aberrant hyper-proliferation of their progenitors (Mariani et al. 2015). On the other side, ablation of one *Foxg1* allele decreases the number of these cells, due to their defective migration from basal forebrain (Shen et al. 2018). Moreover, a reduction of *Foxg1* levels also perturbs interneuronal maturation. It evokes neurite hypertrophy (Shen et al. 2018), it deregulates *Gad2* (Patriarchi et al. 2016) and reduces their electrical activity (Zhu et al. 2019). In this respect, a dampened interneuronal function has been suggested to contribute to seizures occurring in patients with structural *FOXG1* mutations (Mitter et al. 2018; Vegas et al. 2018). Finally, a reduction of *Foxg1* levels in neopallia stem cells is required for their progression to glial lineages (Brancaccio et al. 2010; Falcone et al. 2019).

We speculated that, in addition to its impact on dendritogenesis and laminar identity, persistent expression of *Foxg1* in pyramidal neurons might further modulate their functional regime. We tested this hypothesis *in vivo* and *in vitro*. We found that *Foxg1* upregulation in neocortical

pyramids increased their electrical activity and made *Foxg1*-GOF mice more prone to KA-induced seizures. Unbalanced expression of key genes implicated in GABAergic and glutamatergic transmission likely underlay these phenomena, possibly exacerbated by a concomitant reduction of interneurons and astrocytes. We also found that, in turn, a transient *Foxg1* upregulation was triggered by electrical activity. The resulting, "*Foxg1*/activity" reciprocal loop may make pyramidal neurons sensitive to even small changes of *Foxg1* expression products. That may be relevant to normal control of neocortical functional regime. It may account for neurological aberrancies stemming from *FOXG1* copy number variations (Florian et al. 2011; Seltzer et al. 2014).

MATERIALS AND METHODS

They include: Generation of lentiviral vectors, Mouse handling, Generation and selection of transgenic mouse lines, Histology, Brain immunofluorescence, EEG recordings, Behavioral observation of kainic acid-induced seizures, *In situ* hybridization, Cortico-cerebral cultures, Arc-SARE evaluation of neuronal activity, Ca^{2+} imaging evaluation of neuronal activity, RNASeq, Quantitative RT-PCR, Western blot analysis, Image acquisition, Statistical evaluation of results. For each of them, full details are provided in SUPPLEMENTARY INFORMATION.

RESULTS

Generation of transgenic mice overexpressing *Foxg1* in deep layer neocortical projection neurons. To investigate etiopathogenic mechanisms linking exaggerated *FOXG1* allele dosage to pronounced neuronal hyperactivity peculiar to West syndrome patients, we generated mice gain of function for *Foxg1*, by zygotic lentiviral transgenesis and TetON/OFF technology (**Fig. S1A)**. Three single-transgene-insertion, CD1-congenic male founders, “C”, “D” and “E” were obtained. They were scored for transgene expression, *in vitro* and *in vivo*. Two of them (C and D) performed very poorly and were discarded, the third one (E) was selected and employed for this study.

We investigated the *Tre-Foxg1-IRES-Egfp* spatial-temporal expression pattern in *Foxg1*$^{tTA/+}$*; Tg:Tre-Foxg1-IRES-Egfp*$^{+/-}$ compound mutants (Hanashima et al. 2002), and we compared it with the distribution of the Foxg1 protein, normally detectable throughout telencephalon since E9.5. We found that the transgene was activated at E14.5, when a weak Egfp signal, restricted to the neocortical field, could be found. (**Fig. S2A** and **S3A**). A stronger signal, again limited to neocortex, was detectable at E16.5 (**Fig. 1A, B** and **S2B**). This pattern remained substantially unchanged at later developmental ages (**Fig. 1C** and **S2C**), until P7 (**Fig. 1D, F** and **S2D**) and beyond (not shown). Within neocortex, transgene products showed a dynamic radial distribution. At E14.5, a faint signal was detectable in a few cells located in the uppermost cortical plate (**Fig.**

S3A, arrowheads). At E16.5 a large fraction of cortical plate cells were intensely immunoreactive for Egfp, which also stained large bundles of presumptive cortico-fugal fibers running within the subplate and below it (**Fig. 1B** and **S3B**). A similar pattern was retained at P0 and P7, when - however - the cortical plate signal was prevalently limited to deeper layers (**Fig. S3C**, upper row, and **S3D**) and the Egfp-positive fibers were clustered just above the subventricular zone (**Fig. S3C**, upper row, **and S3D**, arrows) and further detectable while crossing the striatal field (**Fig. S3C**, lower row, arrows)]. Remarkably, at no developmental age subject of analysis transgene activity was detectable within periventricular proliferative layers, where the endogenous *Foxg1* was conversely active, albeit at low levels (**Fig. 1B** and **S3A-C,** asterisks).

Next, we addressed the identity of neural cells expressing the transgene. We found that almost the totality of them were postmitotic neurons, co-expressing Egfp and two established pan-neuronal markers, Tubb3 and NeuN, at E16.5 through P7 (**Fig. 1C, D** and **S4**). Based on obvious morphological criteria (a thin apical dendrite emerging from a radially oriented soma (**Fig. 1C** and **S4**, arrows)), these cells turned out to be pyramidal neurons. Comparison of their P7 radial distribution with DAPI staining as well as with the profiles of three established layer-specific markers, FoxP2 (layer VI), Ctip2 (layer V) and Cux1 (layers IV-II) (Molyneaux et al. 2007), suggested a presumptive layer VI/V identity (**Fig. S5**). To corroborate specific *glutamatergic* identity of these cells, we coimmunoprofiled P7 and P15 brains for Egfp and three GABAergic interneurons' markers, parvalbumin (PV), somatostatin (SST) and calretinin (CR) (Wamsley and Fishell 2017). As expected, no Egfp colocalization with such markers was detected at all (**Fig. 1E**). Finally, we co-immunoprofiled transgenic P7 brains for Egfp and the astrocyte marker S100β (Raponi et al. 2007). Again, no colocalization was observed, confirming that transgene-expressing cells were deep layer projection neurons (**Fig. 1F**).

Neural hyperactivity-hyperexcitability of *Foxg1*-GOF mice

To assess the impact of neuronal *Foxg1* overexpression in neocortical projection neurons on brain activity, P41 *Foxg1*-GOF (*Foxg1*$^{tTA/+}$*;Tg:Tre-Foxg1-IRES-Egfp*$^{+/-}$) mice and wt controls were profiled by electroencephalography (EEG) in basal awake conditions. Electrical activity was monitored within the hippocampus. Albeit not expressing the transgene, in fact, this structure receives extensive neocortical afferences and reverberates them, so acting as a useful proxy of neocortical activity. A bipolar electrode was placed between Cornu Ammonis field 1 (CA1) and dentate gyrus (DG)/hilus regions (**Fig. 2A**). It was secured to the skull and electrical activity was monitored for three days, two hours per day. The EEG was inspected paying special attention to frequency and temporal distribution of spikes (**Fig. 2B**). Interestingly, both total spike frequency and interictal cluster frequency were increased by about 50% in *Foxg1*-GOF mutants as compared to controls (with n=4,4, and p<0.01 and p<0.02, respectively). Ictal cluster frequency was

increased >3 times, however this did not result statistically significant. Isolated spike frequency was unaffected. (**Fig. 2C**). Altogether, these data point to an appreciable increase of coordinated neuronal activity occurring in *Foxg1*-GOF mutants compared to controls.

Next, to corroborate these findings, we challenged *Foxg1*-GOF mutants (as well as *Foxg1*-LOF and wild type mice, as controls) with a proconvulsant glutamatergic agonist, kainic acid (KA). We administered P35 animals with 20 mg of KA per kg of body weight, by intraperitoneal injection, and monitored their behaviour over the following two hours. We specifically paid attention to signs of altered brain activity, such as immobility, rigid posture, head bobbing, forelimb clonus with rearing and falling, etc. Every 10 min, a score was given, according to Racine's staging criteria (Racine 1972) (**Fig. 3A**). The majority of animals did not go above Racine stage (RS) 3, repetitive movements & head bobbing (5/14, 12/17 and 7/9, in case of GOF, WT and LOF, respectively), a subset of them reached RS4, limbic motor seizure (4/14, 4/17 and 2/9, as for GOF, WT and LOF, respectively). Only a few got up to RS5, continuous rearing and falling, and more (5/14, 1/17 and 0/9 in case of GOF, WT and LOF, respectively) ($p<0.073$, χ-square test) (**Fig. 3B**). Longitudinal analysis of data showed that, for each genotype, RS increased progressively from the onset of the experiment to about 1 hour later, then smoothly declining. The RS(t) curve of the GOF group was on average 1.3 units above WT controls (the corresponding GOF/WT gap was only 0.3). In particular, the distance between the GOF and the WT curves peaked at 90 and 100 min, reaching 1.7 and 1.9, respectively, with $p<0.01$ (ANOVA) in both cases (**Fig. 3C**). Altogether, these data point to a remarkable increase of neuronal excitability, occurring in GOF models compared to controls, and rule out that such effect may stem from dominant negative effects.

Finally, upon completion of Racine tests, mice were sacrificed and their brains snap-frozen for subsequent analysis. Brains from animals of different genotypes, reaching different Racine's stages, were sliced and profiled by not radioactive in situ hybridization, for expression of the *Fos* immediate early gene. Within *Foxg1*-GOF brains, *Fos* was strongly activated throughout the hippocampus, including the dentate gyrus (DG), as well as in scattered neocortical cells. In case of *wt* brains, a strong *Fos* signal was present in CA3 and a weaker one in CA1 and DG. Finally, *Fos* activation in *Foxg1*-LOF brains was very weak, or not detectable at all (**Fig. 3D**). This scenario is consistent with behavioural data reported above and strengthens the hypothesis that a specific increase of neuronal excitability occurred in *Foxg1*-GOF mutants.

Histogenetic aberrancies of *Foxg1*-GOF mice

We hypothesized that the neurological profile of our mutants might first reflect gross histogenetic aberrancies, triggered by *Foxg1* overexpression in neocortical projection neurons.

To test this hypothesis, first, we scored *Foxg1*-GOF, P0 and P7 neocortices for their lamination pattern. At P0 (**Fig. 4A**), the layer VI marker FoxP2 was slightly down-regulated, the layer V marker Ctip2 spread into deeper grey matter and Cux1, normally expressed by layers IV-II, was dramatically downregulated. A consistent scenario was detectable at P7 (**Fig. S5**). Closely packaged in VI layer of WT neocortex, $FoxP2^+$ cells were loosely distributed through layers VI and V of GOF mutants. $Ctip2^+$ cells partially spread into layer VI (arrows). $Cux1^+$ layer IV-II was halved in its radial extension. All that points to defective segregation of layer V and layer VI neurons as well as to inhibition of layer IV-II programs.

Next, we inspected the neocortex of P35 GOF mutants for spatial frequency of GABAergic interneurons, expressing parvalbumin (PV), somatostatin (SST) and calretinin (CR). We detected a generalized reduction of PV^+ cells, (-42.57±3.27%, $p<0.0005$, n=3,6) particularly pronounced throughout layers VI-II and rostral neocortex. It did not reflect a dominant negative effect, as *Foxg1*-LOF mutants did not replicate it (**Fig. 4B** and **Table S1**). SST^+ and CR^+ interneurons were mainly unaffected, except a local decline of the former in white matter (-31.09±5.50%, $p<0.020$, n=3,3) and of the latter in medial neocortex (-61.25±14.42%, $p<0.009$, n=3,3) (**Fig. S6** and **Table S1**).

Last, we scored *Foxg1*-GOF cortices for $S100\beta^+$ astrocytes. At P0, the neocortical spatial frequency of these cells was reduced by 21.0±3.6% compared to *wt* controls ($p<0.05$). At the same age *Foxg1*-LOF mutants showed an opposite trend (+28.6±9.3%, compared to *wt*) and the difference between *Foxg1*-GOF and -LOF brains was statistically significant ($p<0.03$) (**Fig. 4C** and **Table S2**). At P7, *Foxg1*-GOF mutants still showed an reduction of $S100\beta^+$ astrocytes (-15.6±2.4%, $p<0.07$, n=3,6), specifically pronounced in lateral neocortex (-15.9±4.1%, $p<0.03$) as well as in layer I and II-IV (-26.4±2.6%, $p<0.05$, and -19.6±4.9%, $p<0.05$, respectively). As suggested by the different distribution of $S100\beta^+$ cells in *Foxg1*-LOF neocortices, this phenomenon hardly reflected a dominant-negative effect (**Fig. 4D** and **Table S2**). Intriguingly, *Fgf9*, a key promoter of astroblast proliferation (Seuntjens et al. 2009), was robustly downregulated in *Foxg1*-GOF mice (**Fig. S7**), suggesting that the decreased astroglial density peculiar to these mutants might originate from a non-cell autonomous, neocortical astrogenic deficit.

Hyperactivity of *Foxg1*-GOF neocortical cultures

To test the hypothesis that *Foxg1* overexpression increases neocortical activity, we generated *Foxg1*-GOF neocortical cultures by somatic lentiviral transgenesis and probed them by a genetically encoded, delayed activity-reporter (Kawashima et al. 2009). Specifically, DIV7 cultures originating from E16.5 neocortical precursors, harboring (1) a TetON-controlled *Foxg1*

transgene, (2) a d2EGFP reporter under the control of the "*Arc*-SARE-enhancer/minimal promoter (ArcSAREp)" neuronal-activity-responsive element, and (3) a constitutively expressed *PGKp-RFP* normalizer, were employed. Upon pre-terminal TTX silencing, they were stimulated by Bdnf and finally profiled by cytofluorometry (**Fig. 5A**). Signal specificity was assessed by dedicated, $Bdnf^{OFF}$ controls (not shown). Interestingly, the median d2EGFP/RFP fluorescence ratio, providing a cumulative index of neuronal activity over the previous 6 hours, was upregulated by 1.60±0.10 folds in *Foxg1*-GOF samples compared to controls ($p<0.003$) (**Fig, 5B**), suggesting that *Foxg1* overexpression promoted neuronal activity.

To strengthen these findings and get insight into cellular mechanisms underlying them, we re-investigated the impact of *Foxg1* on basal synaptic activity of neocortical cultures by fluorescence calcium imaging (Bosi et al. 2015; Rauti et al. 2016). Here, *Foxg1* was dampened by RNAi, or, alternatively, upregulated by TetON transgenesis. In the latter case, transgene overexpression was pan-neural (sustained by the *Pgk1* promoter), or restricted to astrocytes or to neurons (driven by *Gfap*- and *Syn*-promoters, respectively) (**Fig. 6A**). Fluorescence fluctuations were recorded and analysed by dedicated softwares. Three indices, representative of network activity, were calculated: (a) prevalence of spontaneously active neurons among total neurons; (b) occurrence of spontaneous Ca^2 episodes in active cells by cumulative distribution of inter-event intervals (IEIs, i.e. inter-calcium transients intervals); (c) neuronal activity synchronization by measuring cross-correlation factor (CCF) (**Fig. 6B-E**). Results were as follows.

We found that *Foxg1* knock-down reduced the prevalence of spontaneously active neurons (49% vs 83%, with $p<0.001$ and n=4,4) (**Fig. 6B**, panel 3), as well as their CCF (0.14±0.001vs 0.79±0.002, with $p<0.001$ and n=4,4) (**Fig. 6B**, panel 5). Moreover, *Foxg1*-LOF cultures were characterised by transient high frequency bursts of activity interspersed by prolonged silent periods (**Fig. 6B**, panel 2), resulting in a different cumulative distribution of IEIs ($p < 0.01$) (**Fig. 6B**, panel 4). In a few words, knocking down *Foxg1* caused a complex alteration in network dynamics, characterized by unevenly distributed calcium transients, restricted to less numerous, hypo-synchronized neurons.

As expected, generalized *Foxg1* overexpression conversely increased the prevalence of spontaneously active neurons (94% vs 18%, with $p<0.01$, n=3,3) (**Fig. 6C**, panel 3), as well as their CCF (0.90±0.04 vs 0.19±0.02, with n=3,1) (**Fig. 6C**, panel 5), while prevalently shortening their IEIs ($p<0.01$) (**Fig. 6C**, panel 4). That points to a strong functional impact of pan-neural *Foxg1* upregulation on synaptic networks, boosting neuronal activity.

Next, when *Foxg1* overexpression was limited to astrocytes, neither the prevalence of active neurons (29% vs 30%, with n=5,4) nor their CCF (0.9±0.02 vs 0.8±0.02, with n=5,4) were affected (**Fig. 6D**, panels 3,5). Instead, IEIs were significantly increased ($p<0.01$) (**Fig. 6D**, panel 4). This means that *neuronal Foxg1* upregulation is *necessary* to enhance network activity. It

further suggests that *Foxg1*-GOF astrocytes may somehow dampen neuronal activity better than control astrocytes.

Finally, restriction of *Foxg1* overexpression to the neuronal lineage increased the prevalence of active neurons (98% vs 31%, with $p<0.001$ and n=12,12) (**Fig. 6E**, panel 3), and their CCF (0.98±0.01 vs 0.40±0.01, with $p<0.001$ and n=12,12) (**Fig. 6E**, panel 5), while shifting cumulative distribution of IEIs significantly to the left ($p<0.001$) (**Fig. 6E**, panel 4**).** This means that neuronal *Foxg1* upregulation is not only necessary, but also *sufficient* to elicit a powerful stimulating effect on network activity.

Misregulation of *Foxg1*-GOF, neocortical neuron transcriptome.

To cast light on molecular mechanisms underlying overactivity of *Foxg1*-GOF neurons, we profiled the transcriptome of neuronal cultures originating from E16.5 neocortical precursors, transduced by a broadly expressed *Foxg1* transgene and allowed to age up to DIV8 in the presence of AraC. Four *Foxg1*-GOF and four control cultures were profiled. >20M paired reads/sample were collected and aligned against the reference genome, raw read counts were normalized as FPKM values, and results were finally filtered according to standard procedures. 11,500 out of 53,000 genes passed filtering. Among them, 7582 resulted to be differentially expressed in *Foxg1*-GOF vs control cultures (with $p<0.05$ and FDR<0.05). 3876 were upregulated (1816 of them >2-folds) and 3706 downregulated (1631 of them >2-folds). As positive controls, *total Foxg1*-mRNA was increased by 4.4-folds, *Arc* and *Hes1*, expected to robustly arise upon *Foxg1* overexpression (see **Fig. 7** and (Chiola et al. 2018)), were upregulated as well, by 6.6-folds ($p<5.31*10^{-54}$, $FDR<2.53*10^{-52}$) and 34.9-folds ($p<1.12*10^{-136}$, $FDR<2.93*10^{-134}$), respectively, *Emx2* and *Tbr1*, normally dampened by *Foxg1* (Muzio and Mallamaci 2005; Toma et al. 2014), were downregulated by -50.1% ($p<1.26*10^{-03}$, $FDR<3.57*10^{-03}$) and -14.5% ($p<8.31*10^{-03}$, $FDR<1.93*10^{-02}$), respectively (**Table S3**).

To get hints about molecular mechanisms underlying abnormal activity of *Foxg1*-GOF neurons, we focused our attention on specific sets of differentially expressed genes, linked to intracellular signal integration and synaptic transmission. Among them, genes encoding for: (1) plasma membrane, voltage-dependent Na^+, K^+ and Ca^{2+} channels, including those belonging to *Scn*, *Kcn* and *Cacn* families (Catterall 2005; Johnston et al. 2010; Zamponi et al. 2010; Shah and Aizenman 2014), as well as pumps and channels mediating Ca^{2+} fluxes among cytoplasm, ER, mitochondria and extracellular spaces, i.e. PMCAs, NCXs, NCKXs, SERCAs, MCU-, SOCE-, CICR- and IICR-effectors (Kwon et al. 2016; Raffaello et al. 2016); (2) glutamatergic and GABAergic receptors (*Grm*, *Gria*, *Grik*, *Grin*, *Gabr)* (Traynelis et al. 2010; Jembrek and Vlainic 2015; Crupi et al. 2019); (3) neuromodulator receptors (*Chrm*, *Chrn*, *Adr*, *Htr*, *Drd*, *P2rx*, *P2ry*) (Gu 2002); and (4) selected structural components of synapses (Monteiro and Feng 2017). Results were

highly articulated and included a large subset of expression level variations likely contributing to enhanced neuronal activity and synchronization (**Table S3**).

We found a widespread upregulation of *Scn* genes. *Scn1a,* mainly restricted to PV^+ interneurons and required for their inhibitory activity (Sun et al. 2016), was conversely decreased by about 4-folds. Quantification of *Kcn* genes did not show any simple shared trend. *Kcc2*, promoting the transition from GABA-driven depolarization to hyperpolarization (Clayton et al. 1998; Rivera et al. 1999), was upregulated >3-folds. Members of *Cacna1, Cacnb* and *Cacng* subfamilies were prevalently increased and the *Cacna2d2/Cacna2d1* ratio was specifically upregulated by about 28-folds, all pointing to a possible increase of *Cacn*-dependent Ca^{2+} currents (Dolphin 2016). A complex expression pattern was also displayed by other gene sets mastering Ca^{2+} exchanges among cytoplasm and other cell compartments. Implicated in Ca^{2+} extrusion to cell exterior, PMCA-encoding *Atp2b2-4* and NCX-encoding *Slc8a1-3* were upregulated, NCKX-encoding *Slc24a2,4* down-regulated. SOCE effector-encoding genes *Stim1* and *Orai2,* promoting Ca^{2+} influx from cell exterior, were upregulated. Involved in release of ER Ca^{2+}, CICR- and IICR machinery genes *Ryr1,2* and *Itpr1,3,* were down- and up-regulated, respectively. SERCA-encoding *Atp2a2,* implicated in ER Ca^{2+} uptake, was downregulated. Finally, three repressors of the MCU machinery, mediating mitochondial Ca^{2+} uptake, *Mcub*, *Micu2* and *Micu3*, were downregulated, and its stimulator *Slc25a23* was upregulated, altogether prefiguring an increased activity of this machinery.

Next, genes encoding for ionotropic glutamatergic receptors showed a pattern definitively consistent with increased neocortical activity. *Grik1*, restricted to interneurons (Paternain et al. 2003), was downregulated, *Grik3,* active in pyramids and encoding for the principal GluK3 subunit (Wisden and Seeburg 1993), was upregulated, *Grik4* and *Grik5,* both essential for the normal ionotropic function (Fernandes et al. 2009), were increased as well. As for *Gria* family, both *Gria2,* decreasing Ca^{2+} permeability of AMPA receptors, (Sanchez et al. 2001) and *Gria4*, needed to prevent epileptic seizures (Beyer et al. 2008), were downregulated. Finally, concerning *Grin* genes, in addition to *Grin1* decline, *Grin2c*/*Grin2a* and *Grin2d*/*Grin2a* ratios were dramatically upregulated, pointing to likely prolonged opening times of NMDA receptors (Paoletti et al. 2013). *Grin3,* normally limiting Ca^{2+} permeability of these receptors (Wada et al. 2006), was downregulated. Moreover, a collapse of key genes implicated in GABAergic conduction and GABA-mediated homeostasis, *Gad1*, *Gad2, Gabra1, Bdnf* **(Fig. S8** and (Hong et al. 2008)), was also detected.

Dynamics of neuromodulator receptor genes (Gu 2002) was very complex. It included alterations with a potential pro-excitatory (*Chrnb4*, *Adra1b*, *Htr3a, Htr6* and *P2rx4* upregulation, as well as *Grm2* and *Grm8* decline) or pro-inhibitory outcome (*Adra1a* and *P2rx2* downregulation as well as *Grm4* and *Drd2* upregulation). Similar considerations apply to modulation of structural

synaptic genes, some upregulated (e.g., *Homer2*, *Nrxn2,3* and *Shank1,2*), some decreased (e.g. *Homer1*, *Nlgn1*). Finally, a misregulation of layer-specific genes was also evident (**Table S4)**. It included a widespread downregulation of layer 2-4, layer 6 and subplate markers and an upregulation of layer 5 ones, consistent with the laminar phenotype displayed by *Foxg1*-GOF mice (**Fig. 4A** and **S5**).

To strengthen these results, we evaluated mRNA levels of a subset of differentially expressed genes, in sister preparations of *Foxg1*-GOF cultures employed for Ca^{2+} imaging assays, by qRTPCR. To note, here we restricted *Foxg1* overexpression to neurons, under the control of *pSyn* promoter. Moreover, we omitted AraC, so allowing neurons to mature in more biologically plausible conditions, i.e. in the presence of a large astrocyte complement. Interestingly, qRTPCR analysis of these samples reproduced the variation pattern previously detected in RNASeq assays (*Scn11a*, *Grik3*, *Grik4 and Grin2c* upregulated, *Scn1a*, *Grin2a*, *Gabra1*, *Gad1*, *Gad2* and *Bdnf* downregulated, **Fig. 7**), corroborating the scenario emerging from these assays.

Interneuron depletion

We further wondered if, similarly to our *Foxg1*-GOF mouse models, a misregulation of the GABAergic-to-glutamatergic neuron ratio could occur in *Foxg1*-GOF primary preparations, contributing to their abnormal behavior. For this purpose, we set up cultures of E16.5 neocortical precursors originating from $Gad1^{EGFP/+}$ donors (Tamamaki et al. 2003), expressing EGFP in all GABAergic neurons, we engineered and processed them similarly to **Fig. 6** assays, and we evaluated the resulting $EGFP^{+}NeuN^{+}/NeuN^{+}$ cell ratio at DIV8 (**Fig. 8** and **S9**). We found that generalized and neuron-restricted *Foxg1* overexpression, driven by *Pgk1* and *Syn* promoters, respectively, decreased this ratio from 16.8±0.6% to 10.5±1.1% ($p<0.001$, n=4,4) as well as from 10.6±0.4% to 4.0±0.7% ($p<0.0001$, n=4,4), respectively (**Fig. 8B,** graphs 2 and 4 from left**)**. Astrocyte-confined *Foxg1* overexpression, under the control of the *Gfap*-promoter was ineffective (**Fig. 8B,** graph 3**)**. Knock-down of endogenous *Foxg1* reduced this ratio only to a very limited extent, from 13.8±0.4% to 12.7±0.4% ($p<0.04$, n=4,4) (**Fig. 8B,** graph 1**)**. In other words, a pronounced interneuron depletion takes place upon neuronal *Foxg1* upregulation, likely contributing to network hyperactivity evoked by manipulation.

Activity-dependent *Foxg1* upregulation in neocortical neurons and its molecular control.

A reciprocal positive feedback between two network nodes may robustly enhance the output of either node, following an even moderate increase of (a) exogenous inputs feeding them or (b) internode connection weights. In this way, an even subtle alteration of these parameters may result in dramatic changes of the network state. In this respect, we wondered if, able to promote neuronal activity, *Foxg1* would be in turn stimulated by such activity.

To address this issue, we transferred DIV6.5 neural cultures originating from E16.5 neocortical tissue under 25 mM extracellular K^+, namely a robust depolarizing treatment (He et al. 2011) and monitored temporal progression of *Foxg1*-mRNA and -protein (**Fig. 9A**). Both gene products underwent a substantial, transient upregulation. The former arose as early as at 1 hour, peaked up at 3 hours (about 2.75-folds) and later declined, getting back to baseline values by 18-24 hours. (**Fig. 9C**). The latter showed an appreciable increase already at 6 hours, peaked up at around 12 hours (about 1.75-folds) and later declined, rebounding to halved levels at about 24 hours (**Fig. 9D**). Interestingly such positive correlation between *Foxg1* expression and neuronal activity was mainly restricted to hyperactive cultures, as neuron silencing by TTX down-regulated *Foxg1*-mRNA only to a limited extent (**Fig. 9B**).

Looking for mechanisms underlying activity-dependent *Foxg1* regulation, we noticed that the *Foxg1* transcription unit and its surroundings are rich in binding sites for immediate early gene-encoded transcription factors (ieg-TFs), validated by Chromatin-Immuno-Precipitation (ChIP) in non-neural cell lines or predicted *in silico* by Jaspar software (Mathelier et al. 2014) (**Fig. 10A**). Therefore, we hypothesized that these TFs, including pCreb1, nuclear-$RelA^{p65}$, Fos, Egr1, Egr2 and Cebpb, might be instrumental in such regulation.

To test this prediction, first we checked if temporal progression of these TFs would be etiologically compatible with *Foxg1*-mRNA fluctuations, in primary neocortical cultures challenged by high potassium. Two of these effectors, pCreb1 and nuclear-Rel^{p65}, normally tuned by fast post-translational mechanisms (Flavell and Greenberg 2008; de la Torre-Ubieta and Bonni 2011; Sun et al. 2016), peaked up as early as at 20 min and remained above the baseline at least up to 90 min (**Fig. 10C,E**). Consistently, the *d2EGFP*-mRNA products of the pCreb1- and NFkB-activity reporters cAMP.RE_3-p(min)-d2EGFP and NFkB.BS_4-p(min)-d2EGFP, pre-delivered to neural cells by lentiviral transgenesis (**Fig. 10B**) displayed also an early-onset, transient upregulation (**Fig. 10D, F**). Conversely, *Fos*-, *Egr1*-, *Egr2*- and *Cebpb*-mRNAs, largely modulated by transcription-dependent mechanisms (Calella et al. 2007; Flavell and Greenberg 2008), peaked up at 1 hour and then declined (**Fig. 10G**). In synthesis, activity-dependent elevation of all six effectors preceded *Foxg1*-mRNA arousal. As such, the former could be instrumental in achieving the latter.

To corroborate this inference, we systematically knocked-down all six ieg-TFs, by delivering the corresponding dominant-negative (DN) effectors (**Table S5**) (Schwarz et al. 1996; Van Antwerp et al. 1996; Olive et al. 1997; Ahn et al. 1998; Park et al. 1999; Mayer et al. 2008) to primary neuronal cultures. We evaluated the impact of these manipulations, in basal conditions as well as upon culture exposure to 25 mM K^+ for 3 hours. In particular, *Egr1* and *Egr2* were functionally co-silenced with a unique DN construct, CREB-DN expression had to be set to very low levels to

prevent neuronal damage (**Fig. 11A**). Most of the DN-devices employed down-regulated *Foxg1*-mRNA by about 15-40%, both in baseline conditions and in the presence of 25 mM K^+. NFkB-DN was specifically ineffective under high K^+. CREB-DN conversely reduced *Foxg1*-mRNA by about 50% and 90%, in baseline condition and under high K^+, respectively. (**Fig. 11B**, 1st and 3rd graph). Altogether, these results suggest that all six ieg-TFs under analysis contribute to sustain neuronal *Foxg1* transcription, synergically and to various extents, in resting conditions as well as following intense electrical activity. In particular, they point to pCreb1 as a key player in this context.

Finally, inspired by the presence of a number of known Foxg1-binding sites within the *Foxg1* locus (**Fig. 10A** and data not shown), we further speculated that late decrease of *Foxg1* gene products upon prolonged K^+ stimulation (**Fig. 9C, D**) did not simply reflect the delayed decline of its transactivators, but it could be enhanced by *Foxg1* self-inhibition. As expected, the delivery of a neuron restricted *Foxg1* transgene (**Fig. 11A**) downregulated *endogenous Foxg1* by >80%, both in baseline conditions and under high K^+ (**Fig. 11B,** 2nd and 4th graphs). Consistently, the same transgene robustly shifted the *Foxg1*(t) expression curve downwards in aging neocortical cultures (**Fig. S10A, B**).

Hyperactivation of iegs in K^+-stimulated, *Foxg1*-GOF neocortical cultures

We have shown that a reciprocal positive feedback may take place between *Foxg1* overexpression and neocortical activity. This feedback might robustly influence neocortical activity regime, strengthening the electro-clinical phenotype of *Foxg1*-GOF mice and exacerbating EEG abnormalities of human patients with a supranumerary *FOXG1* allele. To get an insight into these phenomena, we investigated the impact of increased *Foxg1* expression on K^+-stimulated neocortical cultures. To this aim, *Foxg1* was upregulated by gentle RNAa (**Fig. 12A**), eliciting a 1.5x - 2.0x expression gain, presumably close to that caused by *FOXG1* duplications, and complying with activity-dependent gene tuning (Fimiani et al. 2016). Then, neural cultures were profiled for activity and expression of selected iegs (**Fig. 12A**), as proxies of ongoing neuronal activity (Flavell and Greenberg 2008) and - meanwhile - promoters of it (Jones et al. 2001; Lopez de Armentia et al. 2007; Jancic et al. 2009; Viosca et al. 2009; Gruart et al. 2012; Penke et al. 2013; Koldamova et al. 2014).

Interestingly, following K^+ stimulation, the *d2EGFP*-mRNA product of the pCreb1-activity reporter was rapidly upregulated in *Foxg1*-GOF samples compared to controls ($ctr_{t=0}$-normalized levels at 1 hour were 1.74±0.11 vs 1.36±0.13, respectively, with $p<0.032$) (**Fig. 12B**, left graph). The corresponding NFkB-activity reporter, upregulated at 50 min in both *Foxg1*-GOF samples and controls (1.15±0.03 and 1.19±0.12, respectively, with $p=0.296$), retained its overexpression

at 2 hours in the former, while declining in the latter (1.22±0.14 vs 0.94±0.08, with $p<0.003$) (**Fig. 12B**, right graph).

A consistent scenario emerged from quantitation of endogenous *Fos*, *Egr1* and *Cebpb*-mRNAs. Peaking at 1 hour in *Foxg1*-GOF samples like in controls, both *Fos*- and *Egr1*-mRNAs showed a delayed rebound towards baseline in *Foxg1*-GOF samples compared to controls ($ctr_{t=0}$-normalized levels at 2 hours were 62.3±2.68 vs 48.87±3.91, with $p<0.015$, and 24.88±4.40 vs 16.65±1.78, with $p<0.049$, respectively) (**Fig. 12C**). *Cebpb*-mRNA was conversely upregulated in *Foxg1*-GOF samples for at least 6 hours after high K^+ exposure (for example, $ctr_{t=0}$-normalized levels at 2 hours were 4.96±0.39 and 3.64±0.24, in GOF and ctr samples, respectively, with $p<0.016$) (**Fig. 12C**).

DISCUSSION

To cast light on the impact of *Foxg1* on neocortical neuronal activity, we took advantage of a novel transgenic mouse model, overexpressing this gene within deep neocortical pyramids (**Fig.1**). These animals showed an abnormal EEG (**Fig. 2**) and resulted more prone to KA-evoked limbic motor seizures (**Fig. 3**). Among phenomena possibly accounting for these symptoms, we detected a prominent interneurons reduction throughout their grey matter, as well as an astroglial deficit mainly confined to lateral superficial neocortex (**Fig. 4**). An involvement of hyperactive neocortical neurons was also predicted. As expected, we found that lentivirus driven *Foxg1* overexpression in dissociated neocortical neurons increased their discharge frequency and synchronization (**Fig. 5,6**). Looking for underlying molecular mechanisms, we profiled the transcriptome of these cells. Results of this analysis included an upregulation of large *Scn* and *Cacn* gene sets, encoding for Na^+ and Ca^{2+} channels, complex anomalies in other key genes governing Ca^{2+} fluxes, aberrancies in *Grin, Gria* and *Grik*, NMDA-, AMPA- and KA-receptor genes, as well as a collapse of the GABAergic axis, including *Gad1*, *Gad2*, *Gabra1* and *Bdnf* (**Fig. 7** and **Table S3**). Finally, we scored the impact of neuronal hyperactivity on *Foxg1* expression. We found a transient upregulation of this gene (**Fig. 9**), mediated by the products of immediate-early genes (**Fig. 10,11**), pointing to a positive feedback between *Foxg1* and neuronal activity (**Fig. 12**).

Originally conceived to achieve pan-telencephalic *Foxg1* overexpression, the transgene employed in *in vivo* assays resulted to be unexpectedly confined to post-mitotic, deep neocortical pyramids. That offered us the serendipitous opportunity to explore the role exerted by our gene of interest in these cells in living mice. As the hippocampus of these animals did not express the transgene, its spontaneous electroclinical signs and KA-evoked hyperactivity were hardly autochthonous.

Rather, they likely reflected abnormal neocortical inputs to this structure, which could be so exploited as a proxy of the neocortical phenotype.

In this respect, two major histological abnormalities characterizing the neocortex of *Foxg1*-GOF mutants, a widespread decrease of interneurons and a more localized astroglial deficit (**Fig. 4B-D)**, might contribute to cortex hyperactivity. To notice, both phenomena originated non cell-autonomously, as neither interneurons nor astrocytes expressed the transgene (**Fig. 1E, F**), and a prominent reduction of GABAergic interneuron prevalence also occurred in *Foxg1*-GOF cultures (**Fig. 8 and S8**). As expected, an increase of neocortical projection neurons activity was detectable *in vitro*, upon *Foxg1* overexpression in dissociated cultures. This increase was primarily inferred by an activity-responsive transgene reporter (Kawashima et al. 2009) (**Fig. 5**) and then confirmed by optical profiling of Ca^{2+} indicators (**Fig. 6**). Remarkably, a positive correlation between *Foxg1* expression levels and neuron network synchronization emerged following generalized, both GOF and LOF *Foxg1* manipulations. Furthermore, neuronal hyperactivity was still prominent when *Foxg1* overexpression was restricted to neurons, pointing to mechanisms mostly taking place in these cells.

Moreover, RNA profiling of *Foxg1*-GOF cultures highlighted pronounced alterations of different specific gene sets, likely contributing to it (**Fig. 7** and **Table S3**). General dynamics of *Scn* and *Cacn* genes, and changes in NCKX, SOCE, IICR and SERCA genes prefigure neuron hyperexcitability. Misregulation of MCU genes, likely enhancing mitochondrial Ca^{2+} uptake, might stimulate respiration and sustain enduring electrical activity (Sanganahalli et al. 2013). Unbalanced expression of *Gria*, *Grik* and *Grin* genes might result into strengthened glutamatergic conduction. Last but not least, the collapse of *Gad* and *Scn1a* genes (largely exceeding the shrinkage of the interneuronal complement) as well as the decline of *Gabra1* and *Bdnf* might jeopardize GABAergic control of neocortical circuits. An *ad hoc* work will be required to test these predictions.

Remarkably, we also found that *Foxg1*-mRNA was transiently upregulated under high $[K^+]_O$ and slightly downregulated upon TTX administration, suggesting that its levels are physiologically sensitive to changes of electric activity (**Fig. 9C**). An upregulation of Foxg1 protein followed the mRNA peak, corroborating its potential relevance (**Fig. 9D**). Intriguingly, bioinformatic inspection of the *Foxg1* locus revealed a number of binding sites for immediate early factors. As expected, (Calella et al. 2007; Flavell and Greenberg 2008; Snow and Albensi 2016), some of them (or their mRNAs) showed a pronounced upregulation, which preceded the *Foxg1*-mRNA maximum at three hours. Specifically, pCreb1 and nuclear-Nfkb peaked at 20 min, *Fos*-, *Egr1*-, *Egr2*- and *Cebpb*-mRNAs at about 1 hour (**Fig. 10**). Their functional knock-down, by dominant negative devices, generally reduced *Foxg1*-mRNA both in basal conditions and under high $[K^+]_O$

(**Fig. 11**). All that points to an involvement of these effectors in mediating the impact of electric activity on *Foxg1* levels. Last, the introduction of an exogenous *Foxg1* transgene dampened the expression of its endogenous counterpart, suggesting that an autologous negative feedback may restrict activity dependent *Foxg1* arousal (**Fig. 11**).

In summary, *Foxg1* expression promotes neocortical electrical activity which, in turn, may stimulate *Foxg1* expression. This feedback suggests a crucial *Foxg1* role in fine tuning of neocortical excitability. In this respect, progressive post-natal decline of *Foxg1* levels (**Fig. S10**) might contribute to reduced excitability of more aged brains, mis-regulation of *Foxg1*-mRNA in patients with *Foxg1* copy number variations might deeply affect neuronal activity, resulting in their Rett-like- and West-like EEG aberrancies (Florian et al. 2011; Seltzer et al. 2014). Consistently, gentle stimulation of *Foxg1* by saRNAs led to a complex upward distortion of fluctuations of pCreb1- and Nfkb-activity, as well as of *Fos*-, *Egr1*- and *Cebp*-mRNAs, evoked by high $[K^+]_O$ (**Fig. 12**). Non mere indices of neuronal hyperactivity, upregulation of pCreb1, Egr1 and Fos *may promote* neuronal hyper-activity and -excitability (Jones et al. 2001; Lopez de Armentia et al. 2007; Jancic et al. 2009; Viosca et al. 2009; Zhou et al. 2009; Yassin et al. 2010; Descalzi et al. 2012; Gruart et al. 2012; Penke et al. 2013; Koldamova et al. 2014; Ryan et al. 2015). Functional relevance of these phenomena to *Foxg1*-associated phenotypes will be subject of a dedicated follow-up study.

REFERENCES

Ahn S, Olive M, Aggarwal S, Krylov D, Ginty DD, Vinson C. 1998. A dominant-negative inhibitor of CREB reveals that it is a general mediator of stimulus-dependent transcription of c-fos. Mol Cell Biol. 18:967–977.

Beyer B, Deleuze C, Letts VA, Mahaffey CL, Boumil RM, Lew TA, Huguenard JR, Frankel WN. 2008. Absence seizures in C3H/HeJ and knockout mice caused by mutation of the AMPA receptor subunit Gria4. Hum Mol Genet. 17:1738–1749.

Bosi S, Rauti R, Laishram J, Turco A, Lonardoni D, Nieus T, Prato M, Scaini D, Ballerini L. 2015. From 2D to 3D: novel nanostructured scaffolds to investigate signalling in reconstructed neuronal networks. Sci Rep. 5.

Brancaccio M, Pivetta C, Granzotto M, Filippis C, Mallamaci A. 2010. Emx2 and Foxg1 Inhibit Gliogenesis and Promote Neuronogenesis. STEM CELLS. N/A-N/A.

Calella AM, Nerlov C, Lopez RG, Sciarretta C, von Bohlen und Halbach O, Bereshchenko O, Minichiello L. 2007. Neurotrophin/Trk receptor signaling mediates C/EBPalpha, -beta and NeuroD recruitment to immediate-early gene promoters in neuronal cells and requires C/EBPs to induce immediate-early gene transcription. Neural Develop. 2:4.

Catterall WA. 2005. International Union of Pharmacology. XLVII. Nomenclature and Structure-Function Relationships of Voltage-Gated Sodium Channels. Pharmacol Rev. 57:397–409.

Chiola S, Do MD, Centrone L, Mallamaci A. 2018. Foxg1 Overexpression in Neocortical Pyramids Stimulates Dendrite Elongation Via Hes1 and pCreb1 Upregulation. Cereb Cortex N Y N 1991.

Clayton GH, Owens GC, Wolff JS, Smith RL. 1998. Ontogeny of cation-Cl- cotransporter expression in rat neocortex. Brain Res Dev Brain Res. 109:281–292.

Crupi R, Impellizzeri D, Cuzzocrea S. 2019. Role of Metabotropic Glutamate Receptors in Neurological Disorders. Front Mol Neurosci. 12.

de la Torre-Ubieta L, Bonni A. 2011. Transcriptional Regulation of Neuronal Polarity and Morphogenesis in the Mammalian Brain. Neuron. 72:22–40.

Descalzi G, Li X-Y, Chen T, Mercaldo V, Koga K, Zhuo M. 2012. Rapid synaptic potentiation within the anterior cingulate cortex mediates trace fear learning. Mol Brain. 5:6.

Dolphin AC. 2016. Voltage-gated calcium channels and their auxiliary subunits: physiology and pathophysiology and pharmacology: Voltage-gated calcium channels. J Physiol. 594:5369–5390.

Falcone C, Santo M, Liuzzi G, Cannizzaro N, Grudina C, Valencic E, Peruzzotti-Jametti L, Pluchino S, Mallamaci A. 2019. *Foxg1* Antagonizes Neocortical Stem Cell Progression to Astrogenesis. Cereb Cortex.

Fernandes HB, Catches JS, Petralia RS, Copits BA, Xu J, Russell TA, Swanson GT, Contractor A. 2009. High-Affinity Kainate Receptor Subunits Are Necessary for Ionotropic but Not Metabotropic Signaling. Neuron. 63:818–829.

Fimiani C, Goina E, Su Q, Gao G, Mallamaci A. 2016. RNA activation of haploinsufficient Foxg1 gene in murine neocortex. Sci Rep. 6.

Flavell SW, Greenberg ME. 2008. Signaling Mechanisms Linking Neuronal Activity to Gene Expression and Plasticity of the Nervous System. Annu Rev Neurosci. 31:563–590.

Florian C, Bahi-Buisson N, Bienvenu T. 2011. FOXG1-Related Disorders: From Clinical Description to Molecular Genetics. Mol Syndromol. 2(3-5):153-163.

Gruart A, Benito E, Delgado-Garcia JM, Barco A. 2012. Enhanced cAMP Response Element-Binding Protein Activity Increases Neuronal Excitability, Hippocampal Long-Term Potentiation, and Classical Eyeblink Conditioning in Alert Behaving Mice. J Neurosci. 32:17431–17441.

Gu Q. 2002. Neuromodulatory transmitter systems in the cortex and their role in cortical plasticity. Neuroscience. 111:815–835.

Hanashima C, Fernandes M, Hebert JM, Fishell G. 2007. The Role of Foxg1 and Dorsal Midline Signaling in the Generation of Cajal-Retzius Subtypes. J Neurosci. 27:11103–11111.

Hanashima C, Li SC, Shen L, Lai E, Fishell G. 2004. Foxg1 suppresses early cortical cell fate. Science. 303:56–59.

Hanashima C, Shen L, Li SC, Lai E. 2002. Brain factor-1 controls the proliferation and differentiation of neocortical progenitor cells through independent mechanisms. J Neurosci Off J Soc Neurosci. 22:6526–6536.

He X-B, Yi S-H, Rhee Y-H, Kim H, Han Y-M, Lee S-H, Lee H, Park C-H, Lee Y-S, Richardson E, Kim B-W, Lee S-H. 2011. Prolonged Membrane Depolarization Enhances Midbrain Dopamine Neuron Differentiation via Epigenetic Histone Modifications. STEM CELLS. 29:1861–1873.

Hong EJ, McCord AE, Greenberg ME. 2008. A biological function for the neuronal activity-dependent component of Bdnf transcription in the development of cortical inhibition. Neuron. 60:610–624.

Jancic D, Lopez de Armentia M, Valor LM, Olivares R, Barco A. 2009. Inhibition of cAMP Response Element-Binding Protein Reduces Neuronal Excitability and Plasticity, and Triggers Neurodegeneration. Cereb Cortex. 19:2535–2547.

Jembrek M, Vlainic J. 2015. GABA Receptors: Pharmacological Potential and Pitfalls. Curr Pharm Des. 21:4943–4959.

Johnston J, Forsythe ID, Kopp-Scheinpflug C. 2010. SYMPOSIUM REVIEW: Going native: voltage-gated potassium channels controlling neuronal excitability: K^+ channels and auditory processing. J Physiol. 588:3187–3200.

Jones MW, Errington ML, French PJ, Fine A, Bliss TV, Garel S, Charnay P, Bozon B, Laroche S, Davis S. 2001. A requirement for the immediate early gene Zif268 in the expression of late LTP and long-term memories. Nat Neurosci. 4:289–296.

Kawashima T, Okuno H, Nonaka M, Adachi-Morishima A, Kyo N, Okamura M, Takemoto-Kimura S, Worley PF, Bito H. 2009. Synaptic activity-responsive element in the Arc/Arg3.1 promoter essential for synapse-to-nucleus signaling in activated neurons. Proc Natl Acad Sci U S A. 106:316–321.

Koldamova R, Schug J, Lefterova M, Cronican AA, Fitz NF, Davenport FA, Carter A, Castranio EL, Lefterov I. 2014. Genome-wide approaches reveal EGR1-controlled regulatory networks associated with neurodegeneration. Neurobiol Dis. 63:107–114.

Kwon S-K, Hirabayashi Y, Polleux F. 2016. Organelle-Specific Sensors for Monitoring Ca2+ Dynamics in Neurons. Front Synaptic Neurosci. 8:29.

Lopez de Armentia M, Jancic D, Olivares R, Alarcon JM, Kandel ER, Barco A. 2007. cAMP Response Element-Binding Protein-Mediated Gene Expression Increases the Intrinsic Excitability of CA1 Pyramidal Neurons. J Neurosci. 27:13909–13918.

Manuel M, Martynoga B, Yu T, West JD, Mason JO, Price DJ. 2010. The transcription factor Foxg1 regulates the competence of telencephalic cells to adopt subpallial fates in mice. Dev Camb Engl. 137:487–497.

Mariani J, Coppola G, Zhang P, Abyzov A, Provini L, Tomasini L, Amenduni M, Szekely A, Palejev D, Wilson M, Gerstein M, Grigorenko EL, Chawarska K, Pelphrey KA, Howe JR, Vaccarino FM. 2015. FOXG1-Dependent Dysregulation of GABA/Glutamate Neuron Differentiation in Autism Spectrum Disorders. Cell. 162:375–390.

Martynoga B, Morrison H, Price DJ, Mason JO. 2005. Foxg1 is required for specification of ventral telencephalon and region-specific regulation of dorsal telencephalic precursor proliferation and apoptosis. Dev Biol. 283:113–127.

Mathelier A, Zhao X, Zhang AW, Parcy F, Worsley-Hunt R, Arenillas DJ, Buchman S, Chen C, Chou A, Ienasescu H, Lim J, Shyr C, Tan G, Zhou M, Lenhard B, Sandelin A, Wasserman WW. 2014. JASPAR 2014: an extensively expanded and updated open-access database of transcription factor binding profiles. Nucleic Acids Res. 42:D142–D147.

Mayer SI, Dexheimer V, Nishida E, Kitajima S, Thiel G. 2008. Expression of the transcriptional repressor ATF3 in gonadotrophs is regulated by Egr-1, CREB, and ATF2 after gonadotropin-releasing hormone receptor stimulation. Endocrinology. 149:6311–6325.

Mitter D, Pringsheim M, Kaulisch M, Plümacher KS, Schröder S, Warthemann R, Abou Jamra R, Baethmann M, Bast T, Büttel H-M, Cohen JS, Conover E, Courage C, Eger A, Fatemi A, Grebe TA, Hauser NS, Heinritz W, Helbig KL, Heruth M, Huhle D, Höft K, Karch S, Kluger G, Korenke GC, Lemke JR, Lutz RE, Patzer S, Prehl I, Hoertnagel K, Ramsey K, Rating T, Rieß A, Rohena L, Schimmel M, Westman R, Zech F-M, Zoll B, Malzahn D, Zirn B, Brockmann K. 2018. FOXG1 syndrome: genotype–phenotype association in 83 patients with FOXG1 variants. Genet Med. 20:98–108.

Miyoshi G, Fishell G. 2012. Dynamic FoxG1 Expression Coordinates the Integration of Multipolar Pyramidal Neuron Precursors into the Cortical Plate. Neuron. 74:1045–1058.

Molyneaux BJ, Arlotta P, Menezes JRL, Macklis JD. 2007. Neuronal subtype specification in the cerebral cortex. Nat Rev Neurosci. 8:427–437.

Monteiro P, Feng G. 2017. SHANK proteins: roles at the synapse and in autism spectrum disorder. Nat Rev Neurosci. 18:147–157.

Muzio L, Mallamaci A. 2005. Foxg1 confines Cajal-Retzius neuronogenesis and hippocampal morphogenesis to the dorsomedial pallium. J Neurosci Off J Soc Neurosci. 25:4435–4441.

Olive M, Krylov D, Echlin DR, Gardner K, Taparowsky E, Vinson C. 1997. A dominant negative to activation protein-1 (AP1) that abolishes DNA binding and inhibits oncogenesis. J Biol Chem. 272:18586–18594.

Paoletti P, Bellone C, Zhou Q. 2013. NMDA receptor subunit diversity: impact on receptor properties, synaptic plasticity and disease. Nat Rev Neurosci. 14:383–400.

Park EA, Song S, Vinson C, Roesler WJ. 1999. Role of CCAAT enhancer-binding protein beta in the thyroid hormone and cAMP induction of phosphoenolpyruvate carboxykinase gene transcription. J Biol Chem. 274:211–217.

Paternain AV, Cohen A, Stern-Bach Y, Lerma J. 2003. A Role for Extracellular Na^+ in the Channel Gating of Native and Recombinant Kainate Receptors. J Neurosci. 23:8641–8648.

Patriarchi T, Amabile S, Frullanti E, Landucci E, Lo Rizzo C, Ariani F, Costa M, Olimpico F, W Hell J, M Vaccarino F, Renieri A, Meloni I. 2016. Imbalance of excitatory/inhibitory synaptic protein expression in iPSC-derived neurons from FOXG1 +/− patients and in foxg1 +/− mice. Eur J Hum Genet. 24:871–880.

Penke Z, Morice E, Veyrac A, Gros A, Chagneau C, LeBlanc P, Samson N, Baumgartel K, Mansuy IM, Davis S, Laroche S. 2013. Zif268/Egr1 gain of function facilitates hippocampal synaptic plasticity and long-term spatial recognition memory. Philos Trans R Soc B Biol Sci. 369:20130159–20130159.

Racine RJ. 1972. Modification of seizure activity by electrical stimulation. II. Motor seizure. Electroencephalogr Clin Neurophysiol. 32:281–294.

Raffaello A, Mammucari C, Gherardi G, Rizzuto R. 2016. Calcium at the Center of Cell Signaling: Interplay between Endoplasmic Reticulum, Mitochondria, and Lysosomes. Trends Biochem Sci. 41:1035–1049.

Raponi E, Agenes F, Delphin C, Assard N, Baudier J, Legraverend C, Deloulme J-C. 2007. S100B expression defines a state in which GFAP-expressing cells lose their neural stem cell potential and acquire a more mature developmental stage. Glia. 55:165–177.

Rauti R, Lozano N, León V, Scaini D, Musto M, Rago I, Ulloa Severino FP, Fabbro A, Casalis L, Vázquez E, Kostarelos K, Prato M, Ballerini L. 2016. Graphene Oxide Nanosheets Reshape Synaptic Function in Cultured Brain Networks. ACS Nano. 10:4459–4471.

Rivera C, Voipio J, Payne JA, Ruusuvuori E, Lahtinen H, Lamsa K, Pirvola U, Saarma M, Kaila K. 1999. The K+/Cl- co-transporter KCC2 renders GABA hyperpolarizing during neuronal maturation. Nature. 397:251–255.

Ryan TJ, Roy DS, Pignatelli M, Arons A, Tonegawa S. 2015. Engram cells retain memory under retrograde amnesia. Science. 348:1007–1013.

Sanchez RM, Koh S, Rio C, Wang C, Lamperti ED, Sharma D, Corfas G, Jensen FE. 2001. Decreased glutamate receptor 2 expression and enhanced epileptogenesis in immature rat hippocampus after perinatal hypoxia-induced seizures. J Neurosci Off J Soc Neurosci. 21:8154–8163.

Sanganahalli BG, Herman P, Hyder F, Kannurpatti SS. 2013. Mitochondrial Calcium Uptake Capacity Modulates Neocortical Excitability. J Cereb Blood Flow Metab. 33:1115–1126.

Schwarz EM, Van Antwerp D, Verma IM. 1996. Constitutive phosphorylation of IkappaBalpha by casein kinase II occurs preferentially at serine 293: requirement for degradation of free IkappaBalpha. Mol Cell Biol. 16:3554–3559.

Seltzer LE, Ma M, Ahmed S, Bertrand M, Dobyns WB, Wheless J, Paciorkowski AR. 2014. Epilepsy and outcome in *FOXG1* -related disorders. Epilepsia. 55:1292–1300.

Seuntjens E, Nityanandam A, Miquelajauregui A, Debruyn J, Stryjewska A, Goebbels S, Nave K-A, Huylebroeck D, Tarabykin V. 2009. Sip1 regulates sequential fate decisions by feedback signaling from postmitotic neurons to progenitors. Nat Neurosci. 12:1373–1380.

Shah NH, Aizenman E. 2014. Voltage-Gated Potassium Channels at the Crossroads of Neuronal Function, Ischemic Tolerance, and Neurodegeneration. Transl Stroke Res. 5:38–58.

Shen W, Ba R, Su Y, Ni Y, Chen D, Xie W, Pleasure SJ, Zhao C. 2018. Foxg1 Regulates the Postnatal Development of Cortical Interneurons. Cereb Cortex 29(4):1547-1560.

Snow WM, Albensi BC. 2016. Neuronal Gene Targets of NF-κB and Their Dysregulation in Alzheimer's Disease. Front Mol Neurosci. 9:118.

Sun Y, Paşca SP, Portmann T, Goold C, Worringer KA, Guan W, Chan KC, Gai H, Vogt D, Chen Y-JJ, Mao R, Chan K, Rubenstein JL, Madison DV, Hallmayer J, Froehlich-Santino WM, Bernstein JA, Dolmetsch RE. 2016. A deleterious Nav1.1 mutation selectively impairs telencephalic inhibitory neurons derived from Dravet Syndrome patients. eLife. 5. pii: e13073.

Tamamaki N, Yanagawa Y, Tomioka R, Miyazaki J-I, Obata K, Kaneko T. 2003. Green fluorescent protein expression and colocalization with calretinin, parvalbumin, and somatostatin in the GAD67-GFP knock-in mouse. J Comp Neurol. 467:60–79.

Toma K, Kumamoto T, Hanashima C. 2014. The Timing of Upper-Layer Neurogenesis Is Conferred by Sequential Derepression and Negative Feedback from Deep-Layer Neurons. J Neurosci. 34:13259–13276.

Traynelis SF, Wollmuth LP, McBain CJ, Menniti FS, Vance KM, Ogden KK, Hansen KB, Yuan H, Myers SJ, Dingledine R. 2010. Glutamate Receptor Ion Channels: Structure, Regulation, and Function. Pharmacol Rev. 62:405–496.

Van Antwerp DJ, Martin SJ, Kafri T, Green DR, Verma IM. 1996. Suppression of TNF-alpha-induced apoptosis by NF-kappaB. Science. 274:787–789.

Vegas N, Cavallin M, Maillard C, Boddaert N, Toulouse J, Schaefer E, Lerman-Sagie T, Lev D, Magalie B, Moutton S, Haan E, Isidor B, Heron D, Milh M, Rondeau S, Michot C, Valence S, Wagner S, Hully M, Mignot C, Masurel A, Datta A, Odent S, Nizon M, Lazaro L, Vincent M, Cogné B, Guerrot AM, Arpin S, Pedespan JM, Caubel I, Pontier B, Troude B, Rivier F, Philippe C, Bienvenu T, Spitz M-A, Bery A, Bahi-Buisson N. 2018. Delineating *FOXG1* syndrome: From congenital microcephaly to hyperkinetic encephalopathy. Neurol Genet. 4:e281.

Viosca J, Lopez de Armentia M, Jancic D, Barco A. 2009. Enhanced CREB-dependent gene expression increases the excitability of neurons in the basal amygdala and primes the consolidation of contextual and cued fear memory. Learn Mem. 16:193–197.

Wada A, Takahashi H, Lipton SA, Chen H-SV. 2006. NR3A modulates the outer vestibule of the "NMDA" receptor channel. J Neurosci Off J Soc Neurosci. 26:13156–13166.

Wamsley B, Fishell G. 2017. Genetic and activity-dependent mechanisms underlying interneuron diversity. Nat Rev Neurosci. 18:299–309.

Wisden W, Seeburg PH. 1993. A complex mosaic of high-affinity kainate receptors in rat brain. J Neurosci Off J Soc Neurosci. 13:3582–3598.

Yassin L, Benedetti BL, Jouhanneau J-S, Wen JA, Poulet JFA, Barth AL. 2010. An Embedded Subnetwork of Highly Active Neurons in the Neocortex. Neuron. 68:1043–1050.

Zamponi GW, Lory P, Perez-Reyes E. 2010. Role of voltage-gated calcium channels in epilepsy. Pflüg Arch - Eur J Physiol. 460:395–403.

Zhou Y, Won J, Karlsson MG, Zhou M, Rogerson T, Balaji J, Neve R, Poirazi P, Silva AJ. 2009. CREB regulates excitability and the allocation of memory to subsets of neurons in the amygdala. Nat Neurosci. 12:1438–1443.

Zhu W, Zhang B, Li M, Mo F, Mi T, Wu Y, Teng Z, Zhou Q, Li W, Hu B. 2019. Precisely controlling endogenous protein dosage in hPSCs and derivatives to model FOXG1 syndrome. Nat Commun. 10(1):928.

Funding

We thank:

(1) Telethon Italy (Grant GGP13034 to A.M.)

(2) Fondation Jerome Lejeune (Grant 1621-MA2017A to A.M.)

(3) SISSA (intramurary funding to A.M. and YounGrant R_SSA-ALTR_YG_PS18_20_NEUR_ ref_gruppo_0477 to R.R., Teresa Sorbo, M.S. and W.T.).

LEGENDS TO MAIN FIGURES

Figure 1. Expression pattern of the *Foxg1-promoter*-tTA-driven, *Foxg1-IRES-EGFP* transgene. (A, B) Restriction of transgene products to the cortical plate of the E16.5 neocortical primordium. In (B), a high-power magnification of the a' boxed region of (A) is shown. The asterisk highlights the vz Foxg1 expression domain. **(C, D)** Confinement of transgene products to Tubb3$^+$ and NeuN$^+$ pyramidal neurons within deep layers of neonatal grey matter. In both rows, high power magnifications in columns 2-4 correspond to boxed insets in column 1 (c' and d', respectively). Arrows in (C, 3rd panel) point to Tubb3$^+$ apical dendrites, connecting neuronal somata to the marginal edge of the cortical wall. **(E, F)** Absence of transgene products in neocortical parvalbumin$^+$ (PV$^+$), somatostatin$^+$ (SST$^+$) and calretinin$^+$ (CR$^+$) interneurons as well as in neocortical S100β$^+$ astrocytes. In (E), high-power pictures refer to dark grey areas within the associated silhouettes, and solid and empty arrowheads point to EGFP$^+$ and interneuron marker$^+$ cells, respectively. In (F), high power magnifications in columns 2-4 correspond to the boxed region in column 1 (f'). Abbreviations: mz, marginal zone; cp, cortical plate; sp, subplate; svz, subventricular zone; vz, ventricular zone; *Foxg1*^{EGFP}, *TREt-Foxg1-IRES-EGFP* transgene-driven EGFP.

Figure 2. EEG recordings of P41 *Foxg1*-GOF (*Foxg1*$^{tTA/+}$*;Tg:Tre-Foxg1-IRES-Egfp*$^{+/-}$) and *wt* (*Foxg1*$^{+/+}$*;Tg:TREt-Foxg1-IRES-Egfp*$^{-/-}$) mice. (A) Schematics of bipolar electrodes placement into the hippocampal field. **(B)** Definition of spikes (as voltage fluctuations exceding

4 standard deviations); classification of spikes (as isolated or clustered, if 1 or ≥2 within 0.5 sec, respectively) and spike clusters (as interictal and ictal, if lasting <4 sec and ≥4 sec, respectively) **(C)** Graphical summary of control-normalized, (1) total spike frequency, (2) isolated spike frequency, (3) interictal spike cluster frequency and (4) ictal spike cluster frequency, in *Foxg1*-GOF and control mice. Absolute, control average values were 500, 150, 95 and 0.25 events/10 min, respectively. Electrical activity monitored over three days, two hours per day, in awake conditions. *n*, number of biological replicates (i.e. individual mice); *, $p<0.05$; **, $p<0.01$.

Figure 3. Comparative behavioral-molecular profiling of *Foxg1*-GOF, *Foxg1*-LOF and wt, P35 mice upon proconvulsant stimulation. (A) Details of proconvulsant mice stimulation and subsequent Racine Staging (RS). **(B)** Distribution of individuals of distinct genotypes in groups reaching different maximal RS values and **(C)** temporal RS (average ± sem) progression in individuals of different genotypes. Statistical significance of results assessed by χ-square (B) and ANOVA (C) assays, respectively. *, $p<0.05$; **, $p<0.01$. **(D)** Acute *c-fos* in situ hybridization of KA-treated mice, upon completion of Racine profiling, mid-frontal brain sections. Throughout Figure 3, "*Foxg1*-GOF" refers to *Foxg1*$^{tTA/+}$*;TREt-Foxg1-IRES-Egfp*$^{+/-}$ mutants, "*wt*" refers to data from pooled *Foxg1*$^{+/+}$*;TREt-Foxg1-IRES-Egfp*$^{-/-}$ and *Foxg1*$^{+/+}$*;TREt-Foxg1-IRES-Egfp*$^{+/-}$ animals (3+3), among which no statistically significant differences were previously found, and "*Foxg1*-LOF" to *Foxg1*$^{tTA/+}$*;TREt-Foxg1-IRES-Egfp*$^{-/-}$ mutants. Abbreviations: KA, kainic acid; $maxRS_i$, Racine stage, maximal animal-specific value; ctx, cortex; DG, dentate gyrus; CA1-3, Cornu Ammonis 1-3 fields.

Figure 4. Histogenetic anomalies of *Foxg1*-GOF mutants. (A) P0 neocortical layering. Shown are neuronal packaging, as assessed by DAPI staining, expression profiles of FoxP2, Ctip2 and Cux1, layer VI, V and II-IV markers, and presumptive laminar architecture of *Foxg1*-GOF mutants (*Foxg1*$^{tTA/+}$*;TREt-Foxg1-IRES-Egfp*$^{+/-}$) vs *wt* controls (*Foxg1*$^{+/+}$*;TREt-Foxg1-IRES-Egfp*$^{-/-}$). **(B)** Comparative quantification of neocortical PV^+ interneurons in neocortices of P35 *Foxg1* mutants and controls. Graphs show normalized densities of PV^+ cells in *Foxg1*-GOF, *wt* (defined as in (A)) and *Foxg1*-LOF (*Foxg1*$^{tTA/+}$*;TREt-Foxg1-IRES-Egfp*$^{-/-}$) mice. Data refer to the dark-grey region of the associated silhouettes. They are presented in a cumulative fashion (T, total), or are categorized along the medial-lateral axis (L, lateral; M, medial), the rostro-caudal axis (R, rostral; I, intermediate; C, caudal), the radial axis (MZ, marginal zone; GM, grey matter; WM, white matter). [Absolute PV^+ cell densities in *wt* animals are reported in **Table S1**]. Examples of anti-PV immunofluorescences refer to the boxed area within the intermediate frontal silhouette. Scale bars: 100μm. **(C, D)** Comparative quantification of $S100\beta^+$ astrocytes in P0 (C) and P7 (D) *Foxg1* mutants and controls. For both ages, graphs show *wt*-normalized densities of

S100β$^+$ cells in neocortices of *Foxg1*-GOF, *wt* and *Foxg1*-LOF mice (genotypes defined as in (A)). Data refer to the dark-grey region of the associated silhouettes. In case of P7 analysis, they are presented in a cumulative fashion (T, total), or are categorized along the medial-lateral axis (L, lateral; M, medial), the rostro-caudal axis (R, rostral; I, intermediate; C, caudal), the radial axis (I, II-IV, V, VI, layers 1, 2-4, 5, 6; WM/SVZ, white matter/subventricular zone). [Absolute S100β$^+$ cell densities in *wt* animals are reported in **Table S2**]. Examples of P0 and P7 anti-S100β and anti-EGFP immunofluorescences refer to the boxed areas within the corresponding silhouettes. Abbreviations: mz, marginal zone; cp, cortical plate; i-vi, layers I-VI; sp, subplate; iz, intermediate zone; wm, white matter; svz, subventricular zone; e, ependyma; *Foxg1*^{EGFP}, *TREt-Foxg1-IRES-EGFP* transgene-driven EGFP. Scale bars: 100μm. Statistical significance evaluated by t-test (one-tailed, unpaired). *, $p<0.05$; **$p<0.01$. *n* is the number of mice analyzed

Fig. 5. Evaluation of neocortical culture activity upon *Foxg1* overexpression, by delayed *arc*-promoter-driven-reporter fluorometry. Cytofluorimetric profiling of *Foxg1*-GOF, DIV7 cultures of dissociated E16.5 neocortical cells, harboring a d2EGFP activity reporter under the control of the "*Arc*-SARE-enhancer/minimal promoter (ArcSAREp)" neuronal-activity-responsive element: **(A)** protocol and **(B)** results. The fluorescence ratio between the d2EGFP reporter and the constitutively expressed product of the cis-associated *PGKp-RFP* normalizer was determined per each cell and the *median* ratio of every biological replicate was plotted against its genotype. Horizontal bars, genotype averages. Data normalized against ctr values. Results evaluated by t-test (unpaired, one-tailed). ** $p<0.01$. *n* = number of biological replicates, i.e. independently transduced samples, each containing 50,000 cells.

Fig. 6. Evaluation of neocortical culture activity upon *Foxg1* expression level modulation, by real time Ca^{2+} imaging. $Ca2^+$-sensor-based, fluorimetric activity profiling of DIV8-10 cultures of dissociated E16.5 neocortical cells, loss- or gain of function (LOF or GOF) for *Foxg1*, and controls. **(A)** Experimental strategy. **(B-E)** Results, referring to LOF (B), as well as to generalized (C), astroglia-restricted (D), and neuron-restricted (E) GOF assays. In each (B-E) row, data presented as follows. In first panel (from left), snapshot of a representative field of manipulated *Foxg1* cultures, stained with Fluo4-AM (B) or Oregon-Green BAPTA 1-AM (C-F) Ca^{2+} indicators; scale bar: 50 μm. In second panel, examples of repetitive Ca^{2+} events spontaneously recorded from control (top) or *Foxg1*$^{LOF/GOF}$ (bottom) neurons. In third panel, the histogram represents percentages of spontaneously active cells in the two experimental contexts. In fourth panel, plot of cumulative inter-event interval (IEI) distributions in active cells of control (ctr) and *Foxg1*$^{LOF/GOF}$ cultures. In fifth panel, the histogram summarizes the cross-correlations factors (CCF) measured under the two experimental conditions. Results evaluated by χ-squared test (spontaneously active neuron frequency), Kolmogorov-Smirnov assay (cumulative IEI

distribution) and Mann-Whitney test (CCF). ** $p<10^{-2}$, *** $p<10^{-3}$. *n* represents: (i) the number of visual fields (each taken from an independently lentivirus-transduced cell sample) scored for assessment of "frequency of spontaneously active neurons" (third panel) and "CCF" (fifth panel); (ii) the number of active neurons inspected for evaluation of "cumulative IEI distribution" (fourth panel).

Fig. 7. qRTPCR profiling of neocortical cultures overexpressing *Foxg1* in their neuronal compartment. (A) Protocol, **(B)** results. Data evaluated by *t*-test (unpaired, one-tailed). ** $p<10^{-2}$, *** $p<10^{-3}$, **** $p<10^{-4}$, ***** $p<10^{-5}$, ****** $p<10^{-6}$. *n* = number of biological replicates, i.e. independently transduced cell samples.

Fig. 8. Interneuron quantification in *Foxg1*-GOF neocortical cultures. (A) Protocol and lentiviruses employed, **(B)** results. Data evaluated by *t*-test (unpaired, one-tailed). * $p<0.05$, ** $p<10^{-2}$, **** $p<10^{-4}$. *n* = number of biological replicates, i.e. independently transduced cell samples.

Fig. 9 Activity-dependent modulation of neocortical *Foxg1* expression. Evaluation of *Foxg1* expression levels in dissociated DIV7 cultures originating from E16.5 neocortical tissue: protocol **(A)** and results **(B-D)**. In (B, C) qRTPCR quantification of *Foxg1*-mRNA in cultures silenced by 1□M TTX for 0-48 hours (B) or stimulated by 25 mM K^+ for 0-24 hours (C). In (D) WB quantification of Foxg1-protein in cultures stimulated by 25 mM K^+ for 1-24 hours. Data double normalized, against *Gapdh* (B, C) or beta-actin (D), and *t*=0 baseline values (B-D). Results evaluated by t-test (unpaired, one-tailed), run against *t*=0 values. * $p<0.05$, ** $p<0.01$, *** $p<0.001$. *n* = number of biological replicates, i.e. independently grown cell samples.

Fig. 10. Selecting putative mediators of *Foxg1* response to high K^+. (A) Localization of iegF- (immediate early gene factor) and Foxg1-BSs (binding sites) within the *Foxg1* locus, as detected by ChIP on selected cell lines (UCSC) or predicted by Jaspar software. **(B-G)** Fluctuations of select iegFs levels and activities evoked by timed exposure of dissociated DIV7 cultures originating from E16.5 neocortex to 25 mM K^+: (B) protocol and (C-G) results. As for *Creb1*, shown are: (C) qIF (quantitative immuno-fluorescence) evaluation of phospho-protein level and (D) qRTPCR evaluation of its pro-transcriptional activity, in cultures stimulated by 25mM K^+ for up to 180 min (activity reporter: *d2EGFP*-mRNA product of the cAMP.RE_3-p(min)-d2EGFP transgene). Concerning $RelA^{p65}$, shown are: (E) qIF evaluation of nuclear protein level and (F) qRTPCR evaluation of its pro-transcriptional activity, in cultures stimulated by 25mM K^+ for up to 120 min (activity reporter: *d2EGFP*-RNA product of the NFkB.BS_4-p(min)-d2EGFP transgene). As for *Fos*, *Egr1*, *Egr2* and *Cebpb*, shown is: (G) qRTPCR evaluation of endogenous

mRNA levels in cultures stimulated by 25 mM K^+ for up to 24 hours. Data normalized against: (C,E) iegF$_{t=0}$; (D,F) *RFP*-mRNA$_{t=ti}$ and (*d2EGFP*-mRNA/*RFP*-mRNA)$_{t=0}$ [*RFP*-mRNA as the product of the *p(Pgk1)-RFP* transgene]; (G) *Gapdh*-mRNA$_{t=ti}$ and (*iegF*-mRNA/*Gapdh*-mRNA)$_{t=0}$. Results evaluated by t-test (unpaired, one-tailed), run against *t*=0 values. **p*<0.05, ***p*<0.01, ****p*<0.001. *n* = number of biological replicates, i.e. (D, F, G) independently *in vitro* grown cell samples, or (C, E) individual neural cells, evenly and randomly taken from the reported number of independently transduced samples.

Fig. 11. Validating putative mediators of *Foxg1* response to high K^+. *Foxg1* regulation in primary neocortical cultures engineered by immediate early gene-dominant negative (*ieg-DN*) or *Foxg1* transgenes: **(A)** protocol and **(B)** results. In (B), shown are endogenous-*Foxg1*-mRNA levels upon expression of *ieg-DNs* or exogenous *Foxg1*, in the presence of physiological $[K^+]_o$ ("no K^+") or under 25mM $[K^+]_o$. *Foxg1*-cds and *Foxg1*-3'UTR amplicons were used as proxies of endogenous *Foxg1* transcripts in graphs 1,3 and 2,4, respectively. ctr is *Plap*. Data double normalized, against *Gapdh*-mRNA and ctr samples. Results evaluated by t-test (unpaired, one-tailed). **p*<0.05, ***p*<0.01, ****p*<0.001. *n* = number of biological replicates, i.e. independently transduced cultures.

Fig. 12. *Foxg1*-driven modulation of ieg response to high K^+. Activities and expression levels displayed by select immediate early genes (ieg) proteins and mRNAs, respectively, in dissociated, lentivector-engineered E16.5+DIV7 neocortical cultures, upon chronic *Foxg1* upregulation via RNA activation (RNAa) and timed culture exposure to 25 mM K^+: protocol **(A)** and results **(B,C)**. In (B), qRTPCR evaluation of pCreb1 and NFkb transcriptional activities; proxies: *d2EGFP*-mRNA products of lentiviral cAMP.RE$_3$-p(min)-d2EGFP and NFkB.BS$_4$-p(min)-d2EGFP transgenes, respectively. In (C), qRTPCR evaluation of *Fos*, *Egr1*, *Egr2* and *Cebpb* mRNA levels. Data normalized against: (B) *RFP*-mRNA$_{t=ti}$ and (*d2EGFP*-mRNA/*RFP*-mRNA)$_{t=0}$ [*RFP*-mRNA product of the lentiviral p(Pgk1)-RFP transgene]; and (C) *Gapdh*-mRNA$_{t=ti}$ and (*iegF*-mRNA/*Gapdh*-mRNA)$_{t=0}$. Results evaluated by t-test (unpaired, one-tailed), run against ctr$_{t=ti}$ values. **p*<0.05, ***p*<0.01, ****p*<0.001. *n* = number of biological replicates, i.e. independently transduced cell samples.

Figure 1

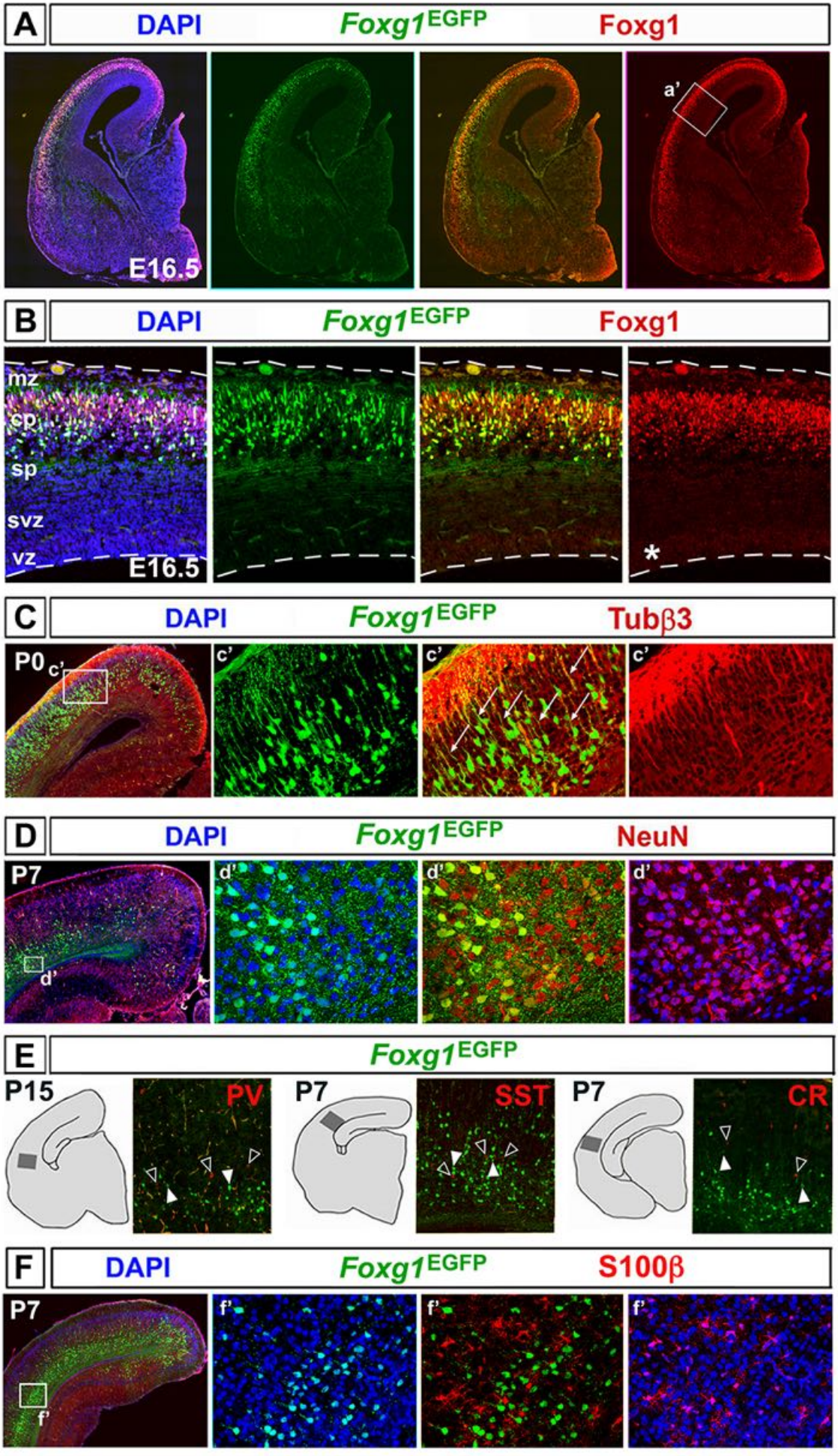
A
DAPI
Foxg1EGFP
Foxg1
a'
E16.5
B
DAPI
Foxg1EGFP
Foxg1
mz
cp
sp
svz
vz
E16.5
*
C
DAPI
Foxg1EGFP
Tubβ3
P0
c'
D
DAPI
Foxg1EGFP
NeuN
P7
d'
E
Foxg1EGFP
P15
PV
P7
SST
P7
CR
F
DAPI
Foxg1EGFP
S100β
P7
f'

Figure 2

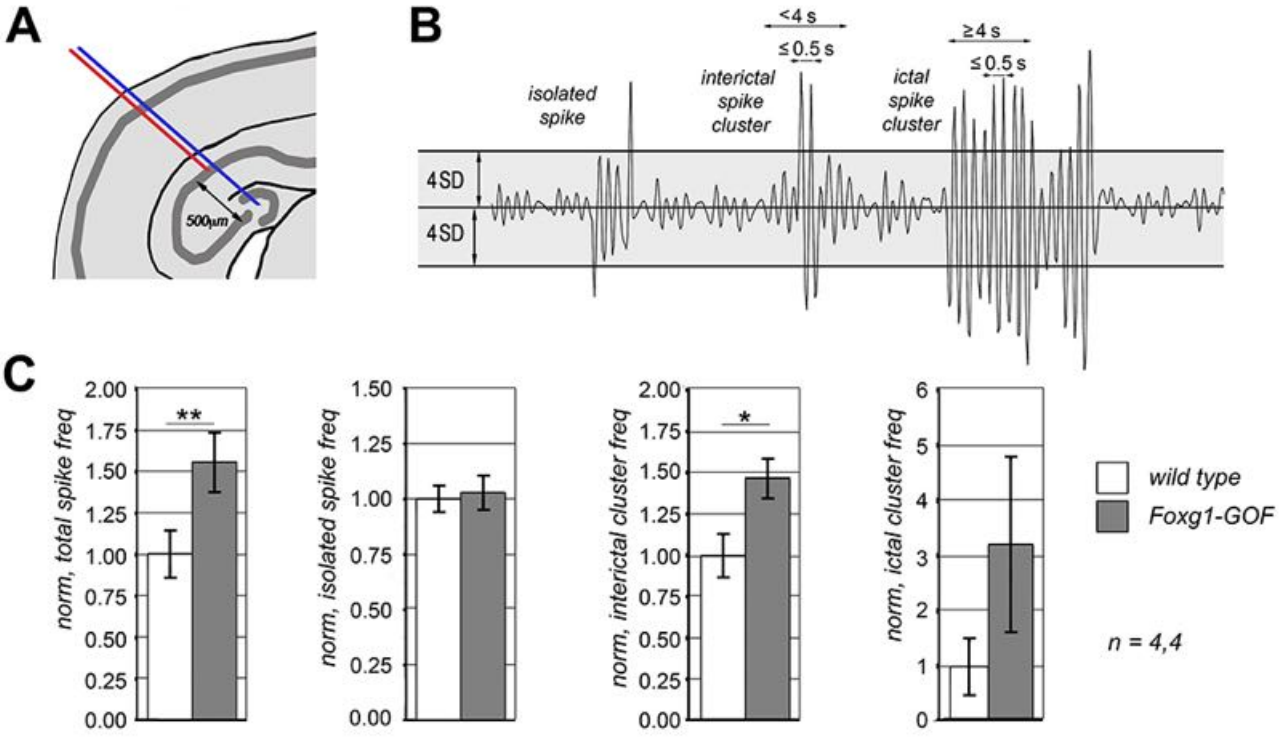
A
500μm
B
<4 s
≤0.5 s
≥4 s
≤0.5 s
isolated spike
interictal spike cluster
ictal spike cluster
4SD
4SD
C
norm, total spike freq
norm, isolated spike freq
norm, interictal cluster freq
norm, ictal cluster freq
**
*
wild type
Foxg1-GOF
n = 4,4

Figure 3

A

KA dose:
20 mg/kg body weight

administration:
intraperitoneal

Racine's stages (RS)
0, normal behavior
1, immobility
2, forelimb and/or tail extension, rigid posture
3, repetitive movements, head bobbing
4, forelimb clonus with rearing and falling (limbic motor seizure)
5, continuous rearing and falling
6, severe whole-body convulsions (tonic–clonic seizures)
7, death

B

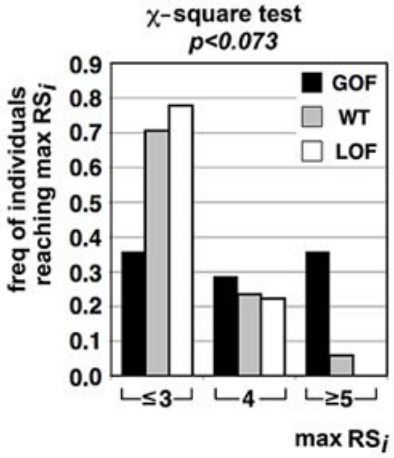

C

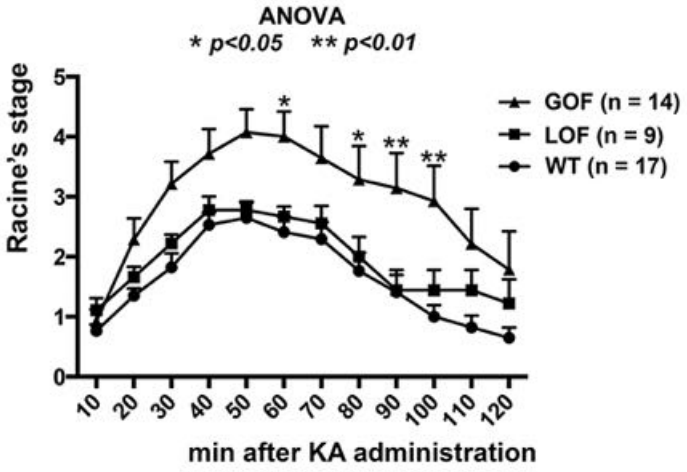

D

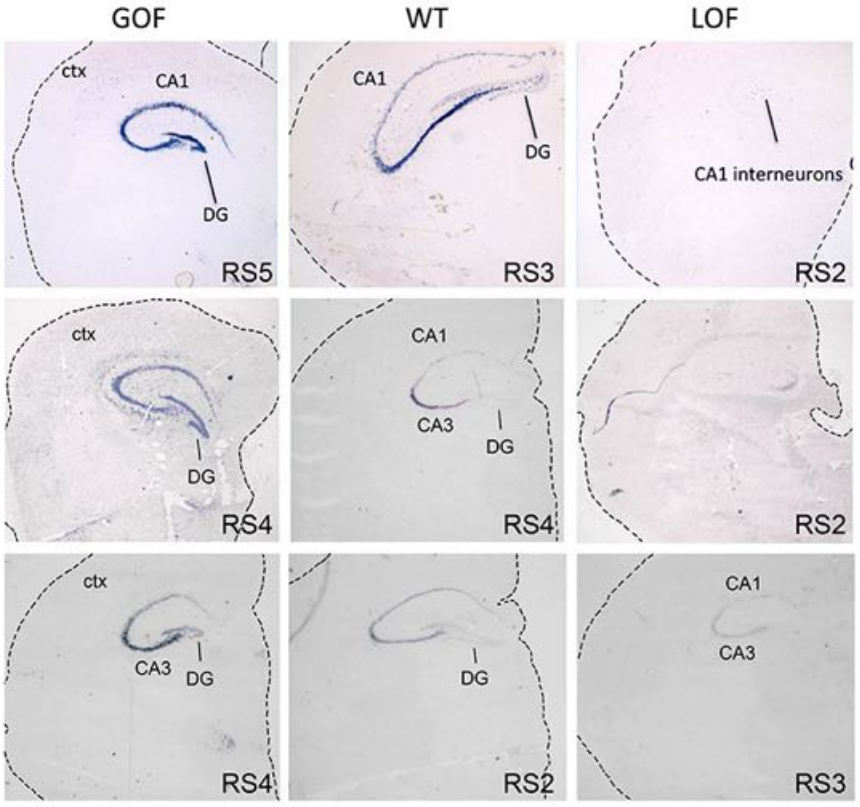

***c-fos*-mRNA, 2 hours after KA administration**

labeling	CA1	strong	weak	weak
	CA3	strong	mid-strong	weak
	DG	strong	weak	no
	ctx	weak	no	no

Figure 4

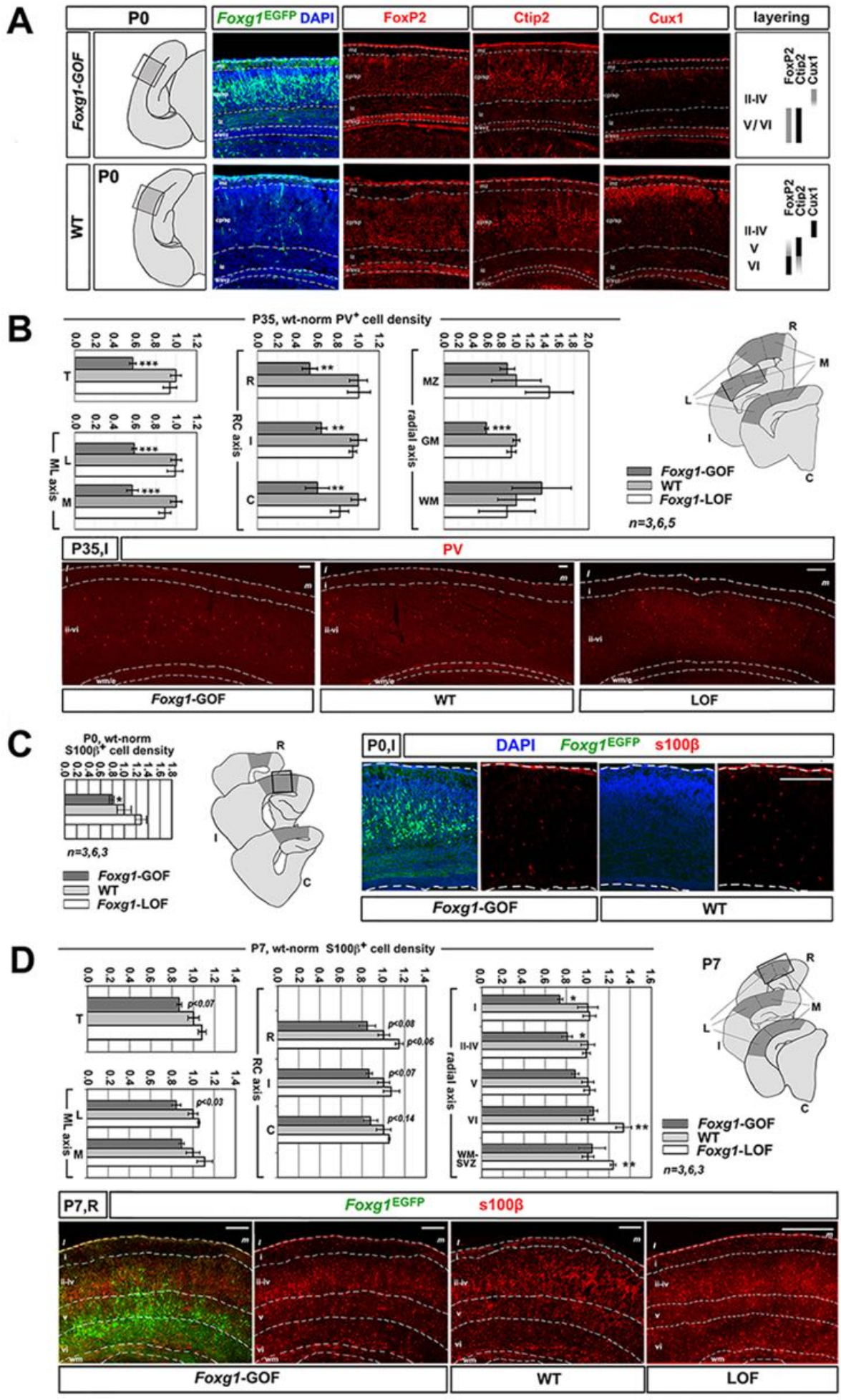
A
P0
Foxg1EGFP DAPI
FoxP2
Ctip2
Cux1
layering
Foxg1-GOF
WT
P0
II-IV
V/VI
V
VI
B
P35, wt-norm PV+ cell density
T
L
M
ML axis
R
I
C
RC axis
MZ
GM
WM
radial axis
Foxg1-GOF
WT
Foxg1-LOF
n=3,6,5
P35,I
PV
Foxg1-GOF
WT
LOF
C
P0, wt-norm S100β+ cell density
n=3,6,3
Foxg1-GOF
WT
Foxg1-LOF
P0,I
DAPI
Foxg1EGFP
s100β
Foxg1-GOF
WT
D
P7, wt-norm S100β+ cell density
p<0,07
p<0,03
p<0,08
p<0,06
p<0,07
p<0,14
II-IV
V
VI
WM-SVZ
P7
Foxg1-GOF
WT
Foxg1-LOF
n=3,6,3
P7,R
Foxg1EGFP
s100β
Foxg1-GOF
WT
LOF

Figure 5

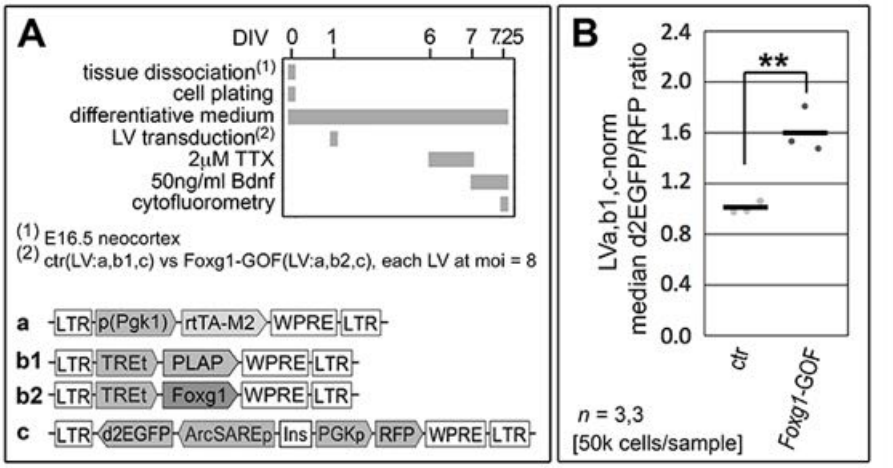
A
DIV 0 1 6 7 7.25
tissue dissociation(1)
cell plating
differentiative medium
LV transduction(2)
2μM TTX
50ng/ml Bdnf
cytofluorometry
(1) E16.5 neocortex
(2) ctr(LV:a,b1,c) vs Foxg1-GOF(LV:a,b2,c), each LV at moi = 8
a LTR p(Pgk1) rtTA-M2 WPRE LTR
b1 LTR TREt PLAP WPRE LTR
b2 LTR TREt Foxg1 WPRE LTR
c LTR d2EGFP ArcSAREp Ins PGKp RFP WPRE LTR
B
LVa,b1,c-norm median d2EGFP/RFP ratio
2.4
2.0
1.6
1.2
0.8
0.4
0.0
**
ctr
Foxg1-GOF
n = 3,3
[50k cells/sample]

Figure 6

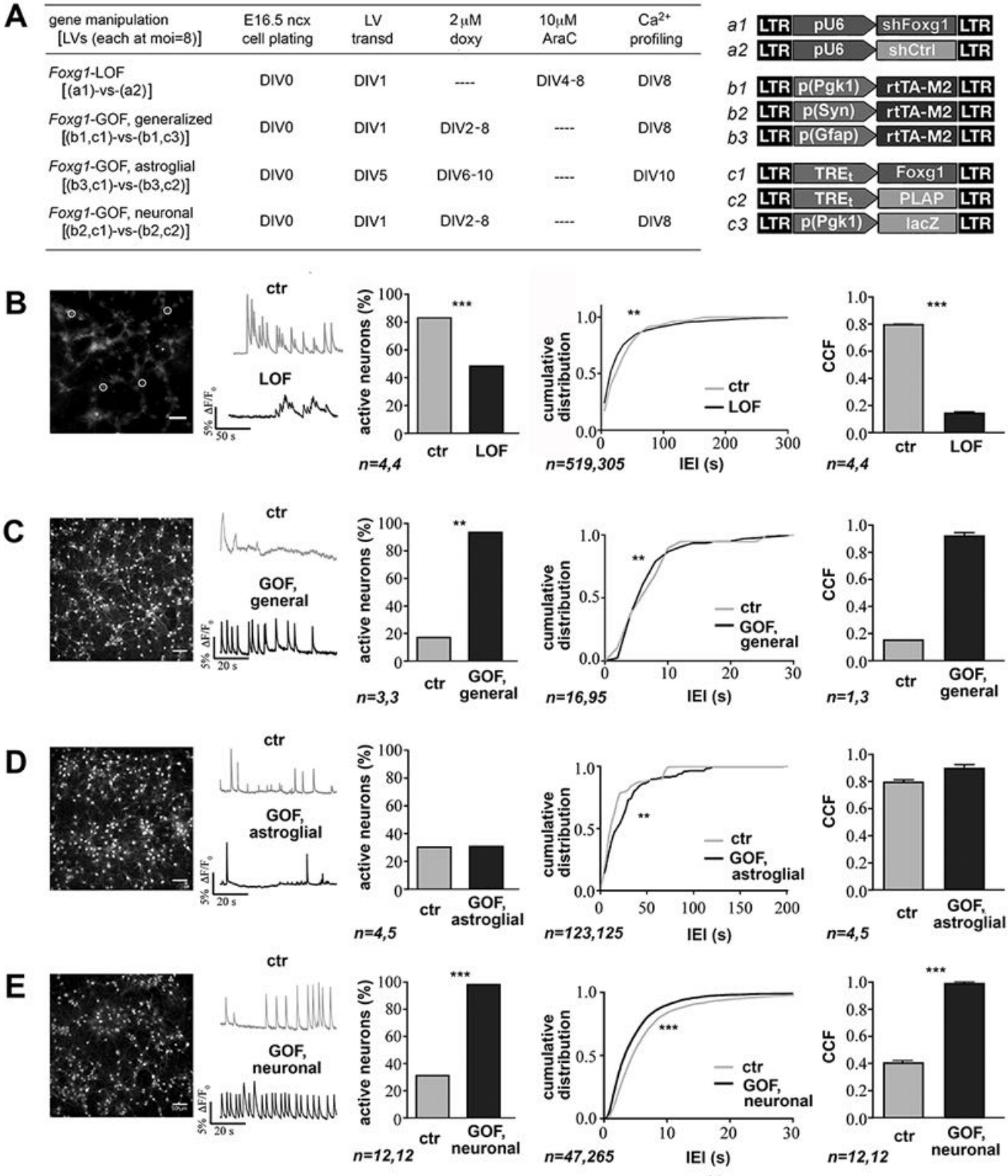
A
gene manipulation [LVs (each at moi=8)]
E16.5 ncx cell plating
LV transd
2μM doxy
10μM AraC
Ca2+ profiling
Foxg1-LOF [(a1)-vs-(a2)]
DIV0 DIV1 ---- DIV4-8 DIV8
Foxg1-GOF, generalized [(b1,c1)-vs-(b1,c3)]
DIV0 DIV1 DIV2-8 ---- DIV8
Foxg1-GOF, astroglial [(b3,c1)-vs-(b3,c2)]
DIV0 DIV5 DIV6-10 ---- DIV10
Foxg1-GOF, neuronal [(b2,c1)-vs-(b2,c2)]
DIV0 DIV1 DIV2-8 ---- DIV8
a1 LTR pU6 shFoxg1 LTR
a2 LTR pU6 shCtrl LTR
b1 LTR p(Pgk1) rtTA-M2 LTR
b2 LTR p(Syn) rtTA-M2 LTR
b3 LTR p(Gfap) rtTA-M2 LTR
c1 LTR TRE$_t$ Foxg1 LTR
c2 LTR TRE$_t$ PLAP LTR
c3 LTR p(Pgk1) lacZ LTR
B
ctr
LOF
5% ΔF/F$_0$
50 s
active neurons (%)
***
ctr LOF
n=4,4
cumulative distribution
**
ctr
LOF
n=519,305
IEI (s)
CCF
***
ctr LOF
n=4,4
C
ctr
GOF, general
20 s
active neurons (%)
**
ctr GOF, general
n=3,3
cumulative distribution
**
ctr
GOF, general
n=16,95
IEI (s)
CCF
ctr GOF, general
n=1,3
D
ctr
GOF, astroglial
20 s
active neurons (%)
ctr GOF, astroglial
n=4,5
cumulative distribution
**
ctr
GOF, astroglial
n=123,125
IEI (s)
CCF
ctr GOF, astroglial
n=4,5
E
ctr
GOF, neuronal
20 s
active neurons (%)
***
ctr GOF, neuronal
n=12,12
cumulative distribution
***
ctr
GOF, neuronal
n=47,265
IEI (s)
CCF
***
ctr GOF, neuronal
n=12,12

Figure 7

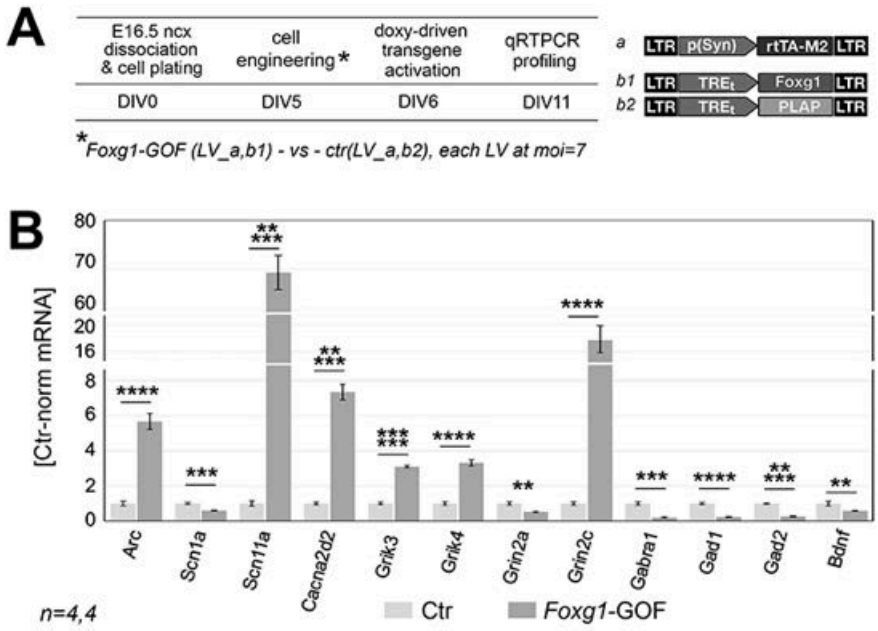
A
E16.5 ncx dissociation & cell plating
cell engineering*
doxy-driven transgene activation
qRTPCR profiling
DIV0
DIV5
DIV6
DIV11
*Foxg1-GOF (LV_a,b1) - vs - ctr(LV_a,b2), each LV at moi=7
a
LTR p(Syn) rtTA-M2 LTR
b1
LTR TRE Foxg1 LTR
b2
LTR TRE PLAP LTR
B
[Ctr-norm mRNA]
80
70
60
20
16
8
6
4
2
0
Arc
Scn1a
Scn11a
Cacna2d2
Grik3
Grik4
Grin2a
Grin2c
Gabra1
Gad1
Gad2
Bdnf
n=4,4
Ctr
Foxg1-GOF

Figure 8

A

exp timing	E16.5 ncx dissociation & cell plating *	cell engineering: t	cell engineering: LVs	cell engineering: moi	2μg/mL doxy-driven transgene activation	profiling
Foxg1-LOF	DIV0	DIV2	(a1)-vs-(a2)	10	----	DIV8
Foxg1-GOF, generalized	DIV0	DIV2	(b1,c1)-vs-(b1,c3)	8+8	DIV3	DIV8
Foxg1-GOF, astroglial	DIV0	DIV5	(b3,c1)-vs-(b3,c2)	8+8	DIV6	DIV8
Foxg1-GOF, neuronal	DIV0	DIV2	(b2,c1)-vs-(b2,c2)	8+8	DIV3	DIV8

* from *Gad1*$^{EGFP/+}$ donors

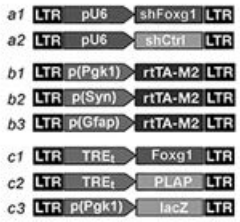

B

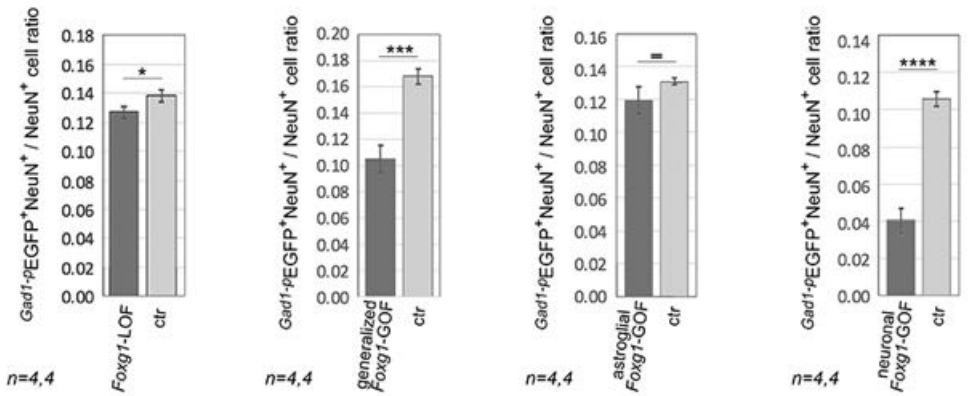

Figure 9

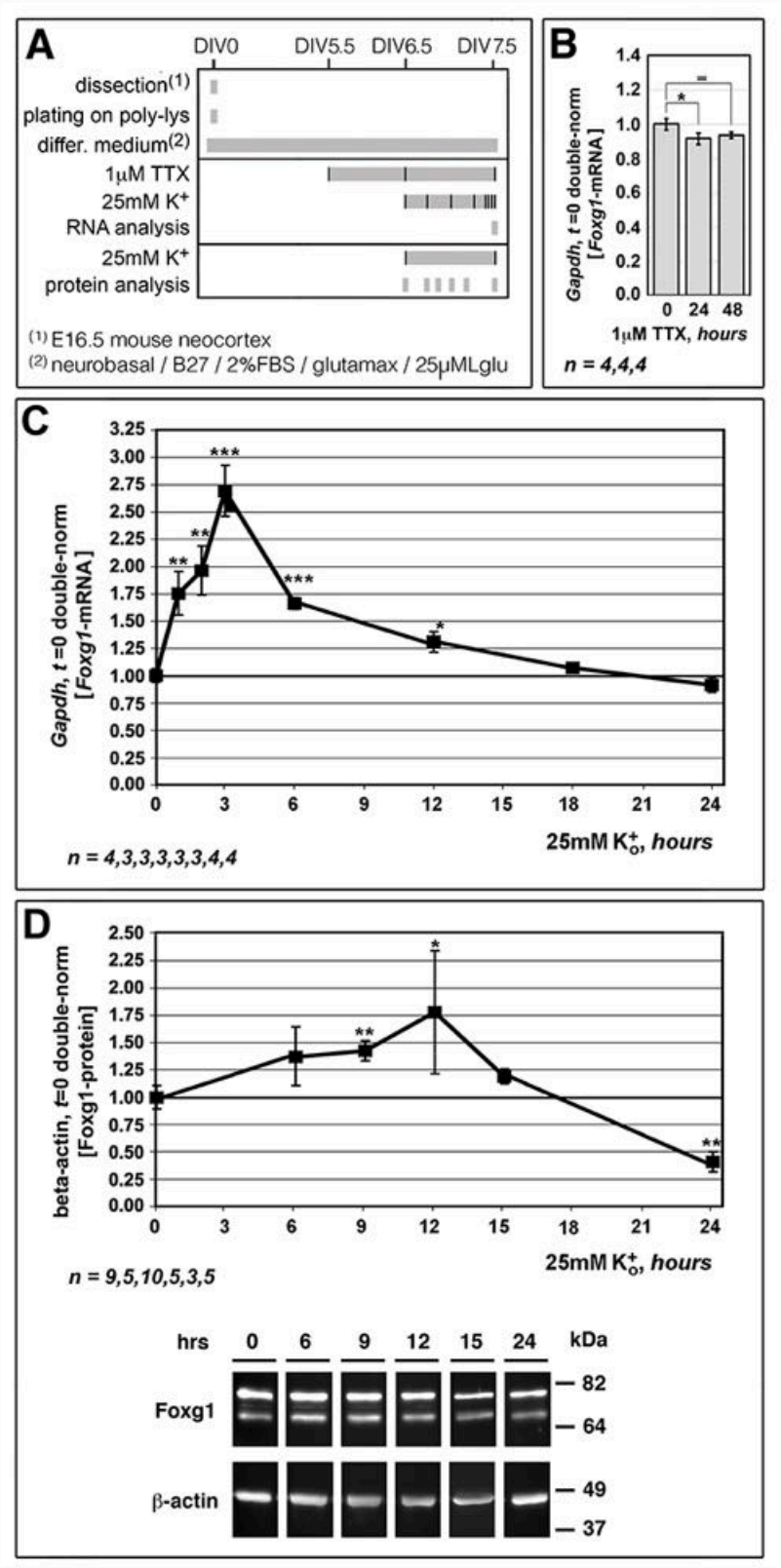
A
DIV0
DIV5.5
DIV6.5
DIV7.5
dissection(1)
plating on poly-lys
differ. medium(2)
1μM TTX
25mM K+
RNA analysis
25mM K+
protein analysis
(1) E16.5 mouse neocortex
(2) neurobasal / B27 / 2%FBS / glutamax / 25μMLglu
B
Gapdh, t=0 double-norm [Foxg1-mRNA]
1μM TTX, hours
n = 4,4,4
C
Gapdh, t=0 double-norm [Foxg1-mRNA]
25mM K+o, hours
n = 4,3,3,3,3,3,4,4
D
beta-actin, t=0 double-norm [Foxg1-protein]
25mM K+o, hours
n = 9,5,10,5,3,5
hrs
0
6
9
12
15
24
kDa
Foxg1
82
64
β-actin
49
37

Figure 10

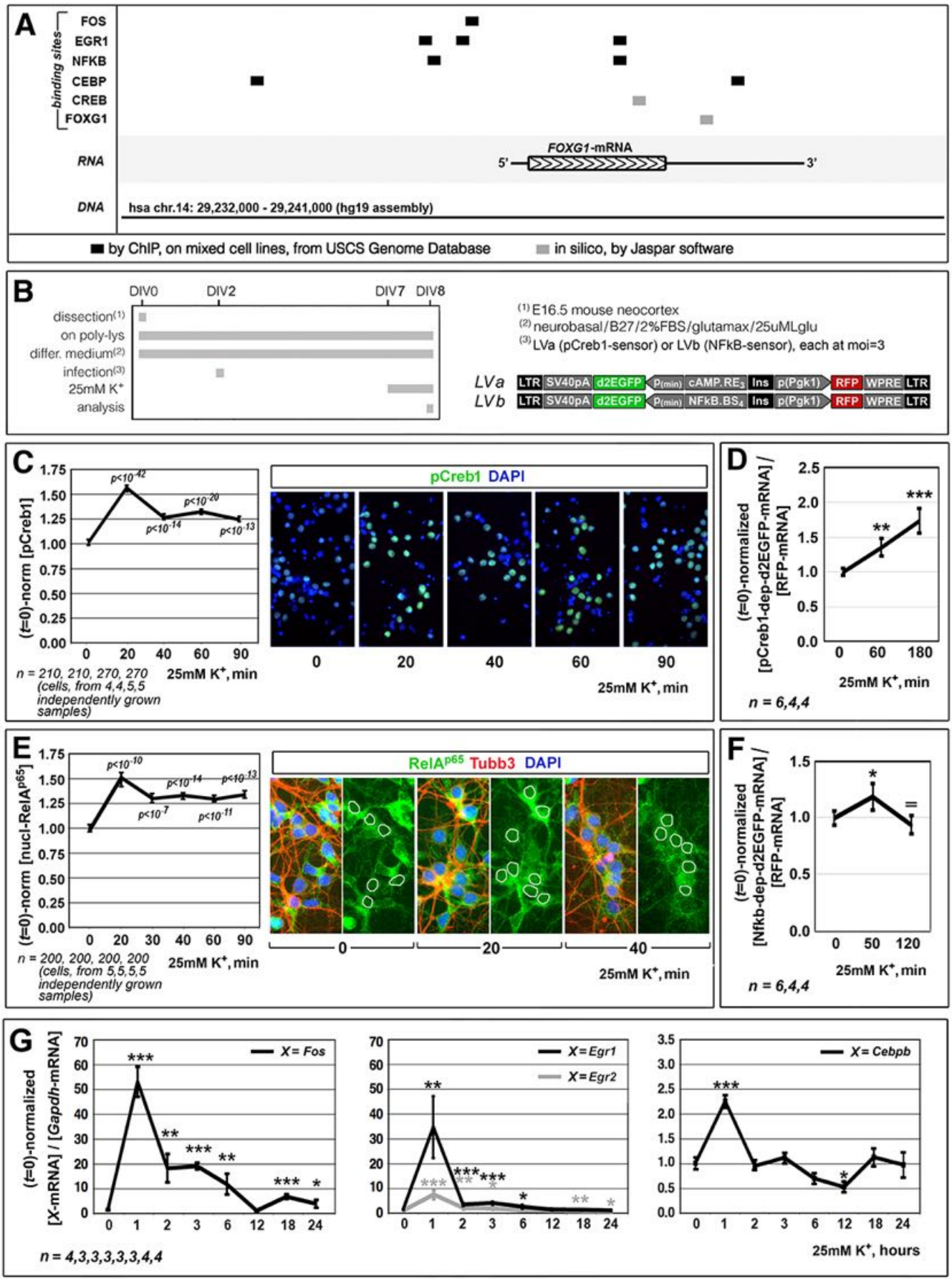
A
binding sites
FOS
EGR1
NFKB
CEBP
CREB
FOXG1
RNA
FOXG1-mRNA
5'
3'
DNA
hsa chr.14: 29,232,000 - 29,241,000 (hg19 assembly)
by ChIP, on mixed cell lines, from USCS Genome Database
in silico, by Jaspar software
B
DIV0
DIV2
DIV7
DIV8
dissection(1)
on poly-lys
differ. medium(2)
infection(3)
25mM K+
analysis
(1) E16.5 mouse neocortex
(2) neurobasal/B27/2%FBS/glutamax/25uMLglu
(3) LVa (pCreb1-sensor) or LVb (NFkB-sensor), each at moi=3
LVa
LVb
LTR
SV40pA
d2EGFP
p(min)
cAMP.RE3
NFkB.BS4
Ins
p(Pgk1)
RFP
WPRE
LTR
C
(t=0)-norm [pCreb1]
p<10-42
p<10-20
p<10-14
p<10-13
n = 210, 210, 270, 270 (cells, from 4,4,5,5 independently grown samples)
25mM K+, min
pCreb1 DAPI
0
20
40
60
90
25mM K+, min
D
(t=0)-normalized [pCreb1-dep-d2EGFP-mRNA] / [RFP-mRNA]
n = 6,4,4
25mM K+, min
E
(t=0)-norm [nucl-RelA p65]
p<10-10
p<10-14
p<10-13
p<10-7
p<10-11
n = 200, 200, 200, 200 (cells, from 5,5,5,5 independently grown samples)
25mM K+, min
RelAp65 Tubb3 DAPI
0
20
40
25mM K+, min
F
(t=0)-normalized [Nfkb-dep-d2EGFP-mRNA] / [RFP-mRNA]
n = 6,4,4
25mM K+, min
G
(t=0)-normalized [X-mRNA] / [Gapdh-mRNA]
X = Fos
X = Egr1
X = Egr2
X = Cebpb
n = 4,3,3,3,3,3,4,4
25mM K+, hours

Figure 11

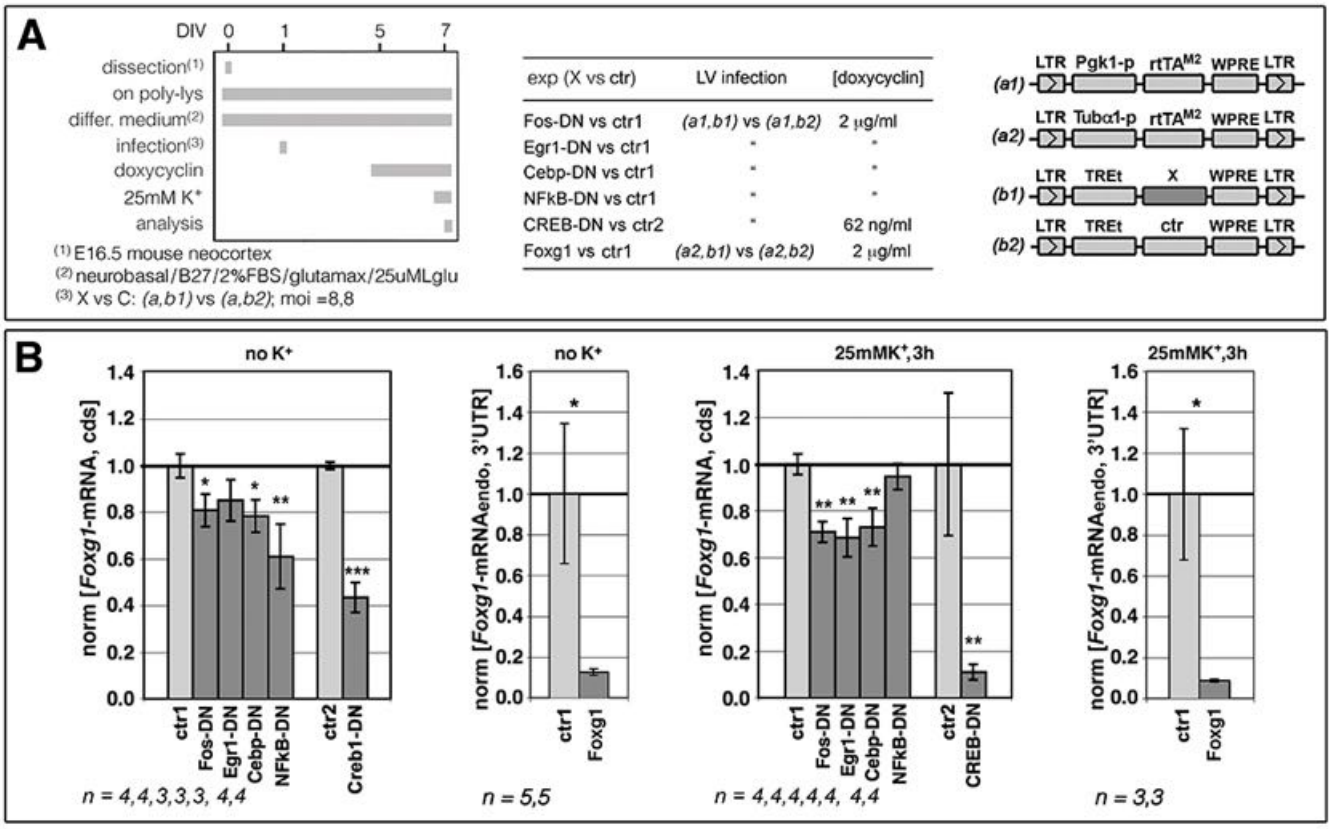
A
DIV 0 1 5 7
dissection(1)
on poly-lys
differ. medium(2)
infection(3)
doxycyclin
25mM K+
analysis
(1) E16.5 mouse neocortex
(2) neurobasal/B27/2%FBS/glutamax/25uMLglu
(3) X vs C: (a,b1) vs (a,b2); moi =8,8
exp (X vs ctr) | LV infection | [doxycyclin]
Fos-DN vs ctr1 | (a1,b1) vs (a1,b2) | 2 μg/ml
Egr1-DN vs ctr1 | " | "
Cebp-DN vs ctr1 | " | "
NFkB-DN vs ctr1 | " | "
CREB-DN vs ctr2 | " | 62 ng/ml
Foxg1 vs ctr1 | (a2,b1) vs (a2,b2) | 2 μg/ml
(a1) LTR Pgk1-p rtTA^M2 WPRE LTR
(a2) LTR Tubα1-p rtTA^M2 WPRE LTR
(b1) LTR TREt X WPRE LTR
(b2) LTR TREt ctr WPRE LTR
B
no K+
norm [Foxg1-mRNA, cds]
ctr1 Fos-DN Egr1-DN Cebp-DN NFkB-DN ctr2 Creb1-DN
n = 4,4,3,3,3, 4,4
no K+
norm [Foxg1-mRNAendo, 3'UTR]
ctr1 Foxg1
n = 5,5
25mMK+,3h
norm [Foxg1-mRNA, cds]
ctr1 Fos-DN Egr1-DN Cebp-DN NFkB-DN ctr2 CREB-DN
n = 4,4,4,4,4, 4,4
25mMK+,3h
norm [Foxg1-mRNAendo, 3'UTR]
ctr1 Foxg1
n = 3,3

Figure 12

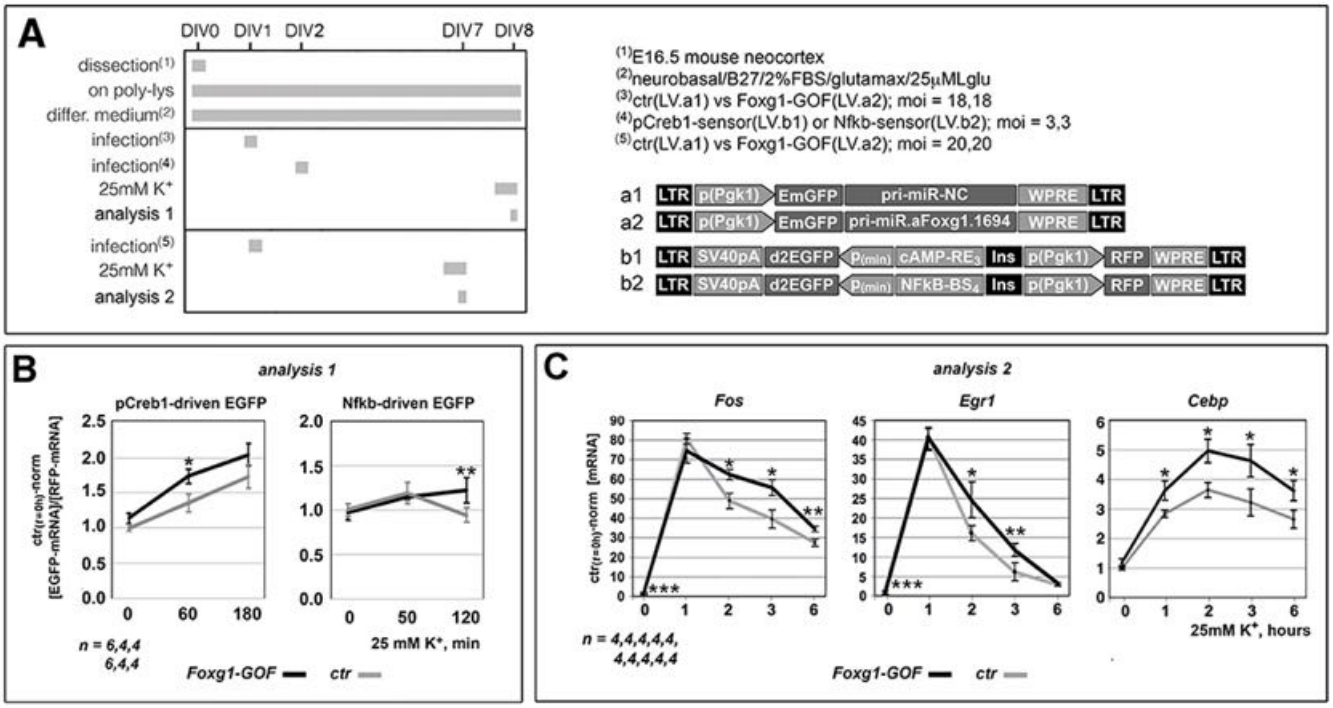
A
DIV0 DIV1 DIV2 DIV7 DIV8
dissection(1)
on poly-lys
differ. medium(2)
infection(3)
infection(4)
25mM K+
analysis 1
infection(5)
25mM K+
analysis 2
(1)E16.5 mouse neocortex
(2)neurobasal/B27/2%FBS/glutamax/25μMLglu
(3)ctr(LV.a1) vs Foxg1-GOF(LV.a2); moi = 18,18
(4)pCreb1-sensor(LV.b1) or Nfkb-sensor(LV.b2); moi = 3,3
(5)ctr(LV.a1) vs Foxg1-GOF(LV.a2); moi = 20,20
a1 LTR p(Pgk1) EmGFP pri-miR-NC WPRE LTR
a2 LTR p(Pgk1) EmGFP pri-miR.aFoxg1.1694 WPRE LTR
b1 LTR SV40pA d2EGFP p(min) cAMP-RE3 Ins p(Pgk1) RFP WPRE LTR
b2 LTR SV40pA d2EGFP p(min) NFkB-BS4 Ins p(Pgk1) RFP WPRE LTR
B
analysis 1
pCreb1-driven EGFP
Nfkb-driven EGFP
ctr(t=0h)-norm [EGFP-mRNA]/[RFP-mRNA]
n = 6,4,4 6,4,4
25 mM K+, min
Foxg1-GOF
ctr
C
analysis 2
Fos
Egr1
Cebp
ctr(t=0h)-norm [mRNA]
n = 4,4,4,4,4,4, 4,4,4,4,4,4
25mM K+, hours
Foxg1-GOF
ctr

Figure S1

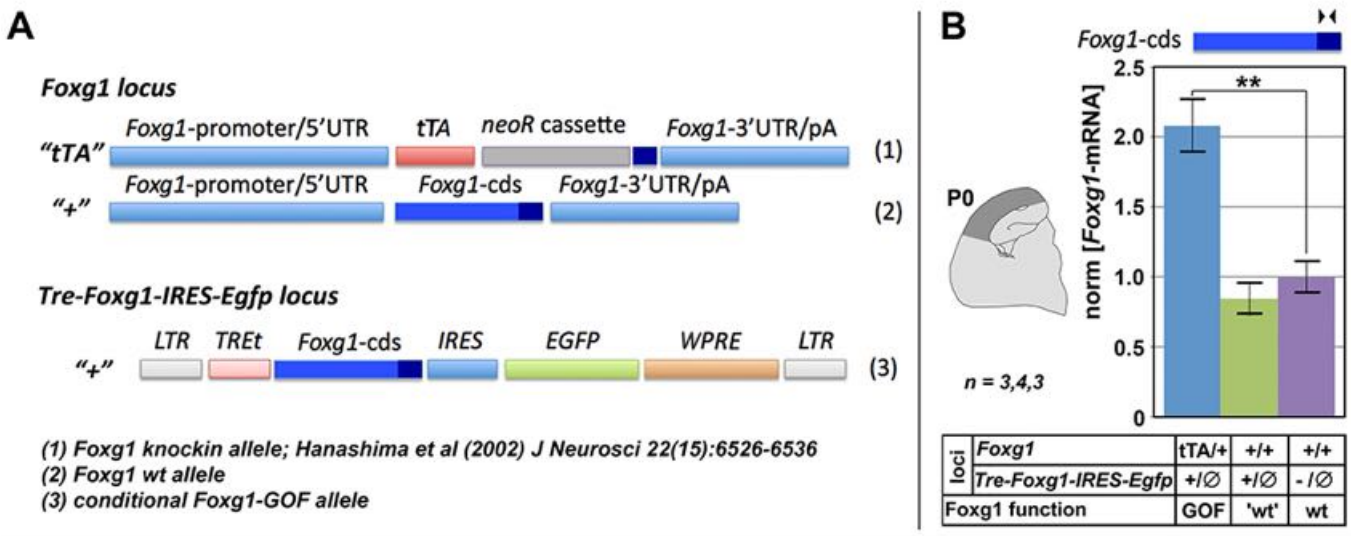
A
Foxg1 locus
"tTA"
Foxg1-promoter/5'UTR
tTA
neoR cassette
Foxg1-3'UTR/pA
(1)
"+"
Foxg1-promoter/5'UTR
Foxg1-cds
Foxg1-3'UTR/pA
(2)
Tre-Foxg1-IRES-Egfp locus
"+"
LTR
TREt
Foxg1-cds
IRES
EGFP
WPRE
LTR
(3)
(1) Foxg1 knockin allele; Hanashima et al (2002) J Neurosci 22(15):6526-6536
(2) Foxg1 wt allele
(3) conditional Foxg1-GOF allele
B
Foxg1-cds
P0
n = 3,4,3
norm [Foxg1-mRNA]
2.5
2.0
1.5
1.0
0.5
0
**
loci
Foxg1
tTA/+
+/+
+/+
Tre-Foxg1-IRES-Egfp
+/∅
+/∅
- /∅
Foxg1 function
GOF
'wt'
wt

Figure S2

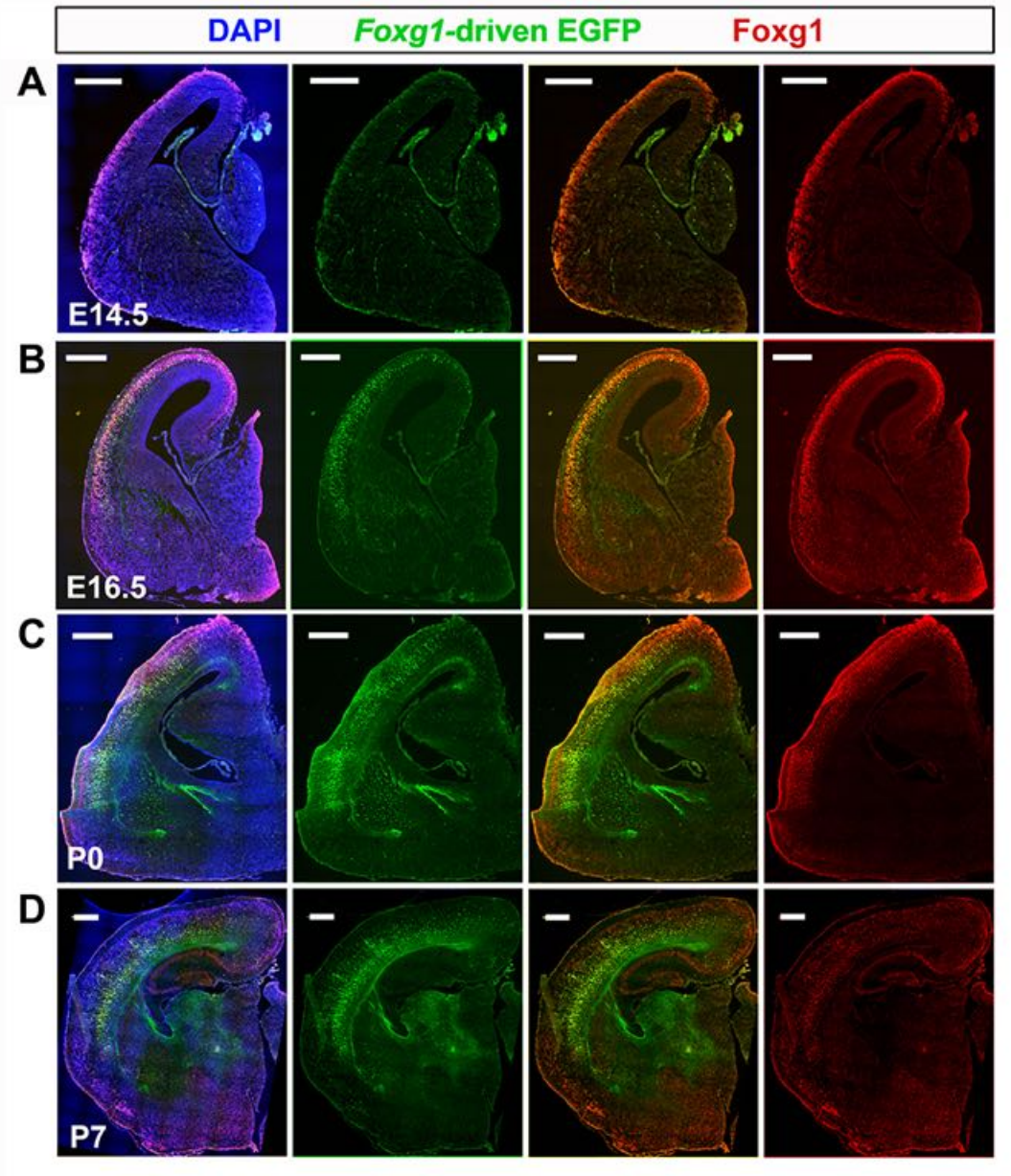

Figure S3

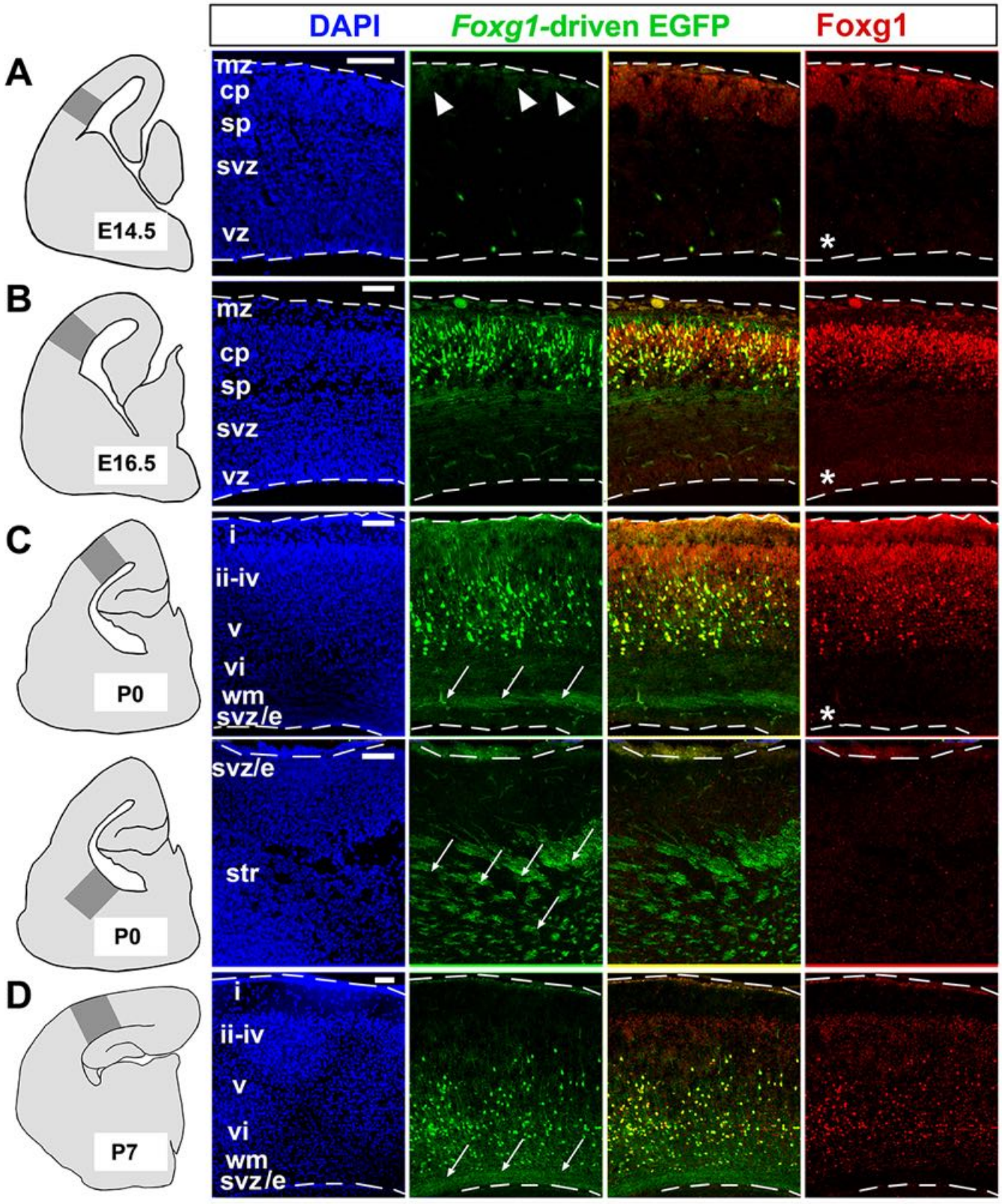
DAPI
Foxg1-driven EGFP
Foxg1
A
E14.5
mz
cp
sp
svz
vz
B
E16.5
mz
cp
sp
svz
vz
C
P0
i
ii-iv
v
vi
wm
svz/e
P0
svz/e
str
D
P7
i
ii-iv
v
vi
wm
svz/e

Figure S4

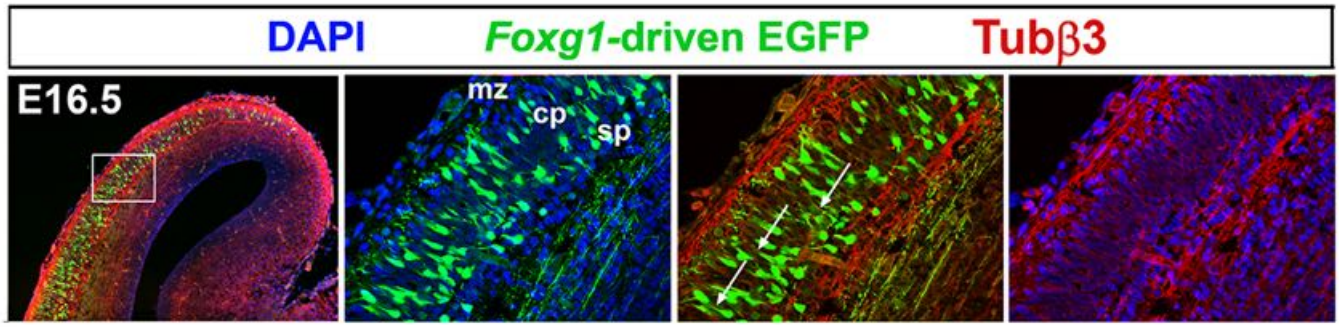

Figure S5

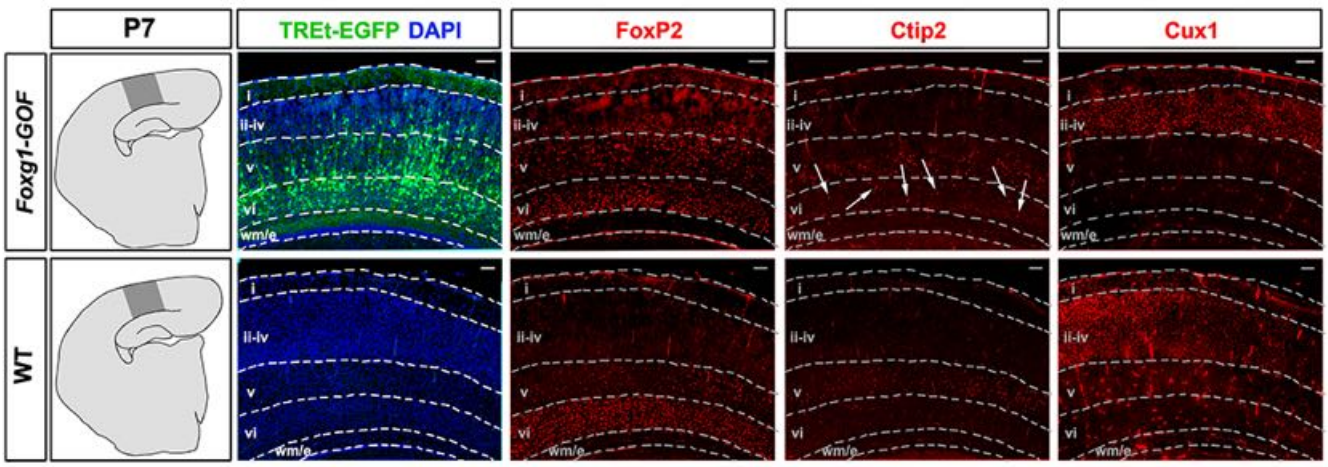

Figure S6

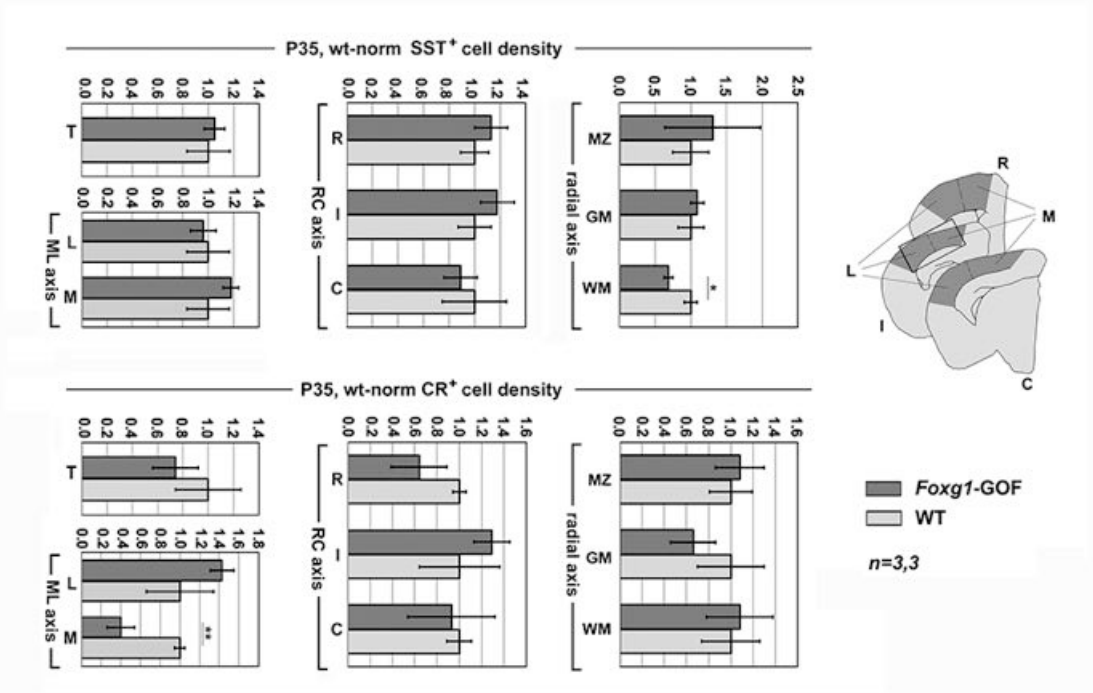
P35, wt-norm SST+ cell density
T
L
M
ML axis
R
I
C
RC axis
MZ
GM
WM
radial axis
*
P35, wt-norm CR+ cell density
**
R
M
L
I
C
Foxg1-GOF
WT
n=3,3

Figure S7

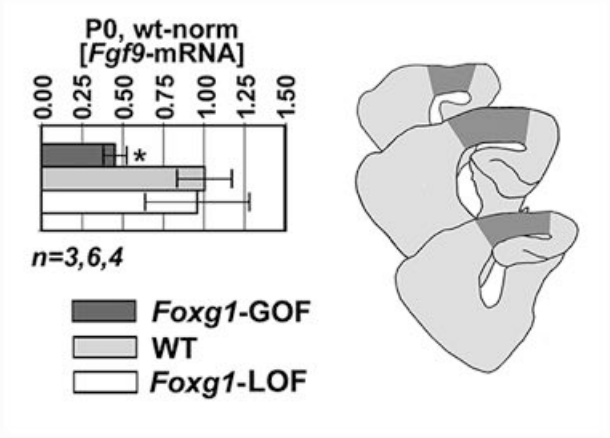
P0, wt-norm
[*Fgf9*-mRNA]
0.00
0.25
0.50
0.75
1.00
1.25
1.50
*
n=3,6,4
Foxg1-GOF
WT
Foxg1-LOF

Figure S8

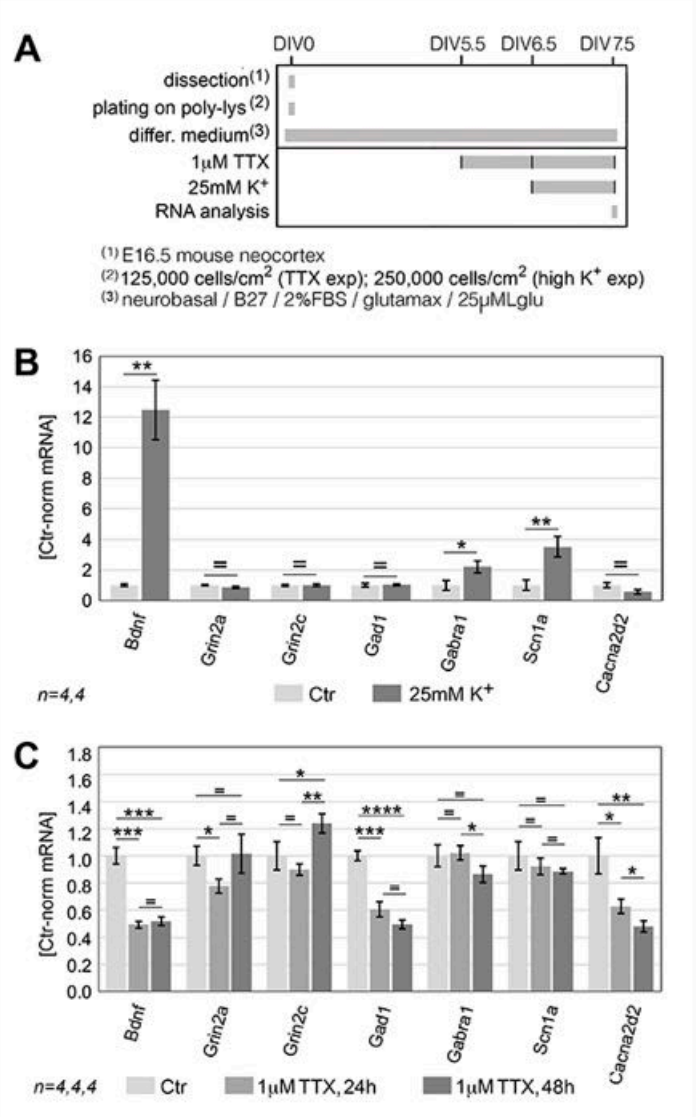
A
DIV0
DIV5.5
DIV6.5
DIV7.5
dissection(1)
plating on poly-lys (2)
differ. medium(3)
1μM TTX
25mM K+
RNA analysis
(1) E16.5 mouse neocortex
(2) 125,000 cells/cm2 (TTX exp); 250,000 cells/cm2 (high K+ exp)
(3) neurobasal / B27 / 2%FBS / glutamax / 25μMLglu
B
[Ctr-norm mRNA]
Bdnf
Grin2a
Grin2c
Gad1
Gabra1
Scn1a
Cacna2d2
n=4,4
Ctr
25mM K+
C
[Ctr-norm mRNA]
Bdnf
Grin2a
Grin2c
Gad1
Gabra1
Scn1a
Cacna2d2
n=4,4,4
Ctr
1μM TTX, 24h
1μM TTX, 48h

Figure S9

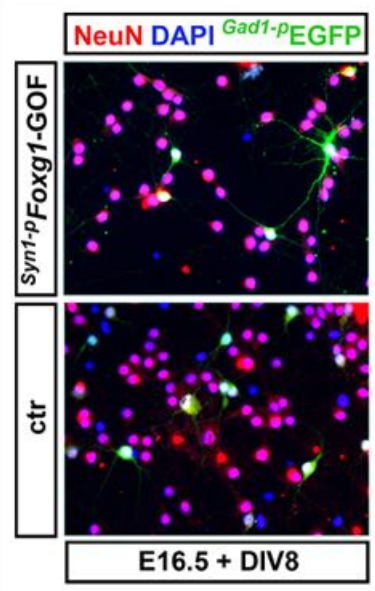

Figure S10

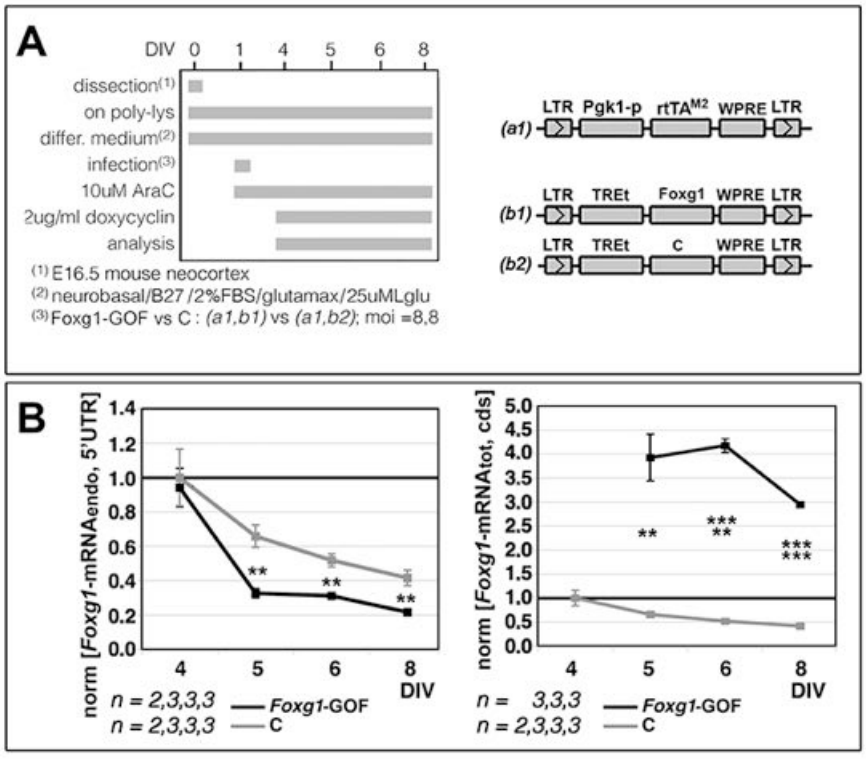
A
DIV 0 1 4 5 6 8
dissection(1)
on poly-lys
differ. medium(2)
infection(3)
10uM AraC
2ug/ml doxycyclin
analysis
(1) E16.5 mouse neocortex
(2) neurobasal/B27 /2%FBS/glutamax/25uMLglu
(3) Foxg1-GOF vs C : (a1,b1) vs (a1,b2); moi =8,8
LTR Pgk1-p rtTA^M2 WPRE LTR
(a1)
LTR TREt Foxg1 WPRE LTR
(b1)
LTR TREt C WPRE LTR
(b2)
B
norm [Foxg1-mRNAendo, 5'UTR]
n = 2,3,3,3 Foxg1-GOF
n = 2,3,3,3 C
DIV
norm [Foxg1-mRNAtot, cds]
n = 3,3,3 Foxg1-GOF
n = 2,3,3,3 C
DIV

6 FINAL REMARKS

During the development of the vertebrate CNS, all neuronal cell types including neurons, astrocytes and oligodendrocytes directly originate form NS-NPCs (Gao et al., 2014), while during CNS degeneration, the damage leads to irreversible neuronal loss, resulting in functional deficits and debilitating pathologies. Anyway, it has been shown that CNS injury can, to some extent, "awake" mechanisms of plasticity usually present during CNS development (Caleo, 2015).

These plasticity events indentify NS-NPCs as essential player even during brain insults which perturb the homeostasis of adult neurogenic niches and the migratory routes of their progeny. In fact, still a spontaneous recruitment of neuroblasts towards pathological sites is observed in a multitude of animal's brain models. For instance, mobilization of neuroblasts from neurogenic niches occurs in response to stroke (Arvidsson et al., 2002), trauma (Kreuzberg et al., 2010) and HD (Kandasamy et al., 2015) in animal models. Since many studies provide evidence for the competence of grafted NS-NPCs to survive, migrate, and differentiate both *in vitro* and *in vivo* systems (Widera, 2004; Wu et al., 2012), the full understanding of NS-NPC's development promises to have a huge impact on future therapeutic approaches (Silver and Miller, 2004; Widera et al., 2007).

Nevertheless, many questions emerge if we think to cells transplantation as the most resolutive way to overcome brain damage. For instance, to which extent can the remaining brain parenchyma accommodate neurons in networks that suffered from neuronal loss due to injury or neurological disease? Would the microenvironment be permissive for neuronal replacement and synaptic integration? Which cells can perform best? Can the loss of function be restored? And finally, how adequate is the new cells participation in the pre-existing circuitry?

In order to answer some of these open questions, with the final goal of evaluating whether these cells could integrate among and communicate with post-mitotic neurons, we established an *in vitro* system of co-culture with different kind of cells, to study single cells and neuronal network properties.

We demonstrated that, when grown in contact with hippocampal neurons, NS-NPCs display a great change in terms of cell maturation, plus the ability to respond and recreate the same kind of synapsis received by hippocampal neurons. These last ones, by the way, confirmed to be an essential *in vitro* control for membrane passive properties and post

synaptic current kinetics as, being so well characterized, they gave the possibility to confirm every improvement in NS-NPCs. In fact in mixed cultures, besides the changes in single cells membrane properties for NS-NPCs, which indicate an increase in cell's size and number of expressed channels, we also observed the formation of a hybrid network with new features different from the ones observed in control cultures (i.e. monocultures of NS-NPCs and hippocampal neurons). Results about the network's behavior are confirmed also by MEAs recordings which suggest that the formation of functional hybrid networks differs from control cultures in terms of their electrophysiological characteristics, resulting in qualitatively and quantitatively different emerging spontaneous episodic synchronization. Many of the differences observed in terms of network activity and cell communication are due to the different balance between excitation and inhibition. In fact, one of the best characterized phenotypes change for NS-NPCs is the switch towards the use of glutamate as excitatory neurotransmitter, a typical hippocampal feature. Such a change led to a different balance of glutamatergic/GABAergic synapses in NS-NPCs, which, together with a higher number of monosynaptically connected neurons, contribute to the whole network activity with a stronger synchronization rate, both in spontaneous conditions and in specifically induced pharmacological ones. The same trend, i.e. the hypothesized decrease of progenitors differentiating into GABAergic neurons, was observed also when NS-NPCs were grown among neuros from SNc/VTA; in this case we also investigated if NS-NPCs result to express the dopaminergic phenotype, but in our preliminary data we never actually found this feature. This may be explained with the evidence that the NS-NPCs - hippocampal neurons mixed cultures had a strong glutamatergic component (about 60% of total number of neurons), while NS-NPCs - SNc/VTA mixed cultures kept only a weaker component of dopaminergic neurons (25% of total neurons). We, in fact, demonstrate that the action potential firing ability held by hippocampal neurons plays a fundamental role in NS-NPCs maturation as well as the astrocytes released factors.

On the other hand, SNc/VTA dissociated neurons culture are not so commonly used as well as the hippocampal dissociated cultures and therefore, the role of dopamine in synapses formation and/or maturation is not well characterized, neither it was evident from our results. Further studies investigating the integration of NPCs among dopaminergic neurons are needed as their potential use in *vivo* would be of great interest for PD.

In conclusion, during the last decade neuronal replacement therapy has become incresingly promising for neurodegenerative diseases therapies because it directly addresses neurodegeneration by replacing lost cells with healthy new ones towards the goal of restoring compromised brain functions (Grade and Götz, 2017). Among the candidates, multipotent neural stem cells (i.e. NS-NPCs derived from embryonic tissue) are the most promising as their protective effects against the host's dysfunctional neurons has been already demonstrated in rodents (Ourednik et al., 2002). However, the mechanisms underlying the functional improvements, have not yet been completely understood, hence it is still questionable how appropriate and to what extent can these new neurons connect in the target zone. The available treatments tend to rescue the remaining neurons, to compensate the lack of synaptic function or to promote functional plasticity or simply to alleviate symptoms. Therefore, despite obvious limitations of *in vitro* studies, our results convincingly suggest that NS-NPCs develop into a more mature electrical phenotype when co-cultured with post-mitotic neurons. This appears to be the first step towards a complete experimental understanding of the electrophysiological properties of NS-NPCs, in the perspective of integrating these cells into neuronal circuits *in vivo.*

7 REFERENCES

Aghajanian, G. K., and Bunney, B. S. (1974). Central dopaminergic neurons: Neurophysiological identification and responses to drugs. *Biochem. Pharmacol.* 23, 523–528. doi:10.1016/0006-2952(74)90074-4.

Anthony, T. E., Klein, C., Fishell, G., and Heintz, N. (2004). Radial Glia Serve as Neuronal Progenitors in All Regions of the Central Nervous System. *Neuron* 41, 881–890. doi:10.1016/S0896-6273(04)00140-0.

Arvidsson, A., Collin, T., Kirik, D., Kokaia, Z., and Lindvall, O. (2002). Neuronal replacement from endogenous precursors in the adult brain after stroke. *Nat. Med.* 8, 963–970. doi:10.1038/nm747.

Ban, J., Bonifazi, P., Pinato, G., Broccard, F. D., Studer, L., Torre, V., et al. (2006). Embryonic Stem Cell-Derived Neurons Form Functional Networks In Vitro. *Stem Cells* 25, 738–749. doi:10.1634/stemcells.2006-0246.

Banasr, M., and Duman, R. (2007). Regulation of Neurogenesis and Gliogenesis by Stress and Antidepressant Treatment. *CNS Neurol. Disord. - Drug Targets* 6, 311–320. doi:10.2174/187152707783220929.

Banker, G. A., and Cowan, W. M. (1977). Rat hippocampal neurons in dispersed cell culture. *Brain Res.* 126, 397–425. doi:10.1016/0006-8993(77)90594-7.

Barker, R. A., Barrett, J., Mason, S. L., and Björklund, A. (2013). Fetal dopaminergic transplantation trials and the future of neural grafting in Parkinson's disease. *Lancet Neurol.* 12, 84–91. doi:10.1016/S1474-4422(12)70295-8.

Benson, D. L., Watkins, F. H., Steward, O., and Banker, G. (1994). Characterization of GABAergic neurons in hippocampal cell cultures. *J. Neurocytol.* 23, 279–95. Available at: http://www.ncbi.nlm.nih.gov/pubmed/8089704 [Accessed January 13, 2019].

Bergami, M., and Berninger, B. (2012). A fight for survival: The challenges faced by a newborn neuron integrating in the adult hippocampus. *Dev. Neurobiol.* 72, 1016–1031. doi:10.1002/dneu.22025.

Bi, B., Salmaso, N., Komitova, M., Simonini, M. V, Silbereis, J., Cheng, E., et al. (2011). Cortical glial fibrillary acidic protein-positive cells generate neurons after perinatal hypoxic injury. *J. Neurosci.* 31, 9205–21. doi:10.1523/JNEUROSCI.0518-11.2011.

Bidarra, S. J., Barrias, C. C., Barbosa, M. A., Soares, R., Amédée, J., and Granja, P. L. (2011). Phenotypic and proliferative modulation of human mesenchymal stem cells via crosstalk with endothelial cells. *Stem Cell Res.* 7, 186–197. doi:10.1016/J.SCR.2011.05.006.

Björklund, A., and Lindvall, O. (2000). Self-repair in the brain. *Nature* 405, 893–895. doi:10.1038/35016175.

Boiani, M., and Schöler, H. R. (2005). Regulatory networks in embryo-derived pluripotent stem cells. *Nat. Rev. Mol. Cell Biol.* 6, 872–881. doi:10.1038/nrm1744.

Brenner, K., You, L., and Arnold, F. H. (2008). Engineering microbial consortia: a new frontier in synthetic biology. *Trends Biotechnol.* 26, 483–489. doi:10.1016/J.TIBTECH.2008.05.004.

Buffo, A., Rite, I., Tripathi, P., Lepier, A., Colak, D., Horn, A.-P., et al. (2008). Origin and progeny of reactive gliosis: A source of multipotent cells in the injured brain. *Proc. Natl. Acad. Sci. U. S. A.* 105, 3581–6. doi:10.1073/pnas.0709002105.

Caleo, M. (2015). Rehabilitation and plasticity following stroke: Insights from rodent models. *Neuroscience* 311, 180–194. doi:10.1016/J.NEUROSCIENCE.2015.10.029.

Campbell, J. J., Davidenko, N., Caffarel, M. M., Cameron, R. E., and Watson, C. J. (2011). A Multifunctional 3D Co-Culture System for Studies of Mammary Tissue Morphogenesis and Stem Cell Biology. *PLoS One* 6, e25661. doi:10.1371/journal.pone.0025661.

Chenn, A., and McConnell, S. K. (1995). Cleavage orientation and the asymmetric inheritance of notchl immunoreactivity in mammalian neurogenesis. *Cell* 82, 631–641. doi:10.1016/0092-8674(95)90035-7.

Conrad, C., and Huss, R. (2005). Adult stem cell lines in regenerative medicine and reconstructive surgery. *J. Surg. Res.* 124, 201–208. doi:10.1016/J.JSS.2004.09.015.

Cottet, S., Corthésy-Theulaz, I., Spertini, F., and Corthésy, B. (2002). Microaerophilic conditions permit to mimic in vitro events occurring during in vivo Helicobacter pylori infection and to identify Rho/Ras-associated proteins in cellular signaling. *J. Biol. Chem.* 277, 33978–86. doi:10.1074/jbc.M201726200.

Deisseroth, K., Singla, S., Toda, H., Monje, M., Palmer, T. D., and Malenka, R. C. (2004). Excitation-Neurogenesis Coupling in Adult Neural Stem/Progenitor Cells. *Neuron* 42, 535–552. doi:10.1016/S0896-6273(04)00266-1.

Ewald, A., Williams, A., Baraban, J., Takai, A., Kass, S., Tohse, N., et al. (1992). Generation of Neurons and Astrocytes from Isolated Cells of the Adult Mammalian Central Nervous System. 1–4.

Fioravante, D., and Regehr, W. G. (2011). Short-term forms of presynaptic plasticity. *Curr. Opin. Neurobiol.* 21, 269–274. doi:10.1016/J.CONB.2011.02.003.

Freed, C. R., Breeze, R. E., Rosenberg, N. L., Schneck, S. A., Kriek, E., Qi, J., et al. (1992). Survival of Implanted Fetal Dopamine Cells and Neurologic Improvement 12 to 46 Months after Transplantation for Parkinson's Disease. *N. Engl. J. Med.* 327, 1549–1555. doi:10.1056/NEJM199211263272202.

Freed, C. R., Greene, P. E., Breeze, R. E., Tsai, W.-Y., DuMouchel, W., Kao, R., et al. (2001). Transplantation of Embryonic Dopamine Neurons for Severe Parkinson's Disease. *N. Engl. J. Med.* 344, 710–719. doi:10.1056/NEJM200103083441002.

Fricker, R. A., Carpenter, M. K., Winkler, C., Greco, C., Gates, M. A., and Björklund, A. (1999). Site-specific migration and neuronal differentiation of human neural progenitor cells after transplantation in the adult rat brain. *J. Neurosci.* 19, 5990–6005. doi:10.1523/JNEUROSCI.19-14-05990.1999.

Gabay, L., Lowell, S., Rubin, L. L., and Anderson, D. J. (2003). Deregulation of Dorsoventral Patterning by FGF Confers Trilineage Differentiation Capacity on CNS Stem Cells In Vitro. *Neuron* 40, 485–499. doi:10.1016/S0896-6273(03)00637-8.

Gao, P., Postiglione, M. P., Krieger, T. G., Hernandez, L., Wang, C., Han, Z., et al. (2014). Deterministic Progenitor Behavior and Unitary Production of Neurons in the Neocortex. *Cell* 159, 775–788. doi:10.1016/J.CELL.2014.10.027.

Goers, L., Freemont, P., and Polizzi, K. M. (2014). Co-culture systems and technologies: taking synthetic biology to the next level. *J. R. Soc. Interface* 11. doi:10.1098/rsif.2014.0065.

Goldberg, A., Mitchell, K., Soans, J., Kim, L., and Zaidi, R. (2017). The use of mesenchymal stem cells for cartilage repair and regeneration: a systematic review. *J. Orthop. Surg. Res.* 12, 39. doi:10.1186/s13018-017-0534-y.

Gonçalves, J. T., Schafer, S. T., and Gage, F. H. (2016). Adult Neurogenesis in the Hippocampus: From Stem Cells to Behavior. *Cell* 167, 897–914. doi:10.1016/J.CELL.2016.10.021.

Götz, M., and Huttner, W. B. (2005). The cell biology of neurogenesis. *Nat. Rev. Mol. Cell Biol.* 6, 777–788. doi:10.1038/nrm1739.

Götz, M., Sirko, S., Beckers, J., and Irmler, M. (2015). Reactive astrocytes as neural stem or progenitor cells: In vivo lineage, In vitro potential, and Genome-wide expression analysis. *Glia* 63, 1452–1468. doi:10.1002/glia.22850.

Grace, A. A., and Onn, S. P. (1989). Morphology and electrophysiological properties of immunocytochemically identified rat dopamine neurons recorded in vitro. *J. Neurosci.* 9, 3463–81. doi:10.1523/JNEUROSCI.09-10-03463.1989.

Grade, S., and Götz, M. (2017). Neuronal replacement therapy: previous achievements and challenges ahead. *npj Regen. Med.* 2, 29. doi:10.1038/s41536-017-0033-0.

Gross, C. G. (2000). Neurogenesis in the adult brain: death of a dogma. *Nat. Rev. Neurosci.* 1, 67–73. doi:10.1038/35036235.

Guo, Y., Wei, Q., Huang, Y., Xia, W., Zhou, Y., and Wang, S. (2013). The effects of astrocytes on differentiation of neural stem cells are influenced by knock-down of the glutamate transporter, GLT-1. *Neurochem. Int.* 63, 498–506. doi:10.1016/J.NEUINT.2013.08.003.

Harel, N. Y., and Strittmatter, S. M. (2006). Can regenerating axons recapitulate developmental guidance during recovery from spinal cord injury? *Nat. Rev. Neurosci.* 7, 603–616. doi:10.1038/nrn1957.

Haubensak, W., Attardo, A., Denk, W., and Huttner, W. B. (2004). Neurons arise in the basal neuroepithelium of the early mammalian telencephalon: a major site of neurogenesis. *Proc.*

Natl. Acad. Sci. U. S. A. 101, 3196–201. doi:10.1073/pnas.0308600100.

Heikkilä, T. J., Ylä-Outinen, L., Tanskanen, J. M. A., Lappalainen, R. S., Skottman, H., Suuronen, R., et al. (2009). Human embryonic stem cell-derived neuronal cells form spontaneously active neuronal networks in vitro. *Exp. Neurol.* 218, 109–116. doi:10.1016/j.expneurol.2009.04.011.

Hofer, S., Magloire, V., Streit, J., and Leib, S. L. (2012). Grafted Neuronal Precursor Cells Differentiate and Integrate in Injured Hippocampus in Experimental Pneumococcal Meningitis. *Stem Cells* 30, 1206–1215. doi:10.1002/stem.1097.

Hokugo, A., Ozeki, M., Kawakami, O., Sugimoto, K., Mushimoto, K., Morita, S., et al. (2005). Augmented Bone Regeneration Activity of Platelet-Rich Plasma by Biodegradable Gelatin Hydrogel. *Tissue Eng.* 11, 1224–1233. doi:10.1089/ten.2005.11.1224.

Hou, S.-W., Wang, Y.-Q., Xu, M., Shen, D.-H., Wang, J.-J., Huang, F., et al. (2008). Functional Integration of Newly Generated Neurons Into Striatum After Cerebral Ischemia in the Adult Rat Brain. *Stroke* 39, 2837–2844. doi:10.1161/STROKEAHA.107.510982.

Howard, M. A., and Baraban, S. C. (2016). Synaptic integration of transplanted interneuron progenitor cells into native cortical networks. *J. Neurophysiol.* 116, 472–478. doi:10.1152/jn.00321.2016.

Hu, Y.-Y., Xu, J., Zhang, M., Wang, D., Li, L., and Li, W.-B. (2015). Ceftriaxone modulates uptake activity of glial glutamate transporter-1 against global brain ischemia in rats. *J. Neurochem.* 132, 194–205. doi:10.1111/jnc.12958.

Husseini, L., Schmandt, T., Scheffler, B., Schröder, W., Seifert, G., Brüstle, O., et al. (2008). Functional Analysis of Embryonic Stem Cell–Derived Glial Cells after Integration into Hippocampal Slice Cultures. *Stem Cells Dev.* 17, 1141–1152. doi:10.1089/scd.2007.0244.

Jeff, G., Schnapp, B. J., and Sheetz, M. P. (1988). Inhibition of pluripotential embryonic stem cell differentiation by purified polypeptides. *Nature* 331, 450.

Kaech, S., and Banker, G. (2007). Culturing hippocampal neurons. doi:10.1038/nprot.2006.356.

Kandasamy, M., Rosskopf, M., Wagner, K., Klein, B., Couillard-Despres, S., Reitsamer, H. A., et al. (2015). Reduction in Subventricular Zone-Derived Olfactory Bulb Neurogenesis in a Rat Model of Huntington's Disease Is Accompanied by Striatal Invasion of Neuroblasts. *PLoS One* 10, e0116069. doi:10.1371/journal.pone.0116069.

Kanthan, S. R., Kavitha, G., Addi, S., Choon, D. S. K., and Kamarul, T. (2011). Platelet-rich plasma (PRP) enhances bone healing in non-united critical-sized defects: A preliminary study involving rabbit models. *Injury* 42, 782–789. doi:10.1016/J.INJURY.2011.01.015.

Kaufman, M. J. E. & M. H. (1981). Establishment in culture of pluripotential cells from mouse embryos. Nature volume 292, pages 154–156. doi:10.1038/292154a0.

Klussmann, S., and Martin-Villalba, A. (2005). Molecular targets in spinal cord injury. *J. Mol. Med.* 83, 657–671. doi:10.1007/s00109-005-0663-3.

Kokaia, Z., Thored, P., Arvidsson, A., and Lindvall, O. (2006). Regulation of Stroke-Induced Neurogenesis in Adult Brain—Recent Scientific Progress. *Cereb. Cortex* 16, i162–i167. doi:10.1093/cercor/bhj174.

Kreuzberg, M., Kanov, E., Timofeev, O., Schwaninger, M., Monyer, H., and Khodosevich, K. (2010). Increased subventricular zone-derived cortical neurogenesis after ischemic lesion. *Exp. Neurol.* 226, 90–99. doi:10.1016/J.EXPNEUROL.2010.08.006.

Larimer, P., Spatazza, J., Stryker, M. P., Alvarez-Buylla, A., and Hasenstaub, A. R. (2017). Development and long-term integration of MGE-lineage cortical interneurons in the heterochronic environment. *J. Neurophysiol.* 118, 131–139. doi:10.1152/jn.00096.2017.

Lepeta, K., Lourenco, M. V, Schweitzer, B. C., Martino Adami, P. V, Banerjee, P., Catuara-Solarz, S., et al. (2016). Synaptopathies: synaptic dysfunction in neurological disorders - A review from students to students. *J. Neurochem.* 138, 785–805. doi:10.1111/jnc.13713.

Li, L., Harms, K. M., Ventura, P. B., Lagace, D. C., Eisch, A. J., and Cunningham, L. A. (2010). Focal cerebral ischemia induces a multilineage cytogenic response from adult subventricular zone that is predominantly gliogenic. *Glia* 58, 1610–1619. doi:10.1002/glia.21033.

Lim, D. A., and Alvarez-Buylla, A. (2016). The Adult Ventricular-Subventricular Zone (V-SVZ) and Olfactory Bulb (OB) Neurogenesis. *Cold Spring Harb. Perspect. Biol.* 8, a018820. doi:10.1101/cshperspect.a018820.

Lovat, V., Pantarotto, D., Lagostena, L., Cacciari, B., Grandolfo, M., Righi, M., et al. (2005). Carbon Nanotube Substrates Boost Neuronal Electrical Signaling. *Nano Lett.* 5, 1107–1110. doi:10.1021/nl050637m.

Lu, J., Manaenko, A., and Hu, Q. (2017). Targeting Adult Neurogenesis for Poststroke Therapy. *Stem Cells Int.* 2017, 5868632. doi:10.1155/2017/5868632.

Luskin, M. B., Pearlman, A. L., and Sanes, J. R. (1988). Cell lineage in the cerebral cortex of the mouse studied in vivo and in vitro with a Recombinant Retrovirus. *Neuron* 1, 635–647. doi:10.1016/0896-6273(88)90163-8.

Madrazo, I., Kopyov, O., Ávila-Rodríguez, M. A., Ostrosky, F., Carrasco, H., Kopyov, A., et al. (2019). Transplantation of Human Neural Progenitor Cells (NPC) into Putamina of Parkinsonian Patients: A Case Series Study, Safety and Efficacy Four Years after Surgery. *Cell Transplant.* 28, 269–285. doi:10.1177/0963689718820271.

Magavi, S. S., Leavitt, B. R., and Macklis, J. D. (2000). Induction of neurogenesis in the neocortex of adult mice. *Nature* 405, 951–955. doi:10.1038/35016083.

Magnusson, J. P., Göritz, C., Tatarishvili, J., Dias, D. O., Smith, E. M. K., Lindvall, O., et al. (2014). A latent neurogenic program in astrocytes regulated by Notch signaling in the mouse. *Science* 346, 237–41. doi:10.1126/science.346.6206.237.

Malatesta, P., Hartfuss, E., and Gotz, M. (2000). Isolation of radial glial cells by fluorescent-activated cell sorting reveals a neuronal lineage. *Development* 127.

Malerba, M., Amin, H., Angotzi, G. N., Maccione, A., and Berdondini, L. (2018). “Fabrication of Multielectrode Arrays for Neurobiology Applications,” in, 147–157. doi:10.1007/978-1-4939-7792-5_12.

Martin, G. R. (1981). Isolation of a pluripotent cell line from early mouse embryos cultured in medium conditioned by teratocarcinoma stem cells. *Proc. Natl. Acad. Sci. U. S. A.* 78, 7634–8. Available at: http://www.ncbi.nlm.nih.gov/pubmed/6950406 [Accessed December 11, 2018].

Martinez-Lozada, Z., Guillem, A. M., and Robinson, M. B. (2016). Transcriptional Regulation of Glutamate Transporters: From Extracellular Signals to Transcription Factors. *Adv. Pharmacol.* 76, 103–45. doi:10.1016/bs.apha.2016.01.004.

Martino, G., and Pluchino, S. (2006). The therapeutic potential of neural stem cells. *Nat. Rev. Neurosci.* 7, 395–406. doi:10.1038/nrn1908.

Matsui, T. K., and Mori, E. (2018). Microglia support neural stem cell maintenance and growth. *Biochem. Biophys. Res. Commun.* 503, 1880–1884. doi:10.1016/j.bbrc.2018.07.130.

McConnell, S. K. (1995). Constructing the cerebral cortex: Neurogenesis and fate determination. *Neuron* 15, 761–768. doi:10.1016/0896-6273(95)90168-X.

McCormick, Z. L., and Hooten, M. (2018). Regenerative Medicine: Ushering in a New Era in Pain Medicine. *Pain Med.* doi:10.1093/pm/pny259.

Méhes, E., Mones, E., Németh, V., and Vicsek, T. (2012). Collective Motion of Cells Mediates Segregation and Pattern Formation in Co-Cultures. *PLoS One* 7, e31711. doi:10.1371/journal.pone.0031711.

Michelsen, K. A., Acosta-Verdugo, S., Benoit-Marand, M., Espuny-Camacho, I., Gaspard, N., Saha, B., et al. (2015). Area-Specific Reestablishment of Damaged Circuits in the Adult Cerebral Cortex by Cortical Neurons Derived from Mouse Embryonic Stem Cells. *Neuron* 85, 982–997. doi:10.1016/J.NEURON.2015.02.001.

Ming, G., and Song, H. (2011). Adult Neurogenesis in the Mammalian Brain: Significant Answers and Significant Questions. *Neuron* 70, 687–702. doi:10.1016/J.NEURON.2011.05.001.

Mistry, S. K., Keefer, E. W., Cunningham, B. a, Edelman, G. M., and Crossin, K. L. (2002). Cultured rat hippocampal neural progenitors generate spontaneously active neural networks. *Proc. Natl. Acad. Sci. U. S. A.* 99, 1621–1626. doi:10.1073/pnas.022646599.

Moon, H. Y., Javadi, S., Stremlau, M., Yoon, K. J., Becker, B., Kang, S.-U., et al. (2019). Conditioned media from AICAR-treated skeletal muscle cells increases neuronal differentiation of adult neural progenitor cells. *Neuropharmacology* 145, 123–130. doi:10.1016/j.neuropharm.2018.10.041.

Moraes, C., Mehta, G., Lesher-Perez, S. C., and Takayama, S. (2012). Organs-on-a-Chip: A Focus on Compartmentalized Microdevices. *Ann. Biomed. Eng.* 40, 1211–1227.

doi:10.1007/s10439-011-0455-6.

Nichols, J., Zevnik, B., Anastassiadis, K., Niwa, H., Klewe-Nebenius, D., Chambers, I., et al. (1998). Formation of Pluripotent Stem Cells in the Mammalian Embryo Depends on the POU Transcription Factor Oct4. *Cell* 95, 379–391. doi:10.1016/S0092-8674(00)81769-9.

Ninkovic, J., and Götz, M. (2013). Fate specification in the adult brain - lessons for eliciting neurogenesis from glial cells. *BioEssays* 35, 242–252. doi:10.1002/bies.201200108.

Noctor, S. C., Martínez-Cerdeño, V., Ivic, L., and Kriegstein, A. R. (2004). Cortical neurons arise in symmetric and asymmetric division zones and migrate through specific phases. *Nat. Neurosci.* 7, 136–144. doi:10.1038/nn1172.

Novo, C. L., Tang, C., Ahmed, K., Djuric, U., Fussner, E., Mullin, N. P., et al. (2016). The pluripotency factor Nanog regulates pericentromeric heterochromatin organization in mouse embryonic stem cells. *Genes Dev.* 30, 1101–15. doi:10.1101/gad.275685.115.

Ohira, K., Furuta, T., Hioki, H., Nakamura, K. C., Kuramoto, E., Tanaka, Y., et al. (2010). Ischemia-induced neurogenesis of neocortical layer 1 progenitor cells. *Nat. Neurosci.* 13, 173–179. doi:10.1038/nn.2473.

Pan, X., Cang, X., Dan, S., Li, J., Cheng, J., Kang, B., et al. (2016). Site-specific Disruption of the Oct4/Sox2 Protein Interaction Reveals Coordinated Mesendodermal Differentiation and the Epithelial-Mesenchymal Transition. *J. Biol. Chem.* 291, 18353–69. doi:10.1074/jbc.M116.745414.

Qian, X., Shen, Q., Goderie, S. K., He, W., Capela, A., Davis, A. A., et al. (2000). Timing of CNS Cell Generation: A Programmed Sequence of Neuron and Glial Cell Production from Isolated Murine Cortical Stem Cells. *Neuron* 28, 69–80. doi:10.1016/S0896-6273(00)00086-6.

Reynolds, B. A., and Weiss, S. (1996). Clonal and Population Analyses Demonstrate That an EGF-Responsive Mammalian Embryonic CNS Precursor Is a Stem Cell. *Dev. Biol.* 175, 1–13. doi:10.1006/DBIO.1996.0090.

Riddle, D. R., and Lichtenwalner, R. J. (2007). *Neurogenesis in the Adult and Aging Brain*. CRC Press/Taylor & Francis Available at: http://www.ncbi.nlm.nih.gov/pubmed/21204350 [Accessed May 16, 2019].

Ross, R., Glomset, J., Kariya, B., and Harker, L. (1974). A platelet-dependent serum factor that stimulates the proliferation of arterial smooth muscle cells in vitro. *Proc. Natl. Acad. Sci. U. S. A.* 71, 1207–10. doi:10.1073/PNAS.71.4.1207.

Ruschenschmidt, C., Koch, P. G., Brustle, O., and Beck, H. (2005). Functional Properties of ES Cell-Derived Neurons Engrafted into the Hippocampus of Adult Normal and Chronically Epileptic Rats. *Epilepsia* 46, 174–183. doi:10.1111/j.1528-1167.2005.01028.x.

Seidenfaden, R., Desoeuvre, A., Bosio, A., Virard, I., and Cremer, H. (2006). Glial conversion of SVZ-derived committed neuronal precursors after ectopic grafting into the adult brain. *Mol.*

Cell. Neurosci. 32, 187–198. doi:10.1016/J.MCN.2006.04.003.

Shihabuddin, L. S., Horner, P. J., Ray, J., and Gage, F. H. (2000). Adult spinal cord stem cells generate neurons after transplantation in the adult dentate gyrus. *J. Neurosci.* 20, 8727–35. doi:10.1523/JNEUROSCI.20-23-08727.2000.

Silver, J., and Miller, J. H. (2004). Regeneration beyond the glial scar. *Nat. Rev. Neurosci.* 5, 146–156. doi:10.1038/nrn1326.

Sirko, S., Behrendt, G., Johansson, P. A., Tripathi, P., Costa, M. R., Bek, S., et al. (2013). Reactive Glia in the Injured Brain Acquire Stem Cell Properties in Response to Sonic Hedgehog. *Cell Stem Cell* 12, 426–439. doi:10.1016/J.STEM.2013.01.019.

Smart, I. H. M., Dehay, C., Giroud, P., Berland, M., and Kennedy, H. (2002). Unique Morphological Features of the Proliferative Zones and Postmitotic Compartments of the Neural Epithelium Giving Rise to Striate and Extrastriate Cortex in the Monkey. *Cereb. Cortex* 12, 37–53. doi:10.1093/cercor/12.1.37.

Sobajima, S., Vadala, G., Shimer, A., Kim, J. S., Gilbertson, L. G., and Kang, J. D. (2008). Feasibility of a stem cell therapy for intervertebral disc degeneration. *Spine J.* 8, 888–896. doi:10.1016/J.SPINEE.2007.09.011.

Song, H., Stevens, C. F., and Gage, F. H. (2002). Astroglia induce neurogenesis from adult neural stem cells. *Nature* 417, 39–44. doi:10.1038/417039a.

Spalding, K. L., Bergmann, O., Alkass, K., Bernard, S., Salehpour, M., Huttner, H. B., et al. (2013). Dynamics of Hippocampal Neurogenesis in Adult Humans. *Cell* 153, 1219–1227. doi:10.1016/J.CELL.2013.05.002.

Stadtfeld, M., and Hochedlinger, K. (2010). Induced pluripotency: history, mechanisms, and applications. *Genes Dev.* 24, 2239–63. doi:10.1101/gad.1963910.

Stephens, C. L., Toda, H., Palmer, T. D., DeMarse, T. B., and Ormerod, B. K. (2012). Adult neural progenitor cells reactivate superbursting in mature neural networks. *Exp. Neurol.* 234, 20–30. doi:10.1016/j.expneurol.2011.12.009.

Suda, Y., Suzuki, M., Ikawa, Y., and Aizawa, S. (1987). Mouse embryonic stem cells exhibit indefinite proliferative potential. *J. Cell. Physiol.* 133, 197–201. doi:10.1002/jcp.1041330127.

Sun Y, and Weber KT. (2000). Infarct scar: a dynamic tissue. [Review] [58 refs]. *Cardiovasc. Res.* 46, 250–256.

Tanouchi, Y., Smith, R. P., and You, L. (2012). Engineering microbial systems to explore ecological and evolutionary dynamics. *Curr. Opin. Biotechnol.* 23, 791–797. doi:10.1016/J.COPBIO.2012.01.006.

Thomson, J. A., Itskovitz-Eldor, J., Shapiro, S. S., Waknitz, M. A., Swiergiel, J. J., Marshall, V. S., et al. (1998). Embryonic stem cell lines derived from human blastocysts. *Science* 282, 1145–7. doi:10.1126/SCIENCE.282.5391.1145.

Thomson, J. A., and Marshall, V. S. (1997). 4 Primate Embryonic Stem Cells. *Curr. Top. Dev. Biol.* 38, 133–165. doi:10.1016/S0070-2153(08)60246-X.

Thored, P., Arvidsson, A., Cacci, E., Ahlenius, H., Kallur, T., Darsalia, V., et al. (2006). Persistent Production of Neurons from Adult Brain Stem Cells During Recovery after Stroke. *Stem Cells* 24, 739–747. doi:10.1634/stemcells.2005-0281.

Tornero, D., Tsupykov, O., Granmo, M., Rodriguez, C., Grønning-Hansen, M., Thelin, J., et al. (2017). Synaptic inputs from stroke-injured brain to grafted human stem cell-derived neurons activated by sensory stimuli. *Brain* 140, aww347. doi:10.1093/brain/aww347.

Tornero, D., Wattananit, S., Madsen, M. G., Koch, P., Wood, J., Tatarishvili, J., et al. (2013). Human induced pluripotent stem cell-derived cortical neurons integrate in stroke-injured cortex and improve functional recovery. *Brain* 136, 3561–3577. doi:10.1093/brain/awt278.

Wang, Y.-C., Yang, J. S., Johnston, R., Ren, Q., Lee, Y.-J., Luan, H., et al. (2014). Drosophila intermediate neural progenitors produce lineage-dependent related series of diverse neurons. *Development* 141, 253–8. doi:10.1242/dev.103069.

Weinandy, F., Ninkovic, J., and Götz, M. (2011). Restrictions in time and space - new insights into generation of specific neuronal subtypes in the adult mammalian brain. *Eur. J. Neurosci.* 33, 1045–1054. doi:10.1111/j.1460-9568.2011.07602.x.

Widera, D. (2004). MCP-1 induces migration of adult neural stem cells. *Eur. J. Cell Biol.* 83, 381–387. doi:10.1078/0171-9335-00403.

Widera, D., Grimm, W.-D., Moebius, J. M., Mikenberg, I., Piechaczek, C., Gassmann, G., et al. (2007). Highly Efficient Neural Differentiation of Human Somatic Stem Cells, Isolated by Minimally Invasive Periodontal Surgery. *Stem Cells Dev.* 16, 447–460. doi:10.1089/scd.2006.0068.

Wise, R. A. (2004). Dopamine, learning and motivation. *Nat. Rev. Neurosci.* 5, 483–494. doi:10.1038/nrn1406.

Wu, Y., Chen, Q., Peng, H., Dou, H., Zhou, Y., Huang, Y., et al. (2012). Directed migration of human neural progenitor cells to interleukin-1β is promoted by chemokines stromal cell-derived factor-1 and monocyte chemotactic factor-1 in mouse brains. *Transl. Neurodegener.* 1, 15. doi:10.1186/2047-9158-1-15.

Xie, Y., Schutte, R. J., Ng, N. N., Ess, K. C., Schwartz, P. H., and O'Dowd, D. K. (2018). Reproducible and efficient generation of functionally active neurons from human hiPSCs for preclinical disease modeling. *Stem Cell Res.* 26, 84–94. doi:10.1016/j.scr.2017.12.003.

Yamashita, T., Ninomiya, M., Hernández Acosta, P., García-Verdugo, J. M., Sunabori, T., Sakaguchi, M., et al. (2006). Subventricular zone-derived neuroblasts migrate and differentiate into mature neurons in the post-stroke adult striatum. *J. Neurosci.* 26, 6627–36. doi:10.1523/JNEUROSCI.0149-06.2006.

Yu, D., Cheng, Z., Ali, A. I., Wang, J., Le, K., Chibaatar, E., et al. (2018). Down-expressed GLT-

1 in PSD astrocytes inhibits synaptic formation of NSC-derived neurons in vitro. *Cell Cycle* 18, 105–114. doi:10.1080/15384101.2018.1560201.

Zeidan, A. A., Rådström, P., and van Niel, E. W. (2010). Stable coexistence of two Caldicellulosiruptor species in a de novo constructed hydrogen-producing co-culture. *Microb. Cell Fact.* 9, 102. doi:10.1186/1475-2859-9-102.

Zhang, W., Fang, X., Zhang, C., Li, W., Wong, W. M., Xu, Y., et al. (2017). Transplantation of embryonic spinal cord neurons to the injured distal nerve promotes axonal regeneration after delayed nerve repair. *Eur. J. Neurosci.* 45, 750–762. doi:10.1111/ejn.13495.